Ferrocene- and ruthenium arene-containing glycomimetics as selective inhibitors of human galectin-1 and -3

Vojtěch Hamala,[a,b] Martin Kurfiřt,[a,b] Lucie Červenková Šťastná,[a] Hedvika Hujerová,[a] Jana Bernášková,[a] Kamil Parkan,[c,d] Jakub Kaminský,[d] Nina Habanová,[d,e] Jaroslav Kozák,[d] Alžběta Magdolenová,[d] Martin Zavřel,[d] Tatiana Staroňová,[f,g] Veronika Ostatná,[g] Lucie Žaloudková,[f,g] Aleš Daňhel,[g] Jitka Holčáková,[h] Petr Voňka,[h] Roman Hrstka,*[h] Jindřich Karban, *[a]

[a] *Institute of Chemical Process Fundamentals of the CAS, v. v. i., Rozvojová 1/135, 165 00 Praha, Czech Republic. E-mail: karban@icpf.cas.cz.*
[b] *Department of Organic Chemistry, University of Chemistry and Technology, Technická 5, 166 28 Praha, Czech Republic.*
[c] *Department of Chemistry of Natural Compounds, University of Chemistry and Technology, Prague, Technická 5, 166 28, Prague, Czech Republic*
[d] *Institute of Organic Chemistry and Biochemistry of the CAS, v. v. i., Flemingovo nám. 542, 160 00 Praha, Czech Republic*
[e] *Department of Analytical Chemistry, University of Chemistry and Technology, Technická 5, 166 28 Praha, Czech Republic.*
[f] *Department of Biochemistry, Faculty of Science, Masaryk University, Kotlářská 2, 602 00, Brno, Czech Republic*
[g] *Institute of Biophysics of the CAS, v. v. i., Královopolská 135, 612 00 Brno, Czech Republic*
[h] *Research Centre for Applied Molecular Oncology, Masaryk Memorial Cancer Institute, Žlutý kopec 7, 656 53 Brno, Czech Republic.*
*E-mail: hrstka@mou.cz, karban@icpf.cas.cz

SUPPORTING INFORMATION I

Experimental procedures

Table of Contents

A. General procedures

Chemicals were used as received. Petroleum ether fraction (with boiling point 40–65 °C) was distilled before use. TLC was carried out with Sigma-Aldrich TLC Silica gel 60 F_{254} and spots were detected by an UV detection at 254 nm or visualized with an anisaldehyde solution (EtOH/AcOH/H_2SO_4). Column chromatography was performed with silica gel 60 (70–230 mesh, Material Harvest) or aluminum oxide 90 active neutral (70–230 mesh, Milipore). If not specified, solutions were concentrated under reduced pressure at temperatures below 45 °C. Anhydrous sodium sulfate was used to dry solutions after aqueous workup. NMR spectra were recorded using Bruker Avance 400 (^{1}H at 400.1 MHz, ^{19}F at 376.4 MHz, ^{13}C at 100.6 MHz) at 25 °C. The ^{1}H and ^{13}C NMR spectra were referenced to the solvent (δ/ppm; δH/δC: $CDCl_3$, 7.26/77.16, MeOH-d_4, 3.31/49.00, dmso-d_6, 2.50/39.52). The ^{19}F NMR spectra were referenced to the line of the internal standard hexafluorobenzene (δ/ppm; −163.00 in $CDCl_3$, −166.62 in MeOD-d_4, −163.86 in DMSO-d_6). The structural assignment of proton and carbon NMR spectra was made by a combination of 1D and 2D NMR measurements: ^{1}H-^{1}H gCOSY, ^{1}H-^{13}C gHSQC, ^{1}H-^{13}C gHMBC, and ^{1}H-^{13}C gHSQC TOCSY. HRMS analyses were done using Bruker MicrOTOF-QIII, using APCI or ESI ionization in the positive mode. The m/z value of an $[M - N_2 + H]^+$ adduct is usually reported for azide-containing sugars because the molecular ion adducts were usually undetectable or extremely weak in abundance. The ruthenium, iron, and copper content in all final compounds were analyzed using inductively coupled plasma mass spectrometry (ICP-MS) with an Agilent 7900 spectrometer (Agilent, Japan) equipped with a quadrupole mass analyzer in a 5% HCl solution. In all cases, the copper content was below the spectrometer's detection limit, while the ruthenium and iron content corresponded with the calculated values. EtOAc stands for ethyl acetate, PE for petroleum ether, DCM for dichloromethane, MeOH for methanol, DMSO for dimethyl sulfoxide and DMF for dimethylformamide.

General procedure for azide-alkyne cycloaddition followed by deacetylation

The starting O-acylated azido-saccharide was dissolved in dimethylformamide ($c \approx 0.05$ M), terminal alkyne (ethynyl ferrocene or phenyl acetylene; 1.2–1.5 equiv per an azido group), $CuSO_4 \cdot 5\ H_2O$ (12 mg, 0.05 mmol), and ascorbic acid (8 mg, 0.05 mmol) were added, and the mixture was stirred for 2 h at 40 °C. The mixture was diluted with water and extracted with DCM (3×). Organic extracts were combined, dried, concentrated. The crude acylated intermediate was dissolved or suspended in the mixture of DCM and MeOH 1:1 ($c \approx 0.01$ M) and a 1 M solution of MeONa in MeOH was added dropwise until pH = 9–10. Reaction mixture was stirred for 12–72 h until the starting material was completely dissolved and TLC (DCM/MeOH) indicated the presence of only one highly polar product. The reaction was neutralized with DOWEX 50W(H$^+$) ion exchange resin, filtered and concentrated. The crude product was purified by column chromatography.

General procedure for azide-alkyne cycloaddition for unprotected saccharides

The starting azido-saccharide was dissolved in dimethylformamide ($c \approx 0.05$ M), ethynyl ferrocene, phenyl acetylene, or propargyl alcohol (1.2–1.5 equiv per an azido group), $CuSO_4 \cdot 5\ H_2O$ (12 mg, 0.05 mmol), and ascorbic acid (8 mg, 0.05 mmol) were added, and the mixture was stirred for 2 h at 40 °C. The reaction mixture was diluted with MeOH, silica gel (approximately 10 g) was added, the solvents were evaporated, and the crude product was dry loaded onto a chromatography column for purification.

General procedure for the preparation of ruthenium arenes

A flask was charged with chloro(pentamethylcyclopentadienyl)ruthenium(II) tetramer (0.28 equiv per one phenyl group) in a glovebox, the flask was equipped with a new septum and removed from the glovebox. Anhydrous CH_3CN was added (2–4 mL) through septum, the reaction mixture was stirred at 65 °C for 2 h under argon until all of the solid tetramer was dissolved, and the reaction mixture was allowed to cool down to rt. A solution of a saccharide (1 equiv) in degassed water ($c \approx 0.01$ M) was added through septum and the reaction mixture was stirred for seven days. The solvents were evaporated, and the crude product was purified by column chromatography on neutral aluminum oxide.

General glycosylation procedure

A mixture of the glycosyl acceptor (1 equiv) and glycosyl donor (1.2–1.3 equiv) was co-evaporated with toluene (3×) and dried for 15 min in the vacuum of an oil pump. Anhydrous DCM ($c \approx 0.1$ M) and 3 Å molecular sieves were added under argon atmosphere and the mixture was stirred at room temperature for 1 h. Reaction was cooled to 0 °C, and NIS (2 equiv) and catalytic amount of triflic acid (20 μL) were added. The reaction mixture was stirred for additional 1–2 h, until TLC indicated the complete absence of one of the starting compounds. The reaction mixture was diluted with DCM (30 mL), quenched by the addition of a saturated aqueous solution of $NaHCO_3$ (5 mL) and 10% aqueous solution of $Na_2S_2O_3$ (5 mL). The reaction mixture was filtered, washed with water, the water phase was extracted with DCM (3×), organic extracts were combined, dried, and concentrated to afford the crude glycosylation product which was purified by column chromatography.

General procedure for oxidative de-O-benzylation

A solution of $NaBrO_3$ (5 equiv) in H_2O ($c \approx 0.15$ M) was added into a solution of a benzyl ether-protected disaccharide in EtOAc ($c \approx 0.02$ M) and the mixture was stirred vigorously. A solution of $Na_2S_2O_4$ (5 equiv) in H_2O ($c \approx 0.075$ M) was slowly added dropwise and the reaction mixture was stirred for 6 h until TLC (EtOAc/PE) indicated the absence of the starting material and the presence of only one polar product. During and/or after the addition of the $Na_2S_2O_4$ solution the colourless two phase mixture turned

orange and then back to colorless. If the color persisted even after TLC indicated the completion of the reaction, the reaction was quenched by addition of a small quantity of a 10% aqueous solution of $Na_2S_2O_3$ (until discoloration of the reaction mixture). The reaction mixture was diluted with DCM, the water phase was saturated with sodium chloride and the phases were separated. The water phase was extracted with DCM (2×). The organic phases were combined and washed with a saturated aqueous solution of $NaHCO_3$, and the water solution was extracted with DCM (2×). Organic extracts were combined, dried and concentrated. The crude product was purified by column chromatography.

General procedure for phthalimide to acetamide conversion.

Ethylenediamine (50 equiv) was added to a solution of a methyl 2-phthalimido-glycoside in MeOH (c ≈ 0.05 M) and the mixture was refluxed for 4 h until TLC (EtOAc) indicated the absence of the starting material and presence of a more polar product. The reaction mixture was concentrated, co-distilled with toluene (3×) and dissolved in MeOH (c ≈ 0.05 M). Acetic anhydride (100 equiv) was added and the reaction mixture was stirred for 2 h at 0 °C until TLC (DCM/MeOH) indicated the absence of a free amine intermediate and presence of a less polar *N*-acetylated product. The reaction mixture was concentrated, co-distilled with toluene (3×) and dry-loaded onto a column for column chromatography for purification.
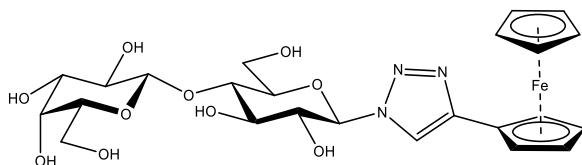
B. Synthesis and characterization of new compounds

B. 1. Synthetic procedures

**(1-β-D-Lactopyranosyl-1*H*-1,2,3-triazol-4-yl)methanol (4)**
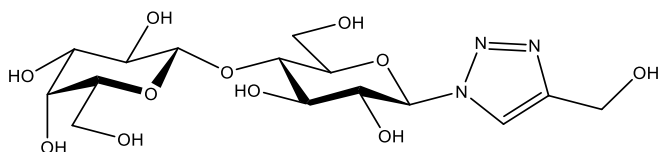
Compound **4** has been prepared according to the known procedure.[1]

1-[4-*O*-(β-D-Galactopyranosyl)-β-D-glucopyranosyl]-4-ferrocenyl-1*H*-1,2,3-triazole (6)

Compound **6** was prepared according to the general procedure for azide-alkyne cycloaddition followed by acetyl deprotection starting from β-D-lactosyl azide peracetate[2] (132 mg, 0.20 mmol), ethynyl ferrocene (50 mg, 0.24 mmol), $CuSO_4 \cdot 5H_2O$ (12 mg, 0.05 mmol), ascorbic acid (8 mg, 0.05 mmol) and DMF (4 mL). The ensuing deacetylation step after aqueous workup was performed using MeOH (10 mL), DCM (10 mL) and 8 drops of 1 M solution of MeONa overnight. Column chromatography in DCM/MeOH 4:1 after DOWEX 50W (H^{+}) neutralization afforded **6** as an orange crystalline solid (93 mg, 81%), mp 261–264 °C (MeOH), R_f 0.10 (DCM/MeOH 5/1), $[\alpha]_D^{20}$ −401 (*c* 1.02, MeOH). ^{1}H NMR (MeOH-d_4, 400 MHz, H-H COSY): δ 8.22 (s, 1H, C*H*$_{Tria}$), 5.64 (d, 1H, *J* = 9.2 Hz, H-1), 4.75, 4.74 (2×q, 2×1H, *J* = 1.8 Hz, C*H*$_{Cp}$), 4.44 (d, 1H, *J* = 7.6 Hz, H-1′), 4.33 (t, 2H, *J* = 1.8 Hz, C*H*$_{Cp}$), 4.08 (s, 5H, C*H*$_{Cp}$), 4.01 (t, 1H, *J* = 9.2 Hz, H-2), 3.97–3.90 (m, 2H, H-6a,6b), 3.83 (dd, 1H, *J* = 3.3, 0.9 Hz, H-4′), 3.81–3.71 (m, 5H, H-3,4,5,6′a,6′b), 3.63 (ddd, 1H, *J* = 7.3, 4.3, 0.9 Hz, H-5′), 3.60 (dd, 1H, *J* = 9.7, 7.6 Hz, H-2′), 3.52 (dd, 1H, *J* = 9.7, 3.3 Hz, H-3′). ^{13}C{^{1}H} NMR (MeOH-d_4, 101 MHz, HSQC, HMBC, HSQC TOCSY): δ 148.1 (*C*$_{q(Tria)}$), 120.6 (*C*H_{Tria}), 105.1 (C-1′), 89.4 (C-1), 79.67, 79.61 (C-3,4), 77.2 (C-5′), 77.0 (C-5), 75.9 (*C*$_{q(Cp)}$), 74.8 (C-3′), 73.7 (C-2), 72.6 (C-2′), 70.6 (5*C*H_{Cp}), 70.3 (C-4′), 69.9 (2*C*H_{Cp}), 67.72, 67.68 (2×*C*H_{Cp}), 62.5 (C-6′), 61.5 (C-6). HRMS-APCI (m/z): [M + H][+] calcd for $C_{24}H_{32}FeN_3O_{10}$, 577.1400; found 577.1406.

1-(4-*O*-(β-D-Galactopyranosyl)-β-D-glucopyranosyl)-4-phenyl-1*H*-1,2,3-triazole (7)
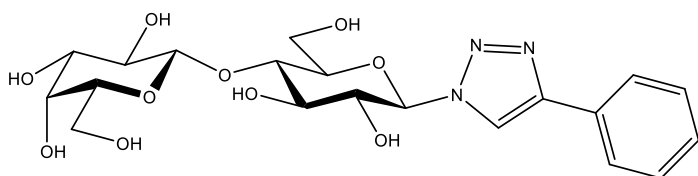
Compound **7** was prepared according to the general procedure for azide-alkyne cycloaddition followed by acetyl deprotection starting from β-D-lactosyl azide peracetate[2] (300 mg, 0.45 mmol), phenyl acetylene (60 μL, 0.55 mmol), $CuSO_4 \cdot 5H_2O$ (12 mg, 0.05 mmol), ascorbic acid (8 mg, 0.05 mmol) and DMF (9 mL). Deacetylation step after aqueous workup was performed using MeOH (20 mL), DCM (20 mL) and 10 drops of 1 M solution of MeONa overnight. Column chromatography in DCM/MeOH 3:1 after DOWEX 50W (H^{+}) neutralization afforded **7** as a white crystalline solid (192 mg, 90% over two steps), mp 267–270 °C (H₂O/MeOH/EtOAc), R_f 0.30 (DCM/MeOH 3:1), $[\alpha]_D^{20}$ +148 (*c* 0.28, MeOH). ^{1}H NMR (DMSO-d_6, 400 MHz, H-H COSY): δ 8.83 (s, 1H, C*H*$_{Tria}$), 7.88 (dd, 2H, *J* = 8.4, 1.3 Hz, C*H*$_{Ph}$), 7.46 (dd, 2H, *J* = 8.4, 7.0 Hz, C*H*$_{Ph}$), 7.35 (tt, 1H, *J* = 7.0, 1.3 Hz, C*H*$_{Ph}$), 5.69 (d, 1H, *J* = 9.3 Hz, H-1), 5.61 (d, 1H, *J* = 5.9 Hz, O*H*-2), 5.14 (d, 1H, *J* = 4.6 Hz, O*H*-2′), 4.93 (d, 1H, *J* = 1.8 Hz, O*H*-3), 4.82 (d, 1H, *J* = 5.3 Hz, O*H*-3′), 4.70–4.66 (m, 2H, O*H*-6, O*H*-6′), 4.55 (d, 1H, *J* = 4.6 Hz, O*H*-4′), 4.28 (d, 1H, *J* = 7.1 Hz, H-1′), 3.91 (ddd, 1H, *J* = 9.3, 8.9, 5.9 Hz, H-2), 3.80 (ddd, 1H, *J* = 12.0, 5.8, 2.1 Hz, H-6a), 3.71 (ddd, 1H, *J* = 9.6, 5.0, 2.1 Hz, H-5), 3.66–3.60 (m, 3H, H-3,6b,4′), 3.58–3.48 (m, 4H, H-4,5′,6′a,6b), 3.41–3.32 (m, 2H, H-2′,3′). ^{13}C{^{1}H} NMR (DMSO-d_6, 101 MHz, HSQC, HMBC, HSQC

TOCSY): δ 146.4 ($C_{q(Tria)}$), 130.6 ($C_{q(Ph)}$), 129.0 ($2CH_{Ph}$), 128.0 (CH_{Ph}), 125.2 ($2CH_{Ph}$), 120.5 (CH_{Tria}), 103.8 (C-1′), 87.2 (C-1), 79.8 (C-4), 77.8 (C-5), 75.6 (C-5′), 75.1 (C-3), 73.3 (C-3′), 72.0 (C-2), 70.6 (C-2′), 68.2 (C-4′), 60.5 (C-6′), 60.1 (C-6). HRMS-APCI (m/z): [M + H]$^+$ calcd for $C_{20}H_{28}N_3O_{10}$, 470.1769; found 470.1765.

(η^5-Pentamethylcyclopentadienyl)[η^6-1-{4-O-(β-D-galactopyranosyl)-β-D-glucopyranosyl}-1H-1,2,3-triazol-4-yl-benzene]ruthenium chloride (8)
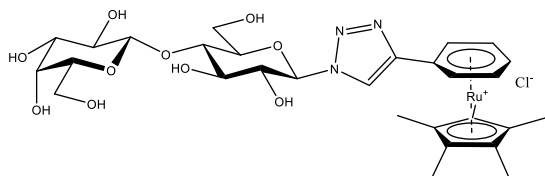
Compound **8** was prepared according to the general procedure for the preparation of ruthenium arenes starting from **7** (85 mg, 0.18 mmol), chloro(pentamethylcyclopentadienyl)ruthenium(II) tetramer (54 mg, 0.05 mmol), anhydrous CH_3CN (4 mL) and degassed water (20 mL). Column chromatography in DCM/MeOH 3:1 on neutral aluminum oxide afforded **8** as a brown amorphous solid (111 mg, 83%), $[\alpha]_D^{20}$ +36 (c 1.09, MeOH). ^{1}H NMR (MeOH-d_4, 400 MHz, H-H COSY): δ 8.90 (s, 1H, CH_{Tria}), 6.57 (d, 2H, J = 6.1 Hz, CH_{Ph}), 6.08 (dd, 2H, J = 6.1, 5.8 Hz, CH_{Ph}), 6.00 (t, 1H, J = 5.8 Hz, CH_{Ph}), 5.77 (d, 1H, J = 9.2 Hz, H-1), 4.47 (d, 1H, J = 7.5 Hz, H-1′), 4.02 (dd, 1H, J = 9.2, 8.8 Hz, H-2), 3.97–3.90 (m, 2H, H-6a,6b), 3.86 (dd, 1H, J = 3.2, 0.9 Hz, H-4′), 3.87–3.77 (m, 4H, H-3,4,5,6′a), 3.75 (dd, 1H, J = 11.3, 4.6 Hz, H-6′b), 3.67–3.64 (m, 1H, H-5′), 3.60 (dd, 1H, J = 9.7, 7.5 Hz, H-2′), 3.54 (dd, 1H, J = 9.7, 3.2 Hz, H-3′), 1.83 (s, 15H, Me). ^{13}C{^{1}H} NMR (MeOH-d_4, 101 MHz, HSQC, HMBC, HSQC TOCSY): δ 142.5 ($C_{q(Tria)}$), 124.3 (CH_{Tria}), 105.1 (C-1′), 98.3 ($C_{q(Cp^*)}$), 93.1 ($C_{q(Ph)}$), 89.4 (C-1), 88.7, 88.62, 88.61, 85.23, 85.17 (5×CH_{Ph}), 79.74,79.73 (C-4,5), 77.1 (C-5′), 76.9 (C-3), 74.8 (C-3′), 73.9 (C-2), 72.5 (C-2′), 70.4 (C-4′), 62.6 (C-6), 61.5 (C-6′), 10.3 (Me_{Cp^*}). HRMS-APCI (m/z): [M − Cl]$^+$ calcd for $C_{30}H_{42}N_3O_{10}Ru$, 706.1916; found 706.1915.

2-(4-Ferrocenyl-1H-1,2,3-triazol-1-yl)ethyl 4-O-(β-D-galactopyranosyl)-β-D-glucopyranoside (10)
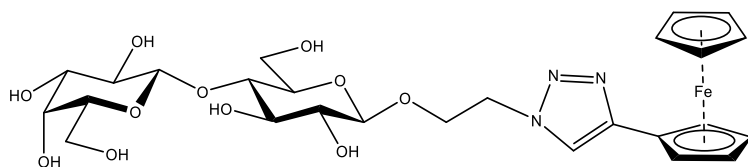
Compound **10** was prepared according to the general procedure for azide-alkyne cycloaddition for unprotected saccharides starting from 2-azidoethyl 4-O-(β-D-galactopyranosyl)-β-D-glucopyranoside[3] (82 mg, 0.20 mmol), ethynyl ferrocene (50 mg, 0.24 mmol), $CuSO_4 \cdot 5H_2O$ (12 mg, 0.05 mmol) and ascorbic acid (8 mg, 0.05 mmol). Column chromatography in DCM/MeOH 3:1 afforded **10** as an orange

crystalline solid (111 mg, 90%), mp 147–150 °C (MeOH/EtOAc), R_f 0.35 (DCM/MeOH 2/1), $[\alpha]_D^{20}$ −408 (c 0.54, MeOH). ^{1}H NMR (MeOH-d_4, 400 MHz, H-H COSY): δ 8.16 (s, 1H, CH_Tria), 4.74 (t, 2H, J = 1.9 Hz, CH_Cp), 4.64 (t, 2H, J = 5.1 Hz, CH_2N), 4.38 (d, 1H, J = 7.8 Hz, H-1), 4.34 (d, 1H, J = 7.5 Hz, H-1′), 4.31 (t, 2H, J = 1.9 Hz, CH_Cp), 4.28 (dt, 1H, J = 11.5, 5.1 Hz, CHHCH$_2$N), 4.07 (s, 5H, CH_Cp), 4.02 (dt, 1H, J = 11.5, 5.1 Hz, CHHCH$_2$N), 3.92 (dd, 1H, J = 12.1, 2.5 Hz, H-6a), 3.83 (dd, 1H, J = 12.1, 4.9 Hz, H-6b), 3.81 (dd, 1H, J = 3.4, 0.7 Hz, H-4′), 3.77 (dd, 1H, J = 11.5, 7.6 Hz, H-6′a), 3.69 (dd, 1H, J = 11.5, 4.6 Hz, H-6′b), 3.59–3.42 (m, 6H, H-3,4,5,2′,3′,5′), 3.29 (dd, 1H, J = 8.8, 7.8 Hz, H-2). ^{13}C{^{1}H} NMR (MeOH-d_4, 101 MHz, HSQC, HMBC, HSQC TOCSY): δ not detected ($C_\text{q(Tria)}$), from HSQC 122.9 (CH_Tria), 105.1 (C-1′), 104.4 (C-1), 80.6 (C-5), 77.1 (C-5′), 76.6,76.4 (C-3,4), not detected ($C_\text{q(Cp)}$), 74.8 (C-3′), 74.7 (C-2), 72.5 (C-2′), 71.5 (5CH$_\text{Cp}$), 70.6 (2CH$_\text{Cp}$), 70.3 (C-4′), 69.1 (OCH$_2$CH$_2$), 68.3 (2CH$_\text{Cp}$), 62.5 (C-6′), 61.9 (C-6), 51.6 (CH_2N). HRMS-APCI (m/z): [M + H]$^+$ calcd for $C_{26}H_{36}FeN_3O_{11}$, 622.1694; found 622.1692.

4-O-(2,3,4,6-Tetra-O-acetyl-β-D-galactopyranosyl)-3,6-di-O-benzyl-2-deoxy-2-phthalimido-β-D-glucopyranosyl azide (13)
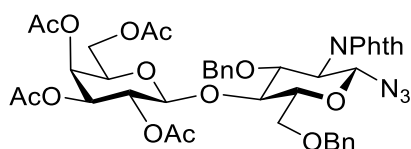
Disaccharide **13** was prepared according to the general glycosylation procedure starting from phenyl 2,3,4,6-tetra-O-acetyl-1-thio-β-D-galactopyranoside[4] (**11**, 579 mg, 1.31 mmol), 3,6-di-O-benzyl-2-deoxy-2-phthalimido-β-D-glucopyranosyl azide[5] (**12**, 520 mg, 1.01 mmol), NIS (455 mg, 2.02 mmol), anhydrous DCM (10 mL), triflic acid (20 μL) and 3 Å molecular sieves (2 g). Column chromatography in EtOAc/PE 2:5 afforded **13** (628 mg, 74%) as a colourless gel, R_f 0.65 (EtOAc/PE 1:1) $[\alpha]_D^{20}$ +129 (c 1.45, CHCl$_3$). ^{1}H NMR (CDCl$_3$, 400 MHz, H-H COSY): δ 7.77–7.62 (m, 4H, CH_Ph), 7.44–7.34 (m, 5H, CH_Ph), 7.01–6.99 (m, 2H, CH_Ph), 6.90–6.83 (m, 3H, CH_Ph), 5.33 (d, 1H, J = 9.4 Hz, H-1), 5.28 (dd, 1H, J = 3.5, 1.2 Hz, H-4′), 5.14 (dd, 1H, J = 10.4, 8.0 Hz, H-2′), 4.85 (dd, 1H, J = 10.4, 3.5 Hz, H-3′), 4.82 (d, 1H, J = 12.1 Hz, CHH O-6Bn), 4.79 (d, 1H, J = 12.3 Hz, CHH O-3Bn), 4.59 (d, 1H, J = 8.0 Hz, H-1′), 4.52 (d, 1H, J = 12.1 Hz, CHH O-6Bn), 4.42 (d, 1H, J = 12.3 Hz, CHH O-3Bn), 4.27 (dd, 1H, J = 10.6, 8.6 Hz, H-3), 4.10 (dd, 1H, J = 10.9, 8.6 Hz, H-4), 4.07 (dd, 1H, J = 10.6, 9.4 Hz, H-2), 4.00 (dd, 1H, J = 11.2, 6.5 Hz, H-6′a), 3.94 (dd, 1H, J = 11.2, 7.2 Hz, H-6′b), 3.80–3.77 (m, 2H, H-6a,6b), 3.65 (ddd, 1H, J = 7.2, 6.5, 1.2 Hz, H-5′), 3.61 (dt, 1H, J = 10.9, 2.4 Hz, H-5), 2.06, 2.03, 2.02, 1.97 (4×s, 4×3H, Me). ^{13}C{^{1}H} NMR (CDCl$_3$, 101 MHz, HSQC, HMBC, HSQC TOCSY): δ 170.5, 170.3, 170.2, 169.3 (4×CO_Ac), from HMBC 167.5, 168.2 (2×CO_Phth), 138.5, 137.8 (2×$C_\text{q(Ph)}$), 134.1 (2CH$_\text{Phth}$), 131.6 (2$C_\text{q(Phth)}$), 128.8 (2CH$_\text{Ph}$), 128.31 (CH_Ph), 128.25, 128.1, 128.0 (3×2CH$_\text{Ph}$), 127.3 (CH_Ph), 123.6 (2CH$_\text{Phth}$), 100.5 (C-1′), 85.9 (C-1), 77.6 (C-4), 77.1 (C-5), 76.5 (C-3), 74.7 (CH$_2$ O-3Bn), 73.9 (CH$_2$ O-

6Bn), 71.1 (C-3′), 70.7 (C-5′), 69.6 (C-2′), 67.2 (C-6), 67.0 (C-4′), 60.8 (C-6′), 55.2 (C-2), 20.9, 20.8, 20.73, 20.70 (4×Me). HRMS-APCI (m/z): $[M - N_2 + H]^+$ calcd for $C_{42}H_{45}N_2O_{15}$, 817.2820; found 817.2814.

## 4-O-(2,3,4,6-Tetra-O-acetyl-β-D-galactopyranosyl)-2-deoxy-2-phthalimido-β-D-glucopyranosyl azide (14)
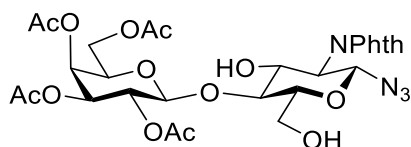
Disaccharide **14** was prepared according to the general procedure for oxidative benzyl deprotection starting from **13** (490 mg, 0.58 mmol) dissolved in EtOAc (15 mL), NaBrO₃ (438 mg, 2.90 mmol) dissolved in H₂O (5 mL) and Na₂S₂O₄ (505 mg, 2.90 mmol) dissolved in H₂O (10 mL). Column chromatography in EtOAc/PE 1:1 afforded **14** (345 mg, 90%) as white amorphous solid, R_f 0.10 (EtOAc/PE 1:1). NMR spectra were in accordance with the lit.[6]

2-Acetamido-2-deoxy-4-O-(β-D-galactopyranosyl)-β-D-glucopyranosyl azide (15)
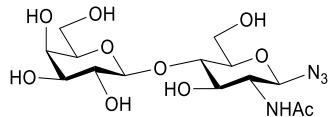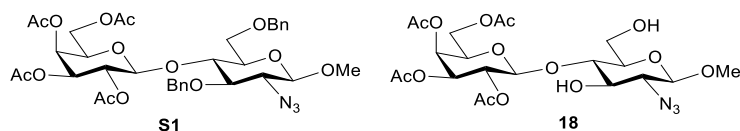

Disaccharide **15** was prepared according to the general procedure for phthalimide to acetamide conversion starting from **14** (330 mg, 0.50 mmol), MeOH (10 mL) and ethylenediamine (1.65 mL, 24.8 mmol) to produce free amine intermediate. Subsequent reaction with acetic anhydride (4.7 mL, 49.7 mmol) in MeOH (10 mL) produced the crude product. Column chromatography in DCM/MeOH 3:1 afforded **15** (170 mg, 84%) as colorless syrup, R_f 0.50 (DCM/MeOH 2:1). $[\alpha]_D^{20}$ +29 (c 0.74, MeOH). ¹H NMR (MeOH-d_4, 400 MHz, H-H COSY): δ 4.53 (d, 1H, J = 9.2 Hz, 1H, H-1), 4.39 (d, 1H, J = 7.4 Hz, H-1′), 3.95 (dd, 1H, J = 12.3, 2.4 Hz, H-6a), 3.88 (dd, 1H, J = 12.3, 4.2 Hz, H-6b), 3.81 (dd, 1H, J = 3.2, 1.0 Hz, H-4′), 3.76 (dd, 1H, J = 11.4, 7.6 Hz, H-6′a), 3.76 (dd, 1H, J = 10.1, 9.2 Hz, H-2), 3.69 (dd, 1H, J = 11.4, 4.6 Hz, H-6′b), 3.66–3.63 (m, 2H, H-3,4), 3.59 (ddd, 1H, J = 7.6, 4.6, 1.0 Hz, H-5′), 3.54 (dd, 1H, J = 9.7, 7.3 Hz, H-2′), 3.54–3.50 (m, 1H, H-5), 3.49 (dd, 1H, J = 9.7, 3.2 Hz, H-3′), 1.99 (s, 3H, Me). ¹³C{¹H} NMR (MeOH-d_4, 101 MHz, HSQC, HMBC, HSQC TOCSY): δ 173.7 (CO), 105.1 (C-1′), 90.2 (C-1), 80.4 (C-4), 78.9 (C-5), 77.2 (C-5′), 74.8 (C-3′), 74.0 (C-3), 72.6 (C-2′), 70.3 (C-4′), 62.5 (C-6′), 61.7 (C-6), 56.1 (C-2), 22.8 (Me). $[M - N_2 + H]^+$ calcd for $C_{14}H_{25}N_2O_{10}$, 381.1509; found 381.1511.

1-(2-Acetamido-2-deoxy-4-*O*-(β-D-galactopyranosyl)-β-D-glucopyranosyl)-4-ferrocenyl-1*H*-1,2,3-triazol (16)
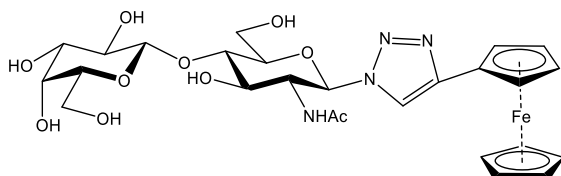
Compound **16** was prepared according to the general procedure for azide-alkyne cycloaddition for unprotected saccharides starting from **15** (108 mg, 0.26 mmol), ethynyl ferrocene (67 mg, 0.32 mmol), $CuSO_4 \cdot 5H_2O$ (12 mg, 0.05 mmol) and ascorbic acid (8 mg, 0.05 mmol). Column chromatography in DCM/MeOH 4:1 afforded **16** as an orange crystalline solid (119 mg, 73%), mp >220 °C (decomp. MeOH), R_f 0.85 (DCM/MeOH 2:1), $[\alpha]_D^{20}$ +2 (*c* 0.87, MeOH). ^{1}H NMR (MeOH-d_4, 400 MHz, H-H COSY): δ 8.19 (s, 1H, C*H*$_{Tria}$), 5.79 (d, 1H, *J* = 9.9 Hz, H-1), 4.75, 4.72 (2×q, 2×1H, *J* = 1.7 Hz, C*H*$_{Cp}$), 4.46 (d, 1H, *J* = 7.6 Hz, H-1′), 4.38 (dd, 1H, *J* = 9.9, 9.7 Hz, H-2), 4.32 (t, 2H, *J* = 1.7 Hz, C*H*$_{Cp}$), 4.07 (s, 5H, C*H*$_{Cp}$), 3.97–3.96 (m, 2H, H-6a,6b), 3.91–3.85 (m, 2H, H-3,4), 3.84 (dd, 1H, *J* = 3.3, 0.9 Hz, H-4′), 3.80 (dd, 1H, *J* = 11.4, 7.6 Hz, H-6′a), 3.78–3.74 (m, 1H, H-5), 3.72 (dd, 1H, *J* = 11.4, 4.8 Hz, H-6′b), 3.63 (ddd, 1H, *J* = 7.6, 4.8, 0.9 Hz, H-5′), 3.59 (dd, 1H, *J* = 9.7, 7.6 Hz, H-2′), 3.52 (dd, 1H, *J* = 9.7, 3.3 Hz, H-3′), 1.81 (s, 3H, *Me*). ^{13}C{^{1}H} NMR (MeOH-d_4, 101 MHz, HSQC, HMBC, HSQC TOCSY): δ 173.2 (*C*O), 148.2 (*C*$_{q(Tria)}$), 119.8 (*C*H$_{Tria}$), 105.1 (C-1′), 88.2 (C-1), 79.9 (C-4), 79.8 (C-5), 77.2 (C-5′), 75.8 (*C*$_{q(Cp)}$), 74.8 (C-3′), 74.2 (C-3), 72.6 (C-2′), 70.7 (5*C*H$_{Cp}$), 70.3 (C-4′), 69.94, 69.92, 67.8, 67.6 (4×*C*H$_{Cp}$), 62.6 (C-6), 61.4 (C-6′), 56.0 (C-2), 22.6 (*Me*). HRMS-ESI (m/z): [M + Na]$^+$ calcd for $C_{26}H_{34}FeN_4O_{10}Na$, 641.1516; found 641.1513.

**Methyl 4-*O*-(2,3,4,6-tetra-*O*-acetyl-β-D-galactopyranosyl)-2-azido-2-deoxy-β-D-glucopyranoside (18)**

Disaccharide **18** was prepared according to the general glycosylation procedure starting from 2,3,4,6-tetra-*O*-acetyl-1-thio-β-D-galactopyranoside[4] (**11**, 430 mg, 0.98 mmol), methyl 2-azido-3,6-di-*O*-benzyl-2-deoxy-β-D-glucopyranosyl[7] (**17**, 325 mg, 0.81 mmol), NIS (366 mg, 1.62 mmol), DCM (6 mL), triflic acid (20 µL) and 3 Å molecular sieves (2 g). Column chromatography in EtOAc/PE 1:2 afforded **S1** (573 mg, 97%) as a colorless gel in about 90% purity, R_f 0.65 (EtOAc/PE 1:1). ^{1}H NMR (CDCl$_3$, 400 MHz, H-H COSY): δ 7.44–7.28 (m, 10H, C*H*$_{Ph}$), 5.26 (dd, 1H, *J* = 3.5, 1.1 Hz, H-4′), 5.11 (dd, 1H, *J* = 10.4, 8.0 Hz, H-2′), 4.97 (d, 1H, *J* = 10.5 Hz, CH*H* O-3Bn), 4.81 (dd, 1H, *J* = 10.4, 3.5 Hz, H-3′),

4.77 (d, 1H, J = 12.1 Hz, CHH O-6Bn), 4.74 (d, 1H, J = 10.5 Hz, CHH O-3Bn), 4.56 (d, 1H, J = 8.0 Hz, H-1′), 4.46 (d, 1H, J = 12.1 Hz, CHH O-6Bn), 4.13–4.10 (m, 1H, H-1), 4.02 (dd, 1H, J = 11.2, 8.0 Hz, H-6′a), 4.02–3.98(m, 1H, H-4), 3.84 (dd, 1H, J = 11.2, 6.0 Hz, H-6′b), 3.76–3.70 (m, 2H, H-6a,6b), 3.58–3.52 (m, 1H, H-5′), 3.55 (s, 3H, MeO), 3.41–3.35 (m, 2H, H-2,3), 3.30 (dt, 1H, J = 10.0, 2.6 Hz, H-5), 2.10, 1.99 (2×s, 2×3H, $Me$$_{Ac}$), 1.97 (2×s, 2×3H, $Me$$_{Ac}$). ^{13}C{^{1}H} NMR (CDCl$_3$, 101 MHz, HSQC, HMBC): δ 170.3 (2×CO), 170.2, 169.3 (2×CO), 138.3, 137.8 (2×$C$$_{q(Ph)}$), 128.8, 128.34 (2×2$CH_{Ph}$), 128.26 ($CH_{Ph}$), 128.2, 128.1 (2×2$CH_{Ph}$), 127.9 ($CH_{Ph}$), 103.0 (C-1), 100.2 (C-1′), 81.1 (C-3), 76.1 (C-4), 75.3 (CH$_2$ O-3Bn), 74.9 (C-5), 73.8 (CH$_2$ O-6Bn), 71.1 (C-3′), 70.6 (C-5′), 69.7 (C-2′), 67.5 (C-6), 66.9 (C-4′), 65.8 (C-2), 60.7 (C-6′), 57.3 (OMe), 20.9, 20.78, 20.75, 20.7 (4×$Me$$_{Ac}$). HRMS-APCI (m/z): [M − N$_2$ + H]$^+$ calcd for C$_{35}$H$_{44}$NO$_{12}$, 702.2756; found 702.2752.

Disaccharide **18** was prepared according to general procedure for oxidative benzyl deprotection starting from **S1** (550 mg, 0.75 mmol) dissolved in EtOAc (25 mL), NaBrO$_3$ (569 mg, 3.77 mmol) dissolved in H$_2$O (10 mL) and Na$_2$S$_2$O$_4$ (595 mg, 3.42 mmol) dissolved in H$_2$O (15 mL). Column chromatography in EtOAc/PE 1:2 followed by recrystallization in EtOAc/PE afforded **18** (270 mg, 65%; 63% over two steps) as a white crystalline solid, mp 149–150 °C (EtOAc/PE), R_f 0.70 (EtOAc) $[\alpha]_D^{20}$ +295 (c 0.65, CHCl$_3$). ^{1}H NMR (CDCl$_3$, 400 MHz, H-H COSY): δ 5.39 (d, 1H, J = 3.4, 1.1 Hz, H-4′), 5.24 (dd, 1H, J = 10.4, 8.0 Hz, H-2′), 5.03 (dd, 1H, J = 10.4, 3.4 Hz, H-3′), 4.64 (d, 1H, J = 8.0 Hz, H-1′), 4.32 (d, 1H, J = 1.4 Hz, OH-3), 4.19 (dd, 1H, J = 11.1, 4.1 Hz, H-6′a), 4.18 (d, 1H, J = 8.3 Hz, H-1), 4.10 (dd, 1H, J = 11.1, 8.5 Hz, H-6′b), 4.05 (ddd, 1H, J = 8.5, 4.1, 1.1 Hz, H-5′), 3.83 (ddd, 1H, J = 12.2, 4.6, 2.2 Hz, H-6a), 3.68–3.61 (m, 2H, H-4,5), 3.63 (ddd, 1H, J = 12.2, 9.5, 3.2 Hz, H-6b), 3.56 (s, 3H, OMe), 3.38–3.25 (m, 2H, H-2,3), 2.17, 2.11, 2.10, 1.98 (4×s, 4×3H, 4×$Me$$_{Ac}$), 1.86 (dd, 1H, J = 9.5, 4.6 Hz, OH-6). ^{13}C{^{1}H} NMR (CDCl$_3$, 101 MHz, HSQC, HMBC): δ 170.7, 170.2, 170.1, 169.6 (4×CO), 102.7 (C-1), 102.2 (C-1′), 81.3 (C-4), 74.3 (C-5), 74.1 (C-3), 71.6 (C-5′), 70.9 (C-3′), 68.9 (C-2′), 67.0 (C-4′), 65.5 (C-2), 62.1 (C-6′), 60.9 (C-6), 57.6 (OMe), 20.80, 20.75, 20.7, 20.6 (4×$Me$$_{Ac}$). HRMS-APCI (m/z): [M − N$_2$ + H]$^+$ calcd for C$_{21}$H$_{32}$NO$_{14}$, 522.1817; found 522.1813.

Methyl 2-deoxy-2-(4-ferrocenyl-1H-1,2,3-triazol-1-yl)-4-O-(β-D-galactopyranosyl)-β-D-glucopyranoside (19)
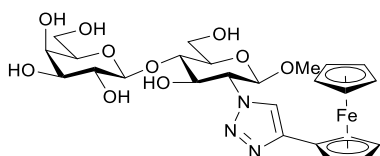
Compound **19** was prepared according to the general procedure for azide-alkyne cycloaddition followed by acetyl deprotection starting from **18** (108 mg, 0.20 mmol), ethynyl ferrocene (50 mg, 0.24 mmol), CuSO$_4$·5H$_2$O (12 mg, 0.05 mmol), ascorbic acid (8 mg, 0.05 mmol) and DMF (4 mL). The ensuing

deacetylation step after aqueous workup was performed using MeOH (10 mL), DCM (10 mL) and 8 drops of 1 M solution of MeONa in MeOH overnight. Column chromatography in DCM/MeOH 6:1 after DOWEX 50W (H$^+$) neutralization afforded **19** as an orange amorphous solid (96 mg, 83%), R_f 0.35 (DCM/MeOH 5:1), $[\alpha]_D^{20}$ +4 (c 1.17, MeOH). ^{1}H NMR (MeOH-d_4, 400 MHz, H-H COSY): δ 8.05 (s, 1H, C*H*$_{Tria}$), 4.92 (d, 1H, J = 8.2 Hz, H-1), 4.75 (t, 2H, J = 1.7 Hz, C*H*$_{Cp}$), 4.44 (d, 1H, J = 7.5 Hz, H-1′), 4.34 (dd, 1H, J = 10.4, 8.2 Hz, H-3), 4.32 (t, 2H, J = 1.7 Hz, C*H*$_{Cp}$), 4.25 (dd, 1H, J = 10.4, 8.2 Hz, H-2), 4.05 (s, 5H, C*H*$_{Cp}$), 4.00 (dd, 1H, J = 12.3, 2.5 Hz, H-6a), 3.96 (dd, 1H, J = 12.3, 4.0 Hz, H-6b), 3.82–3.77 (m, 2H, H-4,4′), 3.75 (dd, 1H, J = 10.7, 7.4 Hz, H-6′a), 3.69–3.65 (m, 2H, H-5,6′b), 3.60 (ddd, 1H, J = 7.4, 4.2, 0.9 Hz, H-5′), 3.57 (dd, 1H, J = 9.7, 7.5 Hz, H-2′), 3.50 (dd, 1H, J = 9.7, 3.3 Hz, H-3′), 3.42 (s, 3H, *Me*). ^{13}C{^{1}H} NMR (MeOH-d_4, 101 MHz, HSQC, HMBC, HSQC TOCSY): δ 147.4 ($C_{q(Tria)}$), 122.8 (*C*H$_{Tria}$), 105.3 (C-1′), 102.8 (C-1), 81.0 (C-4), 77.1 (C-5′), 76.7 (C-5), 76.0 ($C_{q(Cp)}$), 74.9 (C-3′), 74.0 (C-3), 72.6 (C-2′), 70.6 (5*C*H$_{Cp}$), 70.3 (C-4′), 69.8 (2*C*H$_{Cp}$), 67.6 (2*C*H$_{Cp}$, C-2), 62.5 (C-6′), 61.7 (C-6), 57.4 (*Me*). HRMS-ESI (m/z): [M + Na]$^+$ calcd for $C_{25}H_{33}FeN_3O_{10}Na$, 614.1407; found 614.1396.

Methyl 4-*O*-(2,4,6-tri-*O*-acetyl-3-azido-3-deoxy-β-D-galactopyranosyl)-3,6-di-*O*-benzyl-2-deoxy-2-phthalimido-β-D-glucopyranoside (22)
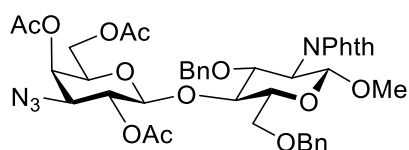
Disaccharide **22** was prepared according to the general glycosylation procedure starting from phenyl 2,4,6-tri-*O*-acetyl-3-azido-3-deoxy-1-thio-β-D-galactopyranoside[8] (**20**, 170 mg, 0.40 mmol), methyl 3,6-di-*O*-benzyl-2-deoxy-2-phthalimido-β-D-glucopyranoside[7] (**21**, 150 mg, 0.30 mmol, NIS (134 mg, 0.60 mmol), DCM (4 mL), triflic acid (10 μL) and 3 Å molecular sieves (2 g). Column chromatography in EtOAc/PE 2:3 afforded **22** (220 mg, 90%) as a colorless gel, R_f 0.65 (EtOAc/PE 1:1). NMR spectra were comparable with those reported in the lit.[6]

Methyl 4-*O*-(2,4,6-tri-*O*-acetyl-3-azido-3-deoxy-β-D-galactopyranosyl)-2-deoxy-2-phthalimido-β-D-glucopyranoside (23)
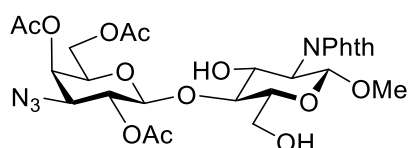
Disaccharide **23** was prepared according to the general procedure for oxidative benzyl deprotection starting from **22** (210 mg, 0.26 mmol) dissolved in EtOAc (12 mL), NaBrO$_3$ (196 mg, 1.30 mmol)

dissolved in H_2O (4 mL) and $Na_2S_2O_4$ (226 mg, 1.30 mmol) dissolved in H_2O (8 mL). Column chromatography in EtOAc/PE 2:1 afforded **23** (145 mg, 89%) as a colorless gel in 95% purity. The impurities were removed in the following step. R_f 0.10 (EtOAc/PE 1:1). ^{1}H NMR (CDCl$_3$, 400 MHz, H-H COSY): δ 7.84, 7.72 (2×dd, 2×2H, J = 5.3, 3.1 Hz, CH_{Ph}), 5.37 (d, 1H, J = 3.4 Hz, H-4′), 5.21 (dd, 1H, J = 10.6, 8.0 Hz, H-2′), 5.19 (d, 1H, J = 8.6 Hz, H-1), 4.64 (d, 1H, J = 8.0 Hz, H-1′), 4.42 (dd, 1H, J = 10.8, 8.4 Hz, H-3), 4.15–4.11 (m, 1H, H-6′a), 4.09 (dd, 1H, J = 10.8, 8.6 Hz, H-2), 3.99–3.94 (m, 2H, H-5′,6′b), 3.91 (dd, 1H, J = 12.2, 2.1 Hz, H-6a), 3.72 (dd, 1H, J = 9.5, 8.4 Hz, H-4), 3.69 (dd, 1H, J = 12.2, 3.1 Hz, H-6b), 3.61 (dd, 1H, J = 10.6, 3.4 Hz, H-3′), 3.56 (ddd, 1H, J = 9.5, 3.1, 2.1 Hz, H-5), 3.44 (s, 3H, OMe), 2.20, 2.15, 1.85 (3×s, 3×3H, Me_{Ac}). ^{13}C{^{1}H} NMR (CDCl$_3$, 101 MHz, HSQC, HMBC, HSQC TOCSY): δ 170.6, 170.0, 169.5 (3×CO_{Ac}), from HMBC 168.1 (2CO_{Phth}), 134.2 (2CH_{Phth}), 131.9 (2$C_{q(Phth)}$), 123.5 (2CH_{Phth}), 102.2 (C-1′), 99.5 (C-1), 82.2 (C-4), 74.2 (C-5), 72.5 (C-5′), 69.8 (C-3,2′), 67.7 (C-4′), 61.9 (C-6′), 61.8 (C-3′), 60.9 (C-6), 57.3 (OMe), 56.0 (C-2), 20.9, 20.7, 20.3 (3×Me_{Ac}). HRMS-APCI (m/z): [M − N_2 + H]$^+$ calcd for $C_{27}H_{33}N_2O_{14}$, 609.1932; found 609.1929.

Methyl 4-*O*-(3-azido-3-deoxy-β-D-galactopyranosyl)-2-acetamido-2-deoxy-β-D-glucopyranoside (24)
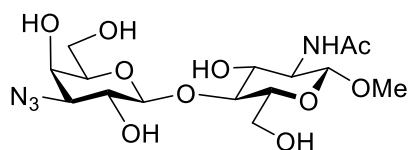
Disaccharide **24** was prepared according to the general procedure for phthalimide to acetamide conversion starting from **23** (300 mg, 0.47 mmol) in MeOH (5 mL) and ethylenediamine (1.5 mL, 22.5 mmol) to produce a free amine intermediate. The subsequent reaction with an excess of acetic anhydride (5 mL, 53 mmol) in MeOH (10 mL) produced the crude product. Column chromatography in DCM/MeOH 6:1 afforded **24** as a white crystalline solid (178 mg, 89%), mp 254–256 °C (MeOH/EtOAc), R_f 0.20 (DCM/MeOH 6:1), $[\alpha]_D^{20}$ +26 (c 0.50, MeOH). ^{1}H NMR (MeOH-d_4, 400 MHz, H-H COSY): δ 4.45 (d, 1H, J = 7.7 Hz, H-1′), 4.32 (d, 1H, J = 8.3 Hz, H-1), 3.93 (dd, 1H, J = 12.2, 2.5 Hz, H-6a), 3.90 (dd, 1H, J = 3.1, 0.9 Hz, H-4′), 3.87 (dd, 1H, J = 12.2, 4.3 Hz, H-6b), 3.73 (dd, 1H, J = 11.5, 7.4 Hz, H-6′a), 3.75–3.61 (m, 6H, H-2,3,4,2′,5′,6′b), 3.46 (s, 3H, OMe), 3.40 (ddd, 1H, J = 9.2, 4.3, 2.5 Hz, H-5), 3.33 (dd, 1H, J = 10.6, 3.1 Hz, H-3′), 1.97 (s, 3H, Me_{Ac}). ^{13}C{^{1}H} NMR (MeOH-d_4, 101 MHz, HSQC, HMBC): δ 173.6 (CO), 105.1 (C-1′), 103.6 (C-1), 80.7 (C-4), 77.8 (C-3), 76.6 (C-5), 74.3 (C-5′), 70.7 (C-2′), 69.4 (C-4′), 66.7 (C-3′), 62.4 (C-6′), 61.8 (C-6), 57.0 (OMe), 56.6 (C-2), 22.9 (Me_{Ac}). HRMS-APCI (m/z): [M − N_2 + H]$^+$ calcd for $C_{15}H_{27}N_2O_{10}$, 395.1660; found 395.1656.

Methyl 4-*O*-{3-deoxy-3-(4-ferrocenyl-1*H*-1,2,3-triazol-1-yl)-β-D-galactopyranosyl}-2-acetamido-2-deoxy-β-D-glucopyranoside (25)
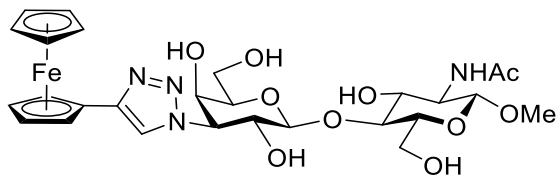
Compound **25** was prepared according to the general procedure for azide-alkyne cycloaddition for unprotected saccharides starting from **24** (165 mg, 0.39 mmol), ethynyl ferrocene (95 mg, 0.45 mmol), $CuSO_4 \cdot 5H_2O$ (12 mg, 0.05 mmol) and ascorbic acid (8 mg, 0.05 mmol). Column chromatography in DCM/MeOH 4:1 afforded **25** as an orange amorphous solid (206 mg, 83%), R_f 0.60 (DCM/MeOH 3:1), $[\alpha]_D^{20}$ +157 (*c* 0.63, MeOH). ^{1}H NMR (MeOH-d_4, 400 MHz, H-H COSY): δ 8.06 (s, 1H, C*H*$_{\text{Tria}}$), 4.81 (dd, 1H, *J* = 11.1, 3.0 Hz, H-3′), 4.74 (t, 2H, *J* = 1.9 Hz, C*H*$_{\text{Cp}}$), 4.67 (d, 1H, *J* = 7.6 Hz, H-1′), 4.36 (d, 1H, *J* = 8.1 Hz, H-1), 4.32 (t, 2H, *J* = 1.9 Hz, C*H*$_{\text{Cp}}$), 4.21 (dd, 1H, *J* = 11.1, 7.6 Hz, H-2′), 4.08–4.06 (m, 1H, H-4′), 4.07 (s, 5H, C*H*$_{\text{Cp}}$), 3.95 (dd, 1H, *J* = 12.2, 2.5 Hz, H-6a), 3.90 (dd, 1H, *J* = 12.2, 4.1 Hz, H-6b), 3.89–3.86 (m, 1H, H-5′), 3.82–3.65 (m, 5H, H-2,3,4,6′a,6′b), 3.47 (s, 3H, O*Me*), 3.44 (ddd, 1H, *J* = 9.4, 4.1, 2.5 Hz, H-5), 1.98 (s, 3H, *Me*$_{\text{Ac}}$). ^{13}C{^{1}H} NMR (MeOH-d_4, 101 MHz, HSQC, HMBC, HSQC TOCSY): δ 173.6 (*C*O), from HMBC 147.4 (*C*$_{\text{q(Tria)}}$), 121.3 (*C*H$_{\text{Tria}}$), 105.4 (C-1′), 103.6 (C-1), 80.8 (C-4), 77.9 (C-5′), 76.6 (C-5), from HMBC 76.3 (*C*$_{\text{q(Cp)}}$), 74.4 (C-3), 70.9 (br s, 5*C*H$_{\text{Cp}}$), 70.0 (br s, 2*C*H$_{\text{Cp}}$), 69.6 (C-4′), 69.2 (C-2′), 67.9 (br s, 2*C*H$_{\text{Cp}}$), 67.4 (C-3′), 62.3 (C-6′), 61.8 (C-6), 57.1 (O*Me*), 56.7 (C-2), 22.9 (*Me*$_{\text{Ac}}$). HRMS-ESI (m/z): $[M + Na]^+$ calcd for $C_{27}H_{36}FeN_4O_{10}Na$, 655.1673; found 655.1674.

Methyl 4-*O*-{3-deoxy-3-(4-phenyl-1*H*-1,2,3-triazol-1-yl)-β-D-galactopyranosyl}-2-acetamido-2-deoxy-β-D-glucopyranoside (26)
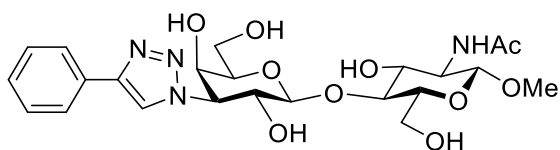
Compound **26** was prepared according to the general procedure for azide-alkyne cycloaddition for unprotected saccharides starting from **24** (150 mg, 0.36 mmol), phenyl acetylene (47 μL, 0.43 mmol), $CuSO_4 \cdot 5H_2O$ (12 mg, 0.05 mmol) and ascorbic acid (8 mg, 0.05 mmol). Column chromatography in DCM/MeOH 4:1 afforded **26** as an white amorphous solid (148 mg, 79%), R_f 0.20 (DCM/MeOH 5:1), $[\alpha]_D^{20}$ +115 (*c* 0.26, MeOH). ^{1}H NMR (MeOH-d_4, 400 MHz, H-H COSY): δ 8.39 (s, 1H, C*H*$_{\text{Tria}}$), 7.85–7.82, 7.46–7.42 (2×m, 2×2H, C*H*$_{\text{Ph}}$), 7.36–7.32 (m, 1H, C*H*$_{\text{Ph}}$), overlapped with MeO*H*-d_4 4.85 (dd, 1H, *J* = 11.1, 3.0 Hz, H-3′), 4.68 (d, 1H, *J* = 7.6 Hz, H-1′), 4.36 (d, 1H, *J* = 8.2 Hz, H-1), 4.25 (dd, 1H, *J* = 11.1, 7.6 Hz, H-2′), 4.08 (dd, 1H, *J* = 3.0, 0.9 Hz, H-4′), 3.95 (dd, 1H, *J* = 12.2, 2.5 Hz, H-6′a), 3.92–

3.88 (m, 2H, H-3,6′b), 3.82–3.64 (m, 5H, H-2,4,6a,6b,5′), 3.47 (s, 3H, O*Me*), 3.43(ddd, 1H, J = 9.3, 4.1, 2.5 Hz, H-5), 1.97 (s, 3H, *Me*$_{Ac}$). ^{13}C{^{1}H} NMR (MeOH-d_4, 101 MHz, HSQC, HMBC, HSQC TOCSY): δ 173.6 (*C*O), 148.4 (*C*$_{q(Tria)}$), 131.9 (*C*$_{q(Ph)}$), 130.0 (2*C*H$_{Ph}$), 129.3 (*C*H$_{Ph}$), 126.7 (2*C*H$_{Ph}$), 121.9 (*C*H$_{Tria}$), 105.4 (C-1′), 103.6 (C-1), 80.8 (C-4), 77.9 (C-3), 76.6 (C-5), 74.4 (C-5′), 69.6 (C-4′), 69.3 (C-2′), 67.6 (C-3′), 62.3 (C-6), 61.8 (C-6′), 57.1 (O*Me*), 56.7 (C-2), 22.9 (*Me*$_{Ac}$). HRMS-APCI (m/z): [M + H]$^+$ calcd for C$_{23}$H$_{33}$N$_4$O$_{10}$, 525.2191; found 525.2186.

(η^5-Pentamethylcyclopentadienyl)[η^5-1-(methyl *N*-acetyl-3′-deoxy-β-D-lactosaminide-3′-yl)-1H-1,2,3-triazol-4-yl-benzene]ruthenium chloride (27)
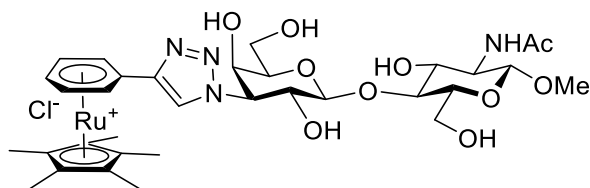
Compound **27** was prepared according to the general procedure for the preparation of ruthenium arenes starting from **26** (60 mg, 0.11 mmol), chloro(pentamethylcyclopentadienyl)ruthenium(II) tetramer (38 mg, 0.03 mmol), anhydrous CH$_3$CN (2 mL) and degassed water (10 mL). Column chromatography in DCM/MeOH 3:1 on neutral aluminum oxide afforded **27** as a brown amorphous solid (75 mg, 82%), $[\alpha]_D^{20}$ −88 (*c* 1.00, MeOH). ^{1}H NMR (MeOH-d_4, 400 MHz, H-H COSY): δ 8.72 (s, 1H, C*H*$_{Tria}$), 6.59 (d, 2H, J = 6.1 Hz, C*H*$_{Ph}$), 6.07 (dd, 2H, J = 6.1, 5.7 Hz, C*H*$_{Ph}$), 5.98 (t, 1H, J = 5.7 Hz, C*H*$_{Ph}$), 4.94 (dd, 1H, J = 11.2, 3.1 Hz, H-3′), 4.71 (d, 1H, J = 7.5 Hz, H-1′), 4.39 (d, 1H, J = 8.2 Hz, H-1), 4.28 (dd, 1H, J = 11.2, 7.5 Hz, H-2′), 4.10 (dd, 1H, J = 3.1, 0.9 Hz, H-4′), 3.96–3.91 (m, 3H, H-3,6a,6b), 3.83–3.65 (m, 5H, H-2,4,5′,6′a, 6′b), 3.50–3.46 (m, 1H, H-5), 3.48 (s, 3H, O*Me*), 2.00 (s, 3H, *Me*$_{Ac}$), 1.83 (s, 15H, *Me*$_{Cp^*}$). ^{13}C{^{1}H} NMR (MeOH-d_4, 101 MHz, HSQC, HMBC, HSQC TOCSY): δ 173.8 (*C*O), 141.8 (*C*$_{q(Tria)}$), 124.7 (*C*H$_{Tria}$), 105.3 (C-1′), 103.6 (C-1), 98.2 (*C*$_{q(Cp^*)}$), 93.5 (*C*$_{q(Ph)}$), 88.62, 88.59, 88.5, 85.1, 85.0 (5×*C*H$_{Ph}$), 80.5 (C-4), 77.9 (C-3), 76.5 (C-5), 74.5 (C-5′), 69.7 (C-4′), 69.1 (C-2′), 67.6 (C-3′), 62.3 (C-6), 61.6 (C-6′), 57.2 (O*Me*), 56.6 (C-2), 23.0 (*Me*$_{Ac}$), 10.3 (*Me*$_{Cp^*}$). HRMS-APCI (m/z): [M − Cl]$^+$ calcd for C$_{33}$H$_{46}$N$_4$O$_{10}$Ru, 761.2339; found 761.2337.

Methyl 4-*O*-{3-deoxy-3-[4-(3-fluorophenyl)-1*H*-1,2,3-triazol-1-yl]-β-D-galactopyranosyl}-2-acetamido-2-deoxy-β-D-glucopyranoside (28)
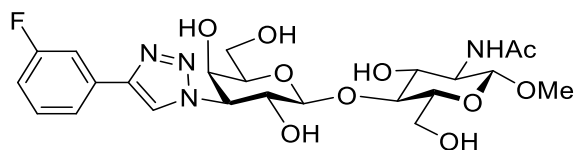
3-Fluorophenyl acetylene (37 μL, 0.32 mmol), CuI (10 mg, 0.05 mmol) and Et$_3$N (30 μL, 0.22 mmol) were subsequently added into a solution of **24** (45 mg, 0.11 mmol) in DMF and the reaction mixture was stirred at 40 °C for 2 hours, filtered through celite and concentrated. Column chromatography in DCM/MeOH 3:1 afforded **28** (51 mg, 88%) as a white amorphous solid, R_f 0.40 (DCM/MeOH 3:1), $[\alpha]_D^{20}$ +1 (*c* 0.22, MeOH/H$_2$O 1:1). ^{1}H NMR (MeOH-*d$_4$*, 400 MHz, H−H COSY): δ 8.45 (s, 1H, C*H*$_{Tria}$), 7.66 (ddd, 1H, *J* = 7.9, 1.5, 1.0 Hz, C*H*$_{Ph}$), 7.60 (ddd, 1H, *J* = 10.2, 2.6, 1.5 Hz, C*H*$_{Ph}$), 7.45 (ddd, 1H, *J* = 8.3, 7.9, 5.9 Hz, C*H*$_{Ph}$), 7.07 (dddd, 1H, *J* = 8.3, 7.1, 2.6, 1.0 Hz, C*H*$_{Ph}$), 4.86 (dd, 1H, *J* = 11.1, 3.1 Hz, H-3′), 4.68 (d, 1H, *J* = 7.6 Hz, H-1′), 4.35 (d, 1H, *J* = 8.1 Hz, H-1), 4.25 (dd, 1H, *J* = 11.1, 7.6 Hz, H-2′), 4.08 (dd, 1H, *J* = 3.1, 0.9 Hz, H-4′), 3.95 (dd, 1H, *J* = 12.2, 2.6 Hz, H-6a), 3.90 (dd, 1H, *J* = 12.2, 4.1 Hz, H-6b), 3.88 (ddd, 1H, *J* = 7.2, 5.1, 0.9 Hz, H-5′), 3.80 (dd, 1H, *J* = 11.4, 7.2 Hz, H-6′a), 3.76 (dd, 1H, *J* = 10.4, 8.1 Hz, H-2), 3.73 (dd, 1H, *J* = 9.4, 8.6 Hz, H-4), 3.72 (dd, 1H, *J* = 11.4, 5.1 Hz, H-6′b), 3.67 (dd, 1H, *J* = 10.4, 8.6 Hz, H-3), 3.47 (s, 3H, O*Me*), 3.43 (ddd, 1H, *J* = 9.4, 4.1, 2.6 Hz, H-5), 1.98 (s, 3H, *Me*$_{Ac}$). ^{13}C{^{1}H} NMR (MeOH-*d$_4$*, 101 MHz, HSQC, HMBC, HSQCTOCSY): δ 173.6 (*C*O), 164.7 (d, $^1J_{(C-F)}$ = 244.3 Hz, *C*F), 147.2 (d, $^4J_{(C-F)}$ = 2.8 Hz, *C*$_{q(Tria)}$), 134.3 (d, $^3J_{(C-F)}$ = 8.5 Hz, *C*$_{q(Ph)}$), 131.9 (d, $^3J_{(C-F)}$ = 8.4 Hz, *C*H_{Ph}), 122.44 (*C*H_{Tria}), 122.44 (d, $^4J_{(C-F)}$ = 2.8 Hz, *C*H_{Ph}), 115.8 (d, $^2J_{(C-F)}$ = 21.4 Hz, *C*H_{Ph}), 113.2 (d, $^2J_{(C-F)}$ = 23.3 Hz, *C*H_{Ph}), 105.4 (C-1′), 103.6 (C-1), 80.8 (C-4), 77.9 (C-5′), 76.6 (C-5), 74.4 (C-3), 69.5 (C-4′), 69.2 (C-2′), 67.7 (C-3′), 62.3 (C-6), 61.8 (C-6′), 57.1 (O*Me*), 56.7 (C-2), 22.9 (*Me*$_{Ac}$). ^{19}F NMR (MeOH-*d$_4$*, 376 MHz, ^{19}F{^{1}H}): δ −116.12 (ddd, $^3J_{(H-F)}$ = 10.2, 7.1 Hz, $^4J_{(H-F)}$ = 5.9 Hz). HRMS-APCI (m/z): [M + H]$^+$ calcd for C$_{23}$H$_{32}$FN$_4$O$_{10}$, 543.2097; found 543.2103.

Methyl 4-*O*-{3-deoxy-3-(4-hydroxymethyl-1*H*-1,2,3-triazol-1-yl)-β-D-galactopyranosyl}-2-acetamido-2-deoxy-β-D-glucopyranoside (29)
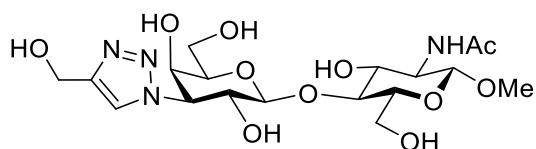
Compound **29** was prepared according to the general procedure for azide-alkyne cycloaddition for unprotected saccharides starting from **24** (50 mg, 0.12 mmol), propargyl alcohol (10 μL, 0.17 mmol), CuSO$_4$·5H$_2$O (12 mg, 0.05 mmol) and ascorbic acid (8 mg, 0.05 mmol). Column chromatography in DCM/MeOH 2:1 afforded **29** as a white foam (48 mg, 85 %), R_f 0.15 (DCM/MeOH 2:1), $[\alpha]_D^{20}$ +121 (*c*
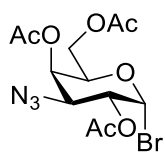
0.41, MeOH) ^{1}H NMR (MeOH-d_4, 400 MHz, H-H COSY): δ 8.01 (s, 1H, CH_{Tria}), 4.80 (dd, 1H, J = 11.1, 3.0 Hz, H-3′), 4.70 (br s, 2H, CH_2OH), 4.64 (d, 1H, J = 7.6 Hz, H-1′), 4.34 (d, 1H, J = 8.1 Hz, H-1), 4.16 (dd, 1H, J = 11.1, 7.6 Hz, H-2′), 4.03 (d, 1H, J = 3.0 Hz, H-4′), 3.93 (dd, 1H, J = 12.1, 2.5 Hz, H-6′a), 3.88 (dd, 1H, J = 12.1, 4.2 Hz, H-6′b), 3.84 (dd, 1H, J = 4.2, 2.5 Hz, H-5′), 3.81–3.67 (m, 4H, H-2,4,6a,6b), 3.65 (dd, 1H, J = 10.1, 8.2 Hz, H-3), 3.47 (s, 3H, OMe), 3.42 (ddd, 1H, J = 9.4, 4.3, 2.5 Hz, H-5), 1.98 (s, 3H, Me_{Ac}). ^{13}C{^{1}H} NMR (MeOH-d_4, 101 MHz, HSQC, HMBC): δ 173.6 (CO), not detected ($C_{\text{q(Tria)}}$, CH$_{\text{Tria}}$), 105.3 (C-1′), 103.6 (C-1), 80.7 (C-4), 77.9 (C-5′), 76.6 (C-5), 74.3 (C-3), 69.5 (C-4′), 69.3 (C-2′), 67.6 (C-3′), 62.3 (C-6), 61.8 (C-6′), 57.1 (OMe), 56.6 (CH_2OH), from HSQC 53.3 (C-2), 22.9 (Me_{Ac}). HRMS-APCI (m/z): [M + H]$^+$ calcd for $C_{18}H_{31}N_4O_{11}$ 479.1983; found 479.1983.

Methyl 4-*O*-{3-deoxy-3-(4-ferrocenyl-1*H*-1,2,3-triazol-1-yl)-β-D-galactopyranosyl}-2-deoxy-2-phthalimido-β-D-glucopyranoside (30)
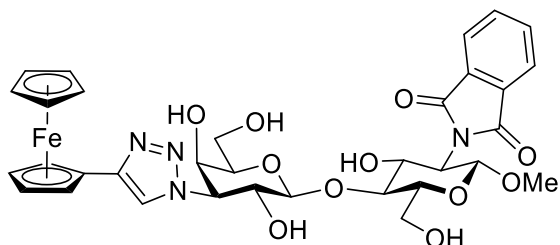
Compound **30** was prepared according to the general procedure for azide-alkyne cycloaddition followed by acetyl deprotection starting from **23** (100 mg, 0.16 mmol), ethynyl ferrocene (40 mg, 0.19 mmol), CuSO$_4$·5H$_2$O (12 mg, 0.05 mmol), ascorbic acid (8 mg, 0.05 mmol) and DMF (4 mL). The deacetylation step following aqueous workup was performed with MeOH (10 mL), DCM (10 mL) and 8 drops of 1 M solution of MeONa in MeOH overnight. Column chromatography in DCM/MeOH 8:1 after DOWEX 50W (H$^+$) neutralization afforded **30** as an orange crystalline solid (78 mg, 69 %), mp 215–219 °C (MeOH/EtOAc), R_f 0.40 (DCM/MeOH 8:1), $[\alpha]_D^{20}$ −17 (*c* 2.24, MeOH/DCM 1:1). ^{1}H NMR (MeOH-d_4, 400 MHz, H-H COSY): δ 8.04 (s, 1H, CH_{Tria}), 7.90–7.83 (m, 4H, CH_{Ph}), 5.13 (d, 1H, J = 8.5 Hz, H-1), 4.80 (dd, 1H, J = 11.2, 3.1 Hz, H-3′), 4.75 (br s, 2H, CH_{Cp}), 4.69 (d, 1H, J = 7.5 Hz, H-1′), 4.44 (dd, 1H, J = 10.9, 8.6 Hz, H-3), 4.33 (br s, 2H, CH_{Cp}), 4.21 (dd, 1H, J = 11.2, 7.5 Hz, H-2′), 4.08 (br s, 5H, CH_{Cp}), 4.06–4.04 (m, 2H, H-2,4′), 3.99–3.97 (m, 2H, H-6a,6b), 3.88–3.75 (m, 3H, H-4,5′,6′a), 3.68 (dd, 1H, J = 11.5, 4.4 Hz, H-6′b), 3.59 (dt, 1H, J = 9.0, 3.2 Hz, H-5), 3.44 (s, 3H, OMe). ^{13}C{^{1}H} NMR (MeOH-d_4, 101 MHz, HSQC, HMBC, HSQC TOCSY): δ not detected (2CO), 147.4 ($C_{\text{q(Tria)}}$), 135.6 (2CH$_{\text{Ph}}$), 133.0 (2$C_{\text{q(Ph)}}$), 124.2 (2CH$_{\text{Ph}}$), 121.2 (CH_{Tria}), 105.4 (C-1′), 100.7 (C-1), 81.1 (C-4), 78.0 (C-5′), from HMBC 76.4 ($C_{\text{q(Cp)}}$), 76.9 (C-5), 71.1 (C-3), 70.6 (5CH$_{\text{Cp}}$), 69.8 (2CH$_{\text{Cp}}$), 69.7 (C-4′), 69.3 (C-2′), 67.7 (2CH$_{\text{Cp}}$), 67.4 (C-3′), 62.4 (C-6′), 61.7 (C-6), 57.8 (C-2), 57.1 (OMe). HRMS-ESI (m/z): [M + Na]$^+$ calcd for $C_{33}H_{36}FeN_4O_{11}$Na, 743.1622; found 743.1620.

2,4,6-Tri-*O*-acetyl-3-azido-3-deoxy-α-D-galactopyranosyl bromide (31)


A solution of 1,2,4,6-tetra-*O*-acetyl-3-azido-3deoxy-D-galactopyranose[9] (500 mg; 1.34 mmol) in dry CH_2Cl_2 (4 mL) was added drowise under vigorous stirring to titanium tetrabromide (295 mg, 0.80 mmol) solution in dry CH_2Cl_2 (8 mL) with a catalytic amount of glacial acetic acid (800 µL, 13.9 µmol). The reaction mixture was left for 1.5 h under microwave irradiation at 55 °C. After complete consumption of the starting material, the reaction mixture was diluted with dry CH_2Cl_2 (100 mL) and washed with saturated $NaHCO_3$ solution (2 × 50 mL), and H_2O (50 mL). The organic phase was separated, dried over anhydrous $MgSO_4$, filtered, and concentrated under vacuum. The residue was purified by flash chromatography on silica (cyclohexane/EtOAc 4:1) to yield product **31** (402 mg; 76%) as a colorless oil. The NMR data were in accordance with lit.[10]

2,3,4,6-Tetra-*O*-acetyl-β-D-galactopyranosyl 2,4,6-tri-*O*-acetyl-3-azido-3-deoxy-1-thio-β-D-galactopyranoside (33)
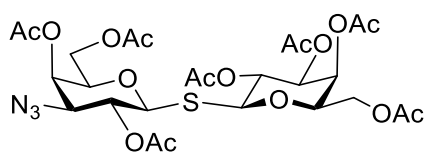
Triisopropylsilyl 2,3,4,6-tetra-*O*-acetyl-1-thio-β-D-galactopyranoside[11] (**32**, 130 mg, 0.25 mmol) and 2,4,6-tri-*O*-acetyl-3-azido-α-D-galactopyranosyl bromide (**31**, 100 mg, 0.25 mmol) were dissolved in anhydrous CH_3CN under argon atmosphere, tetra-n-butylammonium fluoride trihydrate (109 mg, 0.35 mmol) was added and the reaction mixture was stirred for 15 min until TLC indicated absence of either of the starting material and presence of a more polar product. The solvent was evaporated and the crude product was purified on column chromatography affording **33** as a white crystalline solid (151 mg, 89%), mp 165–167 °C (EtOAc/PE), R_f 0.25 (EtOAc/PE 1:1). The NMR spectra were in accordance with the lit.[12]

β-D-Galactopyranosyl 3-deoxy-3-(4-ferrocenyl-1*H*-1,2,3-triazol-1-yl)-1-thio-β-D-galactopyranoside (34)
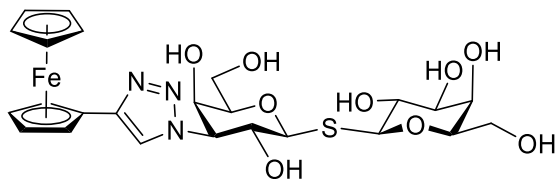
Compound **34** was prepared according to the general procedure for azide-alkyne cycloaddition followed by acetyl deprotection starting from **33** (130 mg, 0.19 mmol), ethynyl ferrocene (52 mg, 0.25 mmol), CuSO$_4$·5H$_2$O (12 mg, 0.05 mmol), ascorbic acid (8 mg, 0.05 mmol) and DMF (4 mL). The deacetylation step after aqueous workup was performed with MeOH (10 mL), DCM (10 mL) and 8 drops of 1 M solution of MeONa in MeOH overnight. Column chromatography in DCM/MeOH 4:1 after DOWEX 50W (H$^+$) neutralization afforded **34** as an orange crystalline solid (92 mg, 81%), mp 158–161 °C (MeOH/EtOAc)., R_f 0.45 (DCM/MeOH 3:1), $[\alpha]_D^{20}$ +3 (*c* 0.62, MeOH/DCM 1:1). ^{1}H NMR (MeOH-d_4, 400 MHz, H-H COSY): δ 8.10 (s, 1H, C*H*$_{Tria}$), 4.88 (d, 1H, *J* = 9.6 Hz, H-1′), 4.80 (dd, 1H, *J* = 10.7, 3.0 Hz, H-3′), 4.75, 4.74 (2×q, 2×1H, *J* = 1.9 Hz, C*H*$_{Cp}$), 4.68 (d, 1H, *J* = 9.8 Hz, H-1), 4.41 (dd, 1H, *J* = 10.7, 9.6 Hz, H-2′), 4.32 (t, 2H, *J* = 1.9 Hz, C*H*$_{Cp}$), 4.12 (dd, 1H, *J* = 3.0, 0.6 Hz, H-4′), 4.07 (s, 5H, C*H*$_{Cp}$), 3.90 (dd, 1H, *J* = 3.4, 1.1 Hz, H-4), 3.84–3.78 (m, 3H, H-6a,5′,6′a), 3.78 (dd, 1H, *J* = 9.8, 9.3 Hz, H-2), 3.72–3.68 (m, 2H, H-6b,6′b), 3.61 (ddd, 1H, *J* = 7.4, 4.4, 1.1 Hz, H-5), 3.52 (dd, 1H, *J* = 9.3, 3.4 Hz, H-3). ^{13}C{^{1}H} NMR (MeOH-d_4, 101 MHz, HSQC, HMBC, HSQC TOCSY): δ 147.3 (*C*$_{q(Tria)}$), 121.2 (*C*H_{Tria}), 86.5 (C-1′), 85.4 (C-1), 81.4 (C-5′), 81.1 (C-5), 76.4 (*C*$_{q(Cp)}$), 76.3 (C-3), 71.7 (C-2), 70.7 (C-4), 70.6 (5*C*H_{Cp}), 69.9 (C-4′), 69.7 (2*C*H_{Cp}), 68.8 (C-3′), 68.5 (C-2′), 67.63, 67.62 (2×*C*H_{Cp}), 63.0 (C-6), 62.7 (C-6′). HRMS-ESI (m/z): [M + Na]$^+$ calcd for C$_{24}$H$_{31}$FeN$_3$O$_9$SNa, 616.1022; found 616.1026.

3-Deoxy-3-(4-ferrocenyl-1*H*-1,2,3-triazol-1-yl)-β-D-galactopyranosyl 3-deoxy-3-(4-ferrocenyl-1*H*-1,2,3-triazol-1-yl)-1-thio-β-D-galactopyranoside (36)
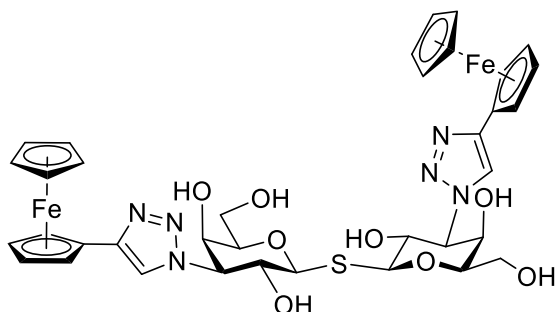
Compound **36** was prepared according to the slightly modified general procedure for azide-alkyne cycloaddition followed by acetyl deprotection starting from 2,4,6-tri-*O*-acetyl-3-azido-3-deoxy-β-D-galactopyranosyl 2,4,6-tri-*O*-acetyl-3-azido-3-deoxy-1-thio-β-D-galactopyranoside[13] (**35**, 130 mg, 0.20 mmol), ethynyl ferrocene (100 mg, 0.48 mmol), CuSO$_4$·5H$_2$O (12 mg, 0.05 mmol), ascorbic acid (8 mg,

0.05 mmol) and DMF (6 mL). The crude intermediate precipitated from the reaction mixture. The obtained orange crystals were filtered, washed with water and suspended in MeOH/DCM 1:1 (120 mL). 30 drops of 1 M solution of MeONa in MeOH were added and the reaction was stirred for 72 h. Column chromatography in DCM/MeOH 8:1 after DOWEX 50W (H$^+$) neutralization afforded **36** as an orange amorphous solid (137 mg, 84%), R_f 0.40 (DCM/MeOH 8:1), $[\alpha]_D^{20}$ −89 (c 0.24, MeOH). ^{1}H NMR (MeOH-d_4, 400 MHz, H-H COSY): δ 8.22 (s, 2H, CH_{Tria}), overlapped with MeOH-d_4 4.92–4.82 (m, 6H, H-1, H-2, H-3), 4.76, 4.71 (2×dt, 2×2H, J = 2.5, 1.3 Hz, CH_{Cp}), 4.29, 4.30 (2×dd, 2×2H, J = 2.5, 1.3 Hz, CH_{Cp}), 4.17 (d, 2H, J = 2.6 Hz, H-4), 4.06 (s, 10H, CH_{Cp}), 3.92–3.87 (m, 4H, H-5,6), 3.75 (dd, 2H, J = 14.7, 7.2 Hz, H-6′). ^{13}C{^{1}H} NMR (MeOH-d_4, 101 MHz, HSQC, HMBC): δ 147.4 ($C_{\text{q(Tria)}}$), 121.3 (CH_{Tria}), 87.1 (C-1), 81.6 (C-5), 76.4 ($C_{\text{q(Cp)}}$), 70.6 (5CH_{Cp}), 69.8 (C-4), 69.74, 69.71 (2×CH_{Cp}), 68.5 (C-2), 68.4 (C-3), 67.6, 67.5 (2×CH_{Cp}), 63.1 (C-6). HRMS-ESI (m/z): [M + Na]$^+$ calcd for C$_{36}$H$_{40}$Fe$_2$N$_6$O$_8$SNa, 851.1220; found 851.1210.

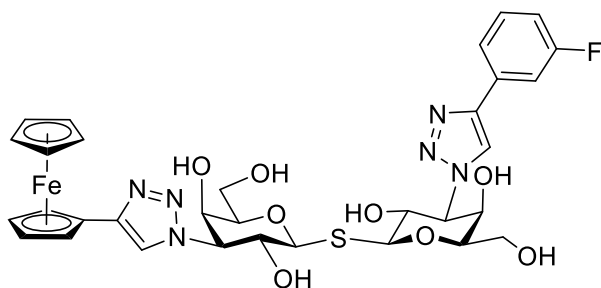**3-deoxy-3-(4-phenyl-1H-1,2,3-triazol-1-yl)-β-D-galactopyranosyl 3-deoxy-3-(4-phenyl-1H-1,2,3-triazol-1-yl)-1-thio-β-D-galactopyranoside (37)**
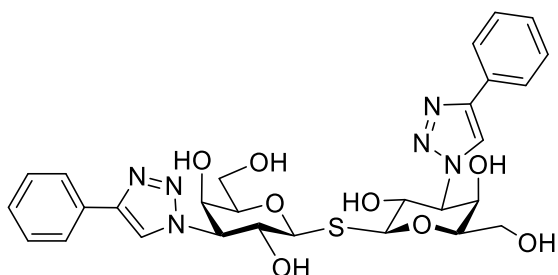
Compound **37** was prepared according to the general procedure for azide-alkyne cycloaddition followed by acetyl deprotection starting from 2,4,6-tri-O-acetyl-3-azido-3-deoxy-β-D-galactopyranosyl 2,4,6-tri-O-acetyl-3-azido-3-deoxy-1-thio-β-D-galactopyranoside[13] (**35**, 230 mg, 0.35 mmol), phenyl acetylene (92 μL, 0.84 mmol), CuSO$_4$·5H$_2$O (12 mg, 0.05 mmol), ascorbic acid (8 mg, 0.05 mmol) and DMF (8 mL). The deacetylation step was performed in MeOH (40 mL), DCM (40 mL) and 12 drops of 1M solution of MeONa in about 72 h. Column chromatography in DCM/MeOH 6:1 after DOWEX 50W (H$^+$) neutralization afforded **37** as a white solid (182 mg, 85%), R_f 0.15 (DCM/MeOH 7:1). The NMR spectra were in accordance with the lit.[14]

3-Deoxy-3-(4-phenyl-1*H*-1,2,3-triazol-1-yl)-β-D-galactopyranosyl 3-deoxy-3-(4-phenyl-1*H*-1,2,3-triazol-1-yl)-1-thio-β-D-galactopyranoside (38)
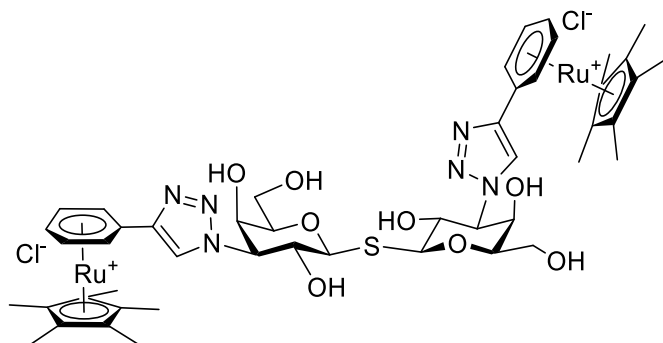
Compound **38** was prepared according to the general procedure for the preparation of ruthenium arenes starting from **37** (52 mg, 0.08 mmol), chloro(pentamethylcyclopentadienyl)ruthenium(II) tetramer (51 mg, 0.05 mmol), anhydrous CH$_3$CN (4 mL) and degassed water (15 mL). Column chromatography in DCM/MeOH 12:1 on neutral aluminum oxide afforded **38** as a brown amorphous solid (61 mg, 62%). ^{1}H NMR (MeOH-d_4, 400 MHz, H-H COSY): δ 8.70 (2×s, 4×2H, C*H*$_{Tria}$), 6.64, 6.58 (2×d, 2×4H, J = 6.1 Hz, C*H*$_{Ph}$), 6.55, 6.48 (2×d, 2×4H, J = 6.0 Hz, C*H*$_{Ph}$), 6.12–5.95 (m, 4×6H, C*H*$_{Ph}$), 4.99 (dd, 4×2H, J = 10.5, 3.2 Hz, H-3), 4.99 (d, 4×2H, J = 9.5 Hz, H-1), 4.63 (d, 4×2H, J = 10.5, 9.5 Hz, H-2), 4.20 (d, 4×2H, J = 3.2 Hz, H-4), 3.92 (dd, 4×2H, J = 7.0, 4.9 Hz, H-5), 3.84 (dd, 4×2H, J = 11.5, 7.0 Hz, H-6), 3.75 (dd, 4×2H, J = 11.5, 4.9 Hz, H-6′), 1.86 (2×s, 2×30H, *Me*), 1.84, 1.83 (2×s, 2×30H, *Me*). ^{13}C{^{1}H} NMR (MeOH-d_4, 101 MHz, HSQC, HMBC): δ 141.8, 141.7 (2×2*C*$_{q(Tria)}$), 124.5, 124.4 (2×2*C*H_{Tria}), 99.3, 98.6, 98.4, 98.3 (4×*C*$_{q(Cp*)}$), 94.0, 93.5 (2×2*C*$_{q(Ph)}$), 88.61, 88.60, 88.58, 88.5 (4×6*C*H_{Ph}), 86.5 (4×C-1), 85.2, 85.1, 85.05, 84.98 (4×4*C*H_{Ph}), 81.3 (4×C-5), 69.8 (4×C-4), 68.9 (4×C-3), 68.5 (4×C-2), 62.7 (4×C-6), 10.3, 10.2, 10.1, 10.0 (4×*Me*$_{Cp*}$). HRMS-APCI (m/z): [M − 2 Cl]$^{2+}$ calcd for C$_{48}$H$_{62}$N$_6$O$_8$Ru$_2$S, 543.1225; found 543.1225.
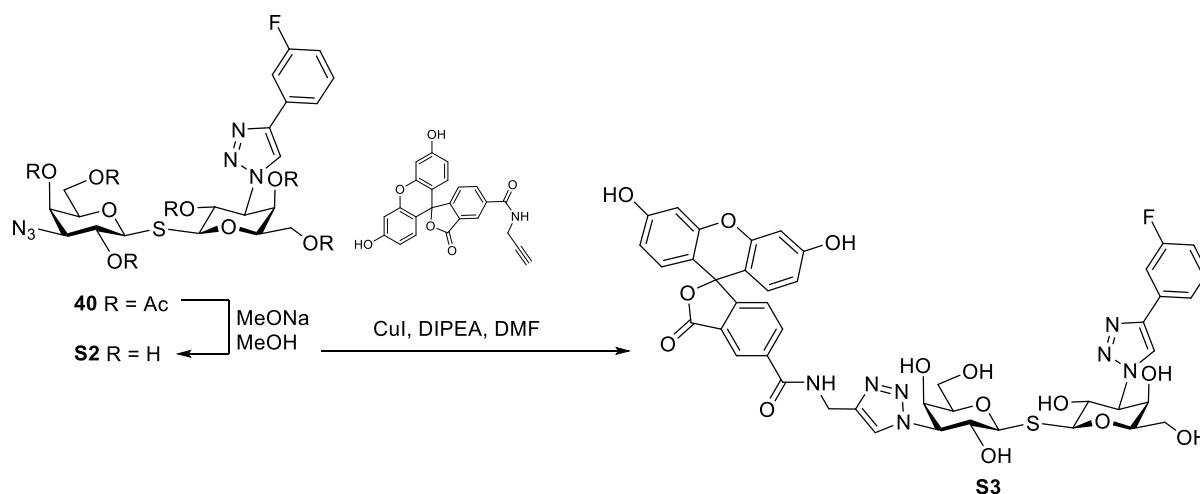
3-Deoxy-3-{4-(3,4,5-trifluorophenyl)-1*H*-1,2,3-triazol-1-yl}-β-D-galactopyranosyl 3-deoxy-3-(4-ferrocenyl-1*H*-1,2,3-triazol-1-yl)-1-thio-β-D-galactopyranoside (41)
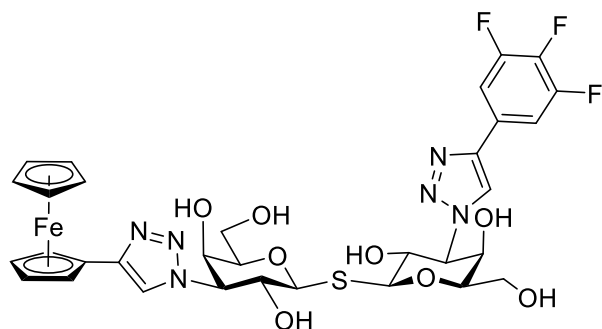
Compound **41** was prepared according to the general procedure for azide-alkyne cycloaddition followed by acetyl deprotection starting from 2,4,6-tri-*O*-acetyl-3-azido-3-deoxy-β-D-galactopyranosyl 2,4,6-tri-

O-acetyl-3-deoxy-3-[4-(3,4,5-trifluorophenyl)-1*H*-1,2,3-triazol-1-yl]-1-thio-β-D-galactopyranoside[15] (**39**, 90 mg, 0.11 mmol), ethynyl ferrocene (28 mg, 0.13 mmol), $CuSO_4 \cdot 5H_2O$ (12 mg, 0.05 mmol), ascorbic acid (8 mg, 0.05 mmol) and DMF (3 mL). The deacetylation step after aqueous workup was performed with MeOH (10 mL), DCM (10 mL) and 8 drops of 1 M solution of MeONa overnight. Column chromatography in DCM/MeOH 7:1 after DOWEX 50W (H^{+}) neutralization afforded **41** as an orange amorphous solid (67 mg, 78%), R_f 0.50 (DCM/MeOH 6:1), $[\alpha]_D^{20}$ −71 (*c* 0.35, MeOH). ^{1}H NMR (MeOH-d_4, 400 MHz, H-H COSY): δ 8.58, 8.21 (2×s, 2×1H, C*H*$_{Tria}$), 7.59 (dd, *J* = 8.6, 6.5 Hz, 2H, C*H*$_{Ph}$), 4.92 (dd, 1H, *J* = 10.7, 2.9 Hz, H-3′), 4.83 (dd, 1H, *J* = 10.8, 3.3 Hz, H-3), 4.91–4.78 (m, 4H, H-1,2,1′,2′), 4.76, 4.70 (2×dt, 2×1H, *J* = 2.5, 1.3 Hz, C*H*$_{Cp}$), 4.31–4.28 (m, 2H, C*H*$_{Cp}$), 4.17 (d, 1H, *J* = 2.9 Hz, H-4′), 4.16 (d, 1H, *J* = 3.3 Hz, H-4), 4.06 (s, 5H, C*H*$_{Cp}$), 3.93–3.75 (m, 5H, H-5,6a, 6b/6′b,5′,6′a), 3.72 (dd, 1H, *J* = 11.3, 4.2 Hz, H-6b/6′b). ^{13}C{^{1}H} NMR (MeOH-d_4, 101 MHz, HSQC, HMBC): δ 152.9 (ddd, $^1J_{(C-F)}$ = 248.0 Hz, $^2J_{(C-F)}$ = 10.1 Hz, $^3J_{(C-F)}$ = 4.2 Hz, 2*C*F), 147.4 ($C_{q(Tria)}$), 145.5 (q, $^{4/5}J_{(C-F)}$ = 2.6 Hz, $C_{q(Tria)}$), 140.5 (dt, $^1J_{(C-F)}$ = 251.0 Hz, $^2J_{(C-F)}$ = 15.4 Hz, *C*F), 128.9 (td, $^3J_{(C-F)}$ = 8.9 Hz, $^4J_{(C-F)}$ = 4.8 Hz, $C_{q(Ph)}$), 122.8, 121.3 (2×*C*H$_{Tria}$), 110.8 (dd, $^2J_{(C-F)}$ = 16.8 Hz, $^3J_{(C-F)}$ = 6.2 Hz, 2*C*H$_{Ph}$), 86.8/86.7 (C-1,1′), 81.5 (C-5,5′), 76.3 ($C_{q(Cp)}$), 70.6 (5*C*H$_{Cp}$), 69.8 (C-4,4′), 69.73 (2*C*H$_{Cp}$), 69.69 (C-4,4′), 68.8 (C-3′), 68.5 (C-3), 68.4 (C-2,2′), 67.6, 67.5 (2×*C*H$_{Cp}$), 63.0, 62.9 (C-6,6′). ^{19}F NMR (MeOH-d_4, 376 MHz): δ −137.68 (dd, $^3J_{(F-F)}$ = 19.7 Hz, $^3J_{(H-F)}$ = 8.6 Hz, 2F), −165.92 (tt, $^3J_{(F-F)}$ = 19.7 Hz, $^4J_{(F-F)}$ = 6.5 Hz, 1F). HRMS-APCI (m/z): [M + H][+] calcd for $C_{32}H_{34}F_3FeN_6O_8S$, 775.1455; found 775.1458.

3-Deoxy-3-{4-(3-fluorophenyl)-1*H*-1,2,3-triazol-1-yl}-β-D-galactopyranosyl 3-deoxy-3-(4-ferrocenyl-1*H*-1,2,3-triazol-1-yl)-1-thio-β-D-galactopyranoside (42)

Compound **42** was prepared according to the general procedure for azide-alkyne cycloaddition followed by acetyl deprotection starting from 2,4,6-tri-*O*-acetyl-3-azido-3-deoxy-β-D-galactopyranosyl 2,4,6-tri-*O*-acetyl-3-deoxy-3-{4-(3-fluorophenyl)-1*H*-1,2,3-triazol-1-yl}-1-thio-β-D-galactopyranoside[15] (80 mg, 0.10 mmol), ethynyl ferrocene (26 mg, 0.12 mmol), $CuSO_4 \cdot 5H_2O$ (12 mg, 0.05 mmol), ascorbic acid (8 mg, 0.05 mmol) and DMF (3 mL). The deacetylation step after aqueous workup was performed with MeOH (15 mL), DCM (15 mL) and 8 drops of 1 M solution of MeONa in overnight. Column chromatography in DCM/MeOH 8:1 after DOWEX 50W (H^{+}) neutralization afforded **42** as an orange amorphous solid (66 mg, 87%), R_f 0.45 (DCM/MeOH 7:1), $[\alpha]_D^{20}$ −53 (*c* 1.31, MeOH). ^{1}H NMR

(MeOH-d_4, 400 MHz, H-H COSY): δ 8.58, 8.22 (2×s, 2×1H, CH_{Tria}), 7.63 (ddd, 1H, J = 7.8, 1.5, 0.8 Hz, CH_{Ph}), 7.58 (ddd, 1H, J = 10.1, 2.6, 1.5 Hz, CH_{Ph}), 7.42 (ddd, 1H, J = 8.1, 7.8, 5.9 Hz, CH_{Ph}), 7.06 (dddd, 1H, J = 9.3, 8.1, 2.6, 0.8 Hz, CH_{Ph}), 4.94–4.82 (m, 6H, H-1,2,3,1′,2′,3′), 4.76, 4.70 (2×dt, 2×1H, J = 2.5, 1.3 Hz, CH_{Cp}), 4.29 (td, 2H, J = 2.5, 1.3 Hz, CH_{Cp}), 4.18 (dd, 1H, J = 2.8, 0.7 Hz, H-4′), 4.16 (dd, 1H, J = 2.2, 0.8 Hz, H-4), 4.06 (s, 5H, CH_{Cp}), 3.93–3.71 (m, 6H, H-5,6a,6b,5′,6′a,6′b). ^{13}C{^{1}H} NMR (MeOH-d_4, 101 MHz, HSQC, HMBC): δ 164.7 (d, $^1J_{\text{(C-F)}}$ = 244.3 Hz, CF), 147.4 ($C_{\text{q(Tria)}}$), 147.2 (d, $^4J_{\text{(C-F)}}$ = 2.8 Hz, $C_{\text{q(Tria)}}$), 134.3 (d, $^3J_{\text{(C-F)}}$ = 8.5 Hz, $C_{\text{q(Ph)}}$), 131.9 (d, $^3J_{\text{(C-F)}}$ = 8.5 Hz $CH_{\text{(Ph)}}$), 122.44 (CH$_{\text{Tria}}$), 122.42 (d, $^4J_{\text{(C-F)}}$ = 3.0 Hz CH$_{\text{(Ph)}}$), 121.3 (CH$_{\text{Tria}}$), 115.8 (d, $^2J_{\text{(C-F)}}$ = 21.5 Hz, CH$_{\text{Ph}}$), 113.1 (d, $^2J_{\text{(C-F)}}$ = 23.3 Hz, CH$_{\text{Ph}}$), 87.0,86.9 (C-1,1′), 81.54,81.52 (C-5,5′), 76.3 ($C_{\text{q(Cp)}}$), 70.6 (5CH$_{\text{Cp}}$), 69.8 (C-4,4′), 69.73 (2CH$_{\text{Cp}}$), 69.71 (C-4,4′), 68.8,68.5 (C-3,3′), 68.4 (C-2,2′), 67.6, 67.5 (2×CH$_{\text{Cp}}$), 63.0, 62.9 (C-6,6′). ^{19}F NMR (MeOH-d_4, 376 MHz): δ −115.98 (ddd, $^3J_{\text{(H-F)}}$ = 10.1, 9.3 Hz, $^4J_{\text{(H-F)}}$ = 5.9 Hz). HRMS-APCI (m/z): [M + H]$^+$ calcd for C$_{32}$H$_{36}$FFeN$_6$O$_8$S, 739.1644; found 739.1641.

The synthesis of the fluorescence probe S3

Scheme S1: Preparation of fluorescence probe **S3**.

3-Azido-3-dideoxy-β-D-galactopyranosyl 3-deoxy-3-[4-(3-fluorophenyl)-1*H*-1,2,3-triazol-1-yl]-1-thio-β-D-galactopyranoside (S2)
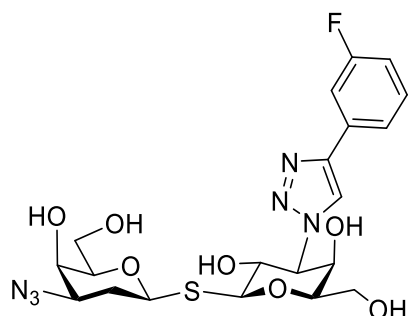
To a solution of 2,4,6-tri-*O*-acetyl-3-deoxy-3-[4-(3-fluorophenyl)-1*H*-1,2,3-triazol-1-yl]-1-thio-β-D-galactopyranose[9] (200 mg; 0.43 mmol) (200 mg; 0.428 mmol) in dry acetone (20 mL), bromide **31** (186 mg; 0.471 mmol), and K_2CO_3 (591 mg; 4.28 mmol) were added under an inert Ar atmosphere. The reaction mixture was then stirred for 4 h at room temperature. After complete consumption of all starting materials, the solvent was evaporated. The residue was diluted with CH_2Cl_2 (50 mL) and washed with H_2O (40 mL) and brine (40 mL). The organic phase was separated, dried over anhydrous $MgSO_4$, filtered, and concentrated under vacuum. The obtained crude product **40** was dissolved in MeOH (10 mL), followed by the addition of NaOMe (1 M, 2 mL), and the resulting solution was stirred for 4 h. After complete consumption of all starting material, the reaction mixture was neutralized with DOWEX 50W (H^+) resin and filtered, the product was purified with column chromatography (CH_2Cl_2/MeOH 6:1) to give **S2** (131 mg, 58%) as an amorphous white solid. The NMR data were in accordance with the literature.[15]

3-Deoxy-3-[4-(fluorescein-5-yl-carbonylaminomethyl)-1*H*-1,2,3-triazol-1-yl]-β-D-galactopyranosyl 3-deoxy-3-[4-(3-fluorophenyl)-1*H*-1,2,3-triazol-1-yl]-1-thio-β-D-galactopyranoside (S3)
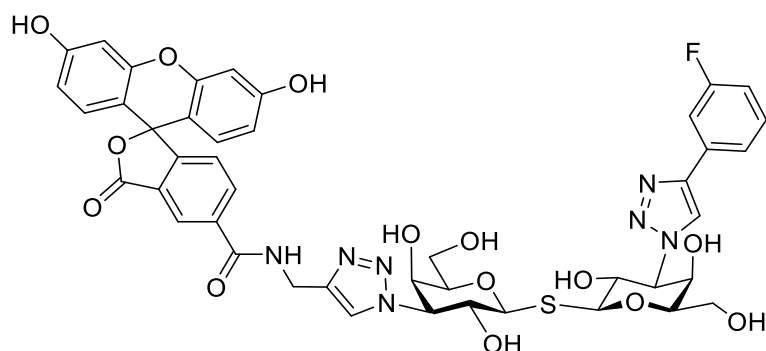
To a solution of azide **S2** (12.0 mg; 23.4 μmol) in dry DMF (3 mL), 6-FAM-alkyne (10.3 mg; 24.9 μmol), CuI (2.2 mg; 11.4 μmol), and DIPEA (8 μL; 45.4 μmol) was added. The reaction mixture was

then stirred in the dark for 2.5 h at 35 °C. After complete consumption of the starting material, the reaction was quenched by adding a saturated solution of NH_4Cl (0.2 mL) and H_2O (2 mL). The resulting mixture was evaporated, and the residue was dissolved in a mixture of dioxane/H_2O (5 mL). The mixture was filtered to remove the obtained salts, and the filtrate was concentrated. The resulting residue was purified by flash chromatography on silica (CH_3CN/H_2O 90:10). Further purification was performed using HPLC on a C18 column (H_2O/MeOH 2 % → 35 %). This purification process yielded product **S3** (18.2 mg; 83%) as an orange solid. This solid was then lyophilized from a mixture of dioxane and H_2O, resulting in 18.2 mg of lyophilized solid. Rf 0.32 (CH_3CN/H_2O 90:1). ^{1}H NMR (MeOH-d_4, 500 MHz): δ 8.56 (s, 1H, H-5-triazole-3), 8.45 (bs, 1H, H-3′-fluoresc), 8.22 (bs, 1H, H-5-triazole-3′), 8.16 (d, 1H, $J_{5',6'}$ = 8.0, H-5′-fluoresc), 7.62 (ddd, 1H, $J_{6,5}$ = 7.8, $J_{6,2}$ = 1.5, $J_{6,4}$ = 1.0, H-6-C_6H_4F), 7.57 (ddd, 1H, $J_{H,F}$ = 10.1, $J_{2,4}$ = 2.6, $J_{2,6}$ = 1.5, H-2-C_6H_4F), 7.42 (ddd, 1H, $J_{5,4}$ = 8.4, $J_{5,6}$ = 7.8, $J_{H,F}$ = 5.9, H-5-C_6H_4F), 7.26 (d, 1H, $J_{6',5'}$ = 8.0, H-6′-fluoresc), 7.04 (dddd, 1H, $J_{H,F}$ = 8.7, $J_{4,5}$ = 8.4, $J_{4,2}$ = 2.6, $J_{4,2}$ = 1.5, H-4-C_6H_4F), 6.69 (d, 2H, $J_{4,2\&5,7}$ = 2.4, H-4,5-fluoresc), 6.65 (bd, 2H, $J_{1,2\&8,7}$ = 8.8, H-1,8-fluoresc), 6.55 (dd, 2H, $J_{2,1\&7,8}$ = 8.8, $J_{2,4\&7,5}$ = 2.4, H-2,7-fluoresc), 4.90 – 4.75 (m, 6H, H-1,1′,2,2′,3,3′), 4.74, 4.68 (2 × bd, 2 × 1H, J_{gem} = 15.2, CH_2N), 4.15, 4.12 (2 × dd, 2 × 1H, $J_{4,3}$ = $J_{4',3'}$ = 2.9, $J_{4,5}$ = $J_{4',5'}$ = 1.0, H-4,4′), 3.88 – 3.75 (m, 4H, H-5,5′,6a,6′a), 3.70, 3.65 (dd, 1H, J_{gem} = 11.3, $J_{6b,5\&6'b,5'}$ = 4.2, H-6b,6′b). ^{13}C NMR (126 MHz, MeOH-d_4): δ 170.84 (COO), 168.54 (CON), 164.67 (d, $J_{C,F}$ = 244.3, C-3-C_6H_4F), 154.85 (CH-4a,4b-fluoresc), 147.17 (C-4-triazole-3), 145.55 (C-4-triazole-3′), 134.33 (d, $J_{C,F}$ = 8.4, C-1-C_6H_4F), 134.18 (CH-5′-fluoresc), 132.02 (C-4′-fluoresc), 131.91 (d, $J_{C,F}$ = 8.5, C-5-C_6H_4F), 130.57 (CH-1,8-fluoresc), 126.57 (CH-6′-fluoresc), 125.85 (CH-3′-fluoresc), 122.48 (CH-5-triazole-3), 122.41 (d, $J_{C,F}$ = 2.8, CH-6-C_6H_4F), 115.78 (d, $J_{C,F}$ = 21.4, CH-4-C_6H_4F), 114.65 (CH-2,7-fluoresc), 113.14 (d, $J_{C,F}$ = 23.2, CH-2-C_6H_4F), 111.65 (C-8a,9a-fluoresc), 103.68 (CH-4,5-fluoresc), 86.82, 86.75 (CH-1,1′), 81.45 (CH-5,5′), 69.83, 69.73 (CH-4,4′), 68.75 (CH-2,2′), 68.36, 68.28 (CH-3,3′), 62.93, 62.86 (CH_2-6,6′), 36.48 (CH_2N) (not detected: C-1′,3,6,9-fluoresc). ^{19}F NMR (470 MHz, MeOH-d_4): δ −110.39 (ddd, $J_{F,H}$ = 10.1, 8.7, 5.9). HRMS-ESI (m/z): [M + H]$^+$ calcd for $C_{44}H_{41}O_{14}N_7FS$ 942.2416; found 942.2415.

B. 2. Estimation of the water solubility for selected compounds

We evaluated the water solubility of the ferrocene inhibitors **10**, **16**, **25**, **30**, **34**, and **36** and ruthenium-arene inhibitors **8** and **27**. For each compound, 3 mg was suspended in 1 mL of distilled water followed by sonication for 15 min. The ferrocene derivatives **10** and **34** and the ruthenium-arene complexes **8** and **27** dissolved completely, whereas the other compounds remained as a suspension of orange solid particles in an orange solution. The suspension was then filtered using a syringe filter equipped with a 0.45 μm MCE membrane. A 0.5 mL aliquot of the filtrate was transferred to a volumetric flask and diluted to 5 mL with 1% HNO_3 aqueous solution. Iron content was determined by atomic emission spectrometer with microwave-induced plasma (MP-AES Agilent Technologies, Inc., USA) equipped with an autosampler model SPS 3 (Agilent Technologies, Inc., USA). Sample was introduced by means of an inert OneNeb nebulizer with a double-pass glass cyclonic spray chamber system and a standard torch. Water solubility was calculated as follows:

ferrocene complex **16**: 0.59 mg/mL

ferrocene complex **25**: 1.69 mg/mL

ferocene complex **30**: 0.21 mg/mL

The iron content in the filtrate of diferrocene inhibitor **36** was below the instrument's detection limit. Therefore, the experiment was repeated in a 10% (v/v) $DMSO/H_2O$, which yielded a solubility value of 1.08 mg/mL.

B. 3. Selected vicinal coupling constant (discussed in the synthesis section of the article)

Table S1. Coupling constant $^3J_{(H-m, H-n,)}$ [Hz] of vicinal protons H-m, H-n in MeOH-d_4 or DMSO-d_6 for selected disaccharides

Compound	m,n											
	1,2	2,3	3,4	4,5	5,6a	5,6b	1′,2′	2′,3′	3′,4′	4′,5′	5′,6′a	5′,6′b
6	9.2	9.2	a	a	a	a	7.6	9.7	3.3	0.9	7.3	4.3
8	9.2	8.8	a	a	a	a	7.5	9.7	3.2	0.9	a	4.6
10	7.8	8.8	a	a	2.5	4.9	7.5	a	3.4	0.7	7.6	4.6
16	9.9	9.7	a	a	a	a	7.6	9.7	3.3	0.9	7.6	4.8
19	8.2	10.4	8.2	a	2.5	4.0	7.5	9.7	3.3	0.9	7.4	4.2
25	8.1	a	a	9.4	2.5	4.1	7.6	11.1	3.0	a	a	a
27	8.2	a	a	a	a	a	7.5	11.2	3.1	0.9	a	a
29	8.5	10.9	8.6	9.0	3.2	3.2	7.5	11.2	3.1	a	a	4.4.
33	9.8	9.3	3.4	1.1	7.4	4.4	9.6	10.7	3.0	0.6	a	a
35	9.5	10.5	3.1	0.0	6.3	6.3	-	-	-	-	-	-
36	a	a	2.6	0.0	a	7.2	-	-	-	-	-	-
37	9.5	10.5	3.2	0.0	7.0	4.9	-	-	-	-	-	-
39	a	10.8	3.3	0.0	a	a	a	10.7	2.9	0.0	a	a

^{a} The signals of protons are overlapped.

B. 4. The electrochemical behavior of compounds 6, 25 and 36

The experiments were carried out in 50 mM sodium phosphate buffer (NaPh) with pH 7.0 using cyclic voltammetry (CV) at a basal-plane pyrolytic graphite electrode (bPGE).[16,17] Fig. S1 shows the obtained results, from which the parameters characterizing the redox system and its reversibility: half-wave potential ($E_{1/2} = (E_p^a+E_p^c)/2$), peak-to-peak potential difference ($\Delta E_p = E_p^a-E_p^c$) and a peak current density ratio (j_p^a/j_p^c) were evaluated (Tab. S2).
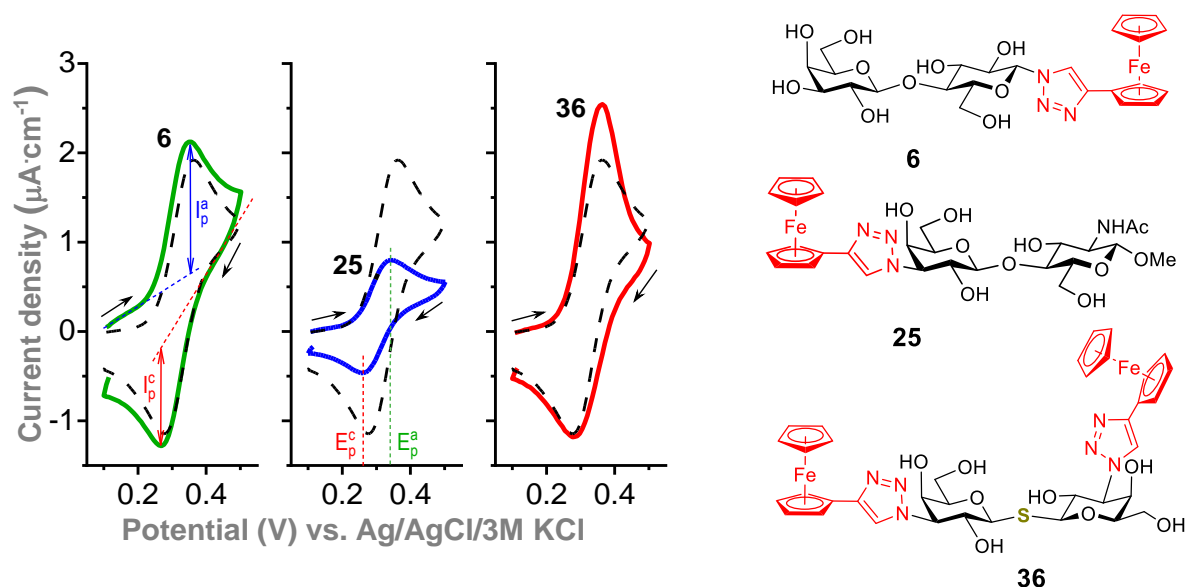
Figure S1. Electrochemical activity of 216 µM 1-substituted lactose **6** (green line), 100 µM 3′-substituted lactosamine inhibitor **25** (blue line) and 100 µM 3,3′-disubstituted thiodigalactoside inhibitor **36** (red line) in comparison to 100 µM ferrocenecarboxylic acid (black dash lines in all three panels) measured by CV (scan rate 100 mV·s⁻¹) at bPGE in 50 mM NaPh pH 7.0.

Table S2. Evaluation of quasi-reversibility of the studied ferrocene-disaccharide conjugates using half wave potential ($E_{1/2} = (E_p^a+E_p^c)/2$), peak to peak potential difference ($\Delta E_p = E_p^a-E_p^c$) and by peak current density ratio (j_p^a/j_p^c) observed by CV (100 mV·s⁻¹) at bPGE.

Ferrocene complex	$E_{1/2}$, V	ΔE_p, V	j_p^a/j_p^c
FeCOOH (100 µM)	0.320	0.084	1.73
6 (216 µM)	0.310	0.078	1.67
25 (100 µM)	0.300	0.070	1.75
36 (100 µM)	0.323	0.077	2.14

Fig. S1 shows how peak current density is influenced by concentration and the number of electroactive ferrocene tags. A solution containing 216 µM of the inhibitor **6** provides about twice higher peak current densities compared to 100-µM solution of the inhibitor **25**, both having only one ferrocene tag, and

comparable peak current densities with **36** at the concentration of 100 µM, which offers two ferrocene redox centers. Surprising results were obtained during the determination of electrode processes occurring at bPGE using CV scan rates between 20 and 2000 mV·s^{-1} (Fig. S2). While **FcCOOH** oxidation and reduction at bPGE were driven by diffusion, together with **6** and **25**, the electrochemical oxidation/reduction of **36** was driven by adsorption. This is obviously caused by the presence of two ferrocene tags resulting in higher structural symmetry lowering its polarity and increasing adsorption capability on bPGE. This phenomenon apparently lowered the limit of detection (LOD, S/N = 3) down to 0.1 µM (**35**) using CV in comparison to LOD = 1 µM for **FcCOOH** and **25**, or 2 µM for **6**. The quasi-reversibility of the electrode process allowed to decrease LOD of **FcCOOH** and **25** down to 0.1 µM, or 0.5 µM for **6**. Corresponding calibration curves and their parameters are shown in Figure S3, S4, and Table S3 respectively.
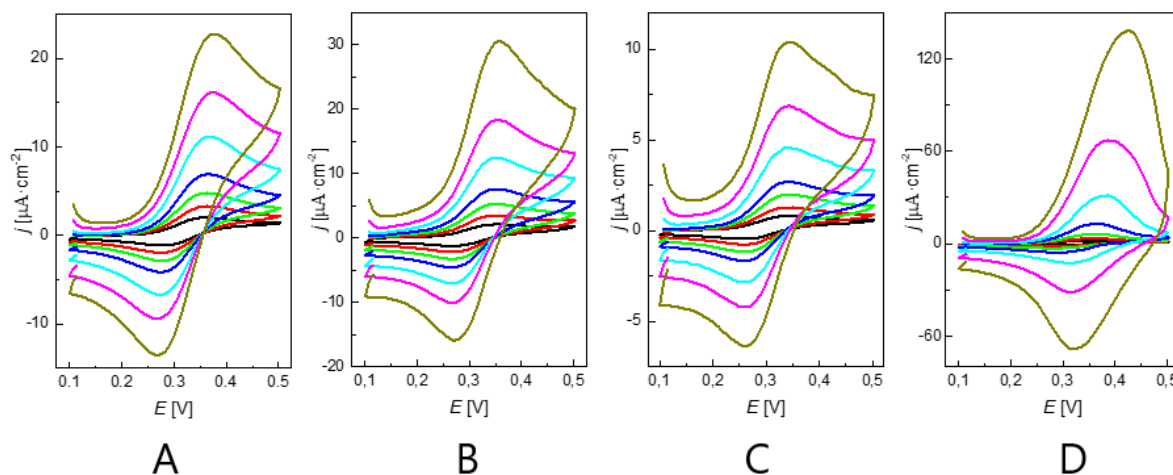
Figure S2 Cyclic voltammograms of the studied compounds: 100 µM **FcCOOH** (A), 216 µM **6** (B), 100 µM **25** (C), 100 µM **36** (D) measured at basal-plane pyrolytic graphite electrode (bPGE) in 50 mM sodium phosphate buffer (NaPh) pH 7.0 using scan rate (V·s^{-1}): 0.02 (black), 0.05 (red), 0.1 (green), 0.2 (blue), 0.5 (cyan), 1.0 (magenta), and 2.0 (dark yellow).

The dependence of the signal heights (I_p) on the scan rate (v, or square root of the scan rate ($v^{0.5}$)) of polarization provides information about the process controlling the electrochemical oxidation or reduction taking place at the bPGE surface. The evaluations of the linear dependencies, including the slopes (A) and the intercepts (B), are summarized in Tab. S2, and the resulting process of each peak is evaluated by equation (1) in the case of a diffusion-controlled process, and by equation (2) if it is a process controlled by adsorption.

$$I_p = \text{A} \cdot v^{0.5} + \text{B} \qquad (1)$$
$$I_p = \text{A} \cdot v + \text{B} \qquad (2)$$

Table S3: Summary of the linear curve parameters evaluated from the CVs (Fig. S2 above) in dependence on scan rate (v) within the range $0.02 - 2.0$ V·s^{-1}.

Compound	Peak	Slope [μA·s$^{1/2}$·V$^{-1/2}$]	Intercept [μA]	R^2
FeCOOH	$I_p^a = A \cdot v^{0.5} + B$	3.52 ± 0.14	0.14 ± 0.11	0.9920
	$I_p^c = A \cdot v^{0.5} + B$	-1.73 ± 0.12	-0.341 ± 0.091	0.9754
6	$I_p^a = A \cdot v^{0.5} + B$	4.12 ± 0.20	-0.31 ± 0.15	0.9879
	$I_p^c = A \cdot v^{0.5} + B$	-2.431 ± 0.062	-0.010 ± 0.046	0.9968
25	$I_p^a = A \cdot v^{0.5} + B$	1.642 ± 0.035	-0.093 ± 0.026	0.9978
	$I_p^c = A \cdot v^{0.5} + B$	-0.904 ± 0.073	-0.038 ± 0.054	0.9687
36	$I_p^a = A \cdot v + B$	$16.00 \pm 0.57^*$	0.38 ± 0.49	0.9935
	$I_p^c = A \cdot v + B$	$-1.45 \pm 0.23^*$	-0.64 ± 0.20	0.8902

* … [μA·s·V^{-1}]

The concentration dependences of studied compounds **FcCOOH**, **6**, **25**, and **36** were measured by CV and square wave voltammetry (SWV) at bPGE. Each measurement has been repeated three times and average values together with the error bars corresponding to ±standard deviations are shown in **Chyba! N enalezen zdroj odkazů.**4. Parameters of the calibration straight lines are evaluated according to equation (3) and summarized in Table S3.

$$j^a = a \cdot c + b \tag{3}$$
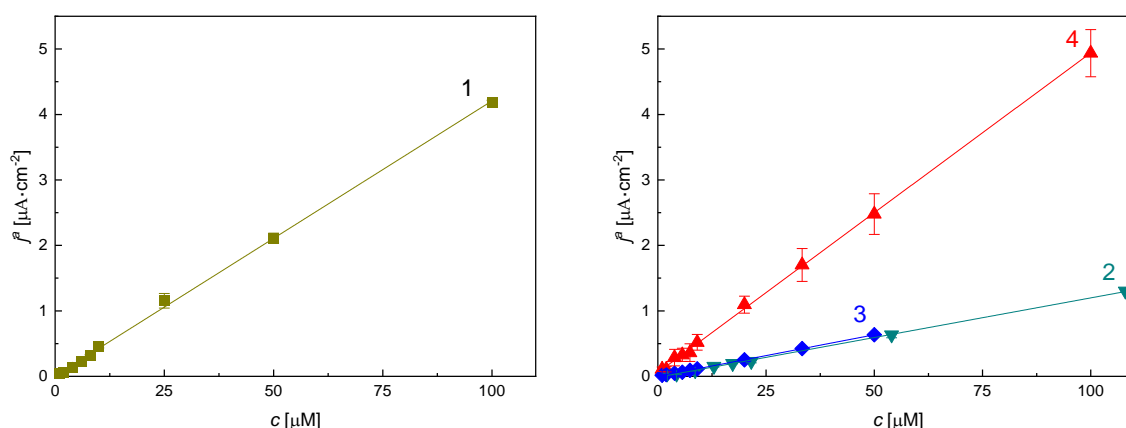
Figure S31 Concentration dependencies of studied compounds: **FcCOOH** (1), **6** (2), **25** (3), **36** (4), measured by CV (scan rate 100 mV·s^{-1}) at bPGE in 50 mM NaPh pH 7.0.
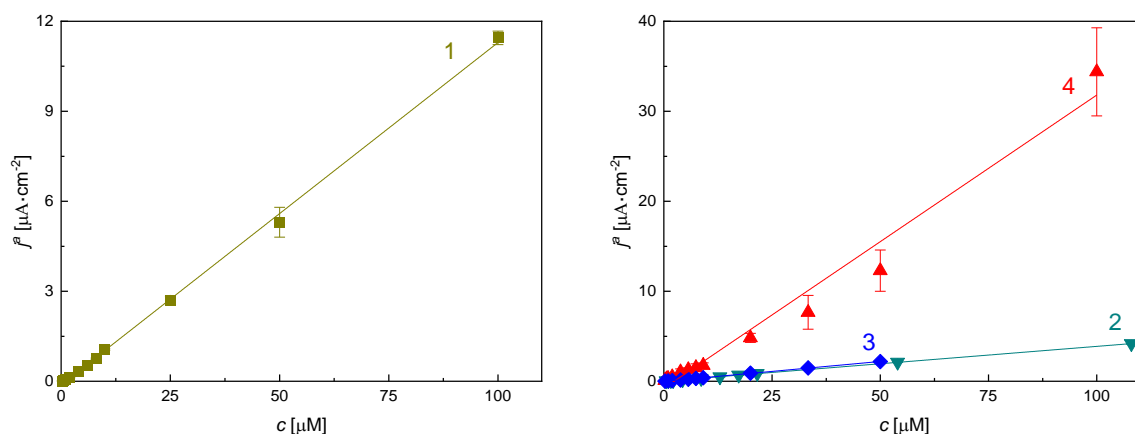
Figure S4 Concentration dependencies of studied compounds: **FcCOOH** (1), **6** (2), **25** (3), **36** (4), measured by SWV (frequency 20 Hz) at bPGE in 50 mM NaPh pH 7.0.

Since ferrocene is considered an outer-sphere redox system relatively insensitive to PGE surface composition,[18] small differences in the electrochemical behavior of the studied compounds **6**, **25** and **36** at the heterogeneous bPGE's surface can be attributed to minor structural variance, primarily to the number of ferrocene tags attached to disaccharide subunits. Thanks to the proven electrochemical activity of these potential galectin inhibitors, voltammetric methods could potentially be used to study their mutual interaction.

C. Preparation of galectins

Preparation and purification of human galectin-1 (*h*gal-1) and -3 (*h*gal-3)

The coding sequences of *h*gal-1 and -3 (NM_002305.4 and NM_002306) were cloned using Gateway recombination technology (Invitrogen) into the pDEST15 vector containing an N-terminal His6-GST tag cleavable by TEV protease (Tobacco Etch Virus nuclear-inclusion-a endopeptidase). Both cloned genes were expressed in *E. coli* BL21 RILP. The bacteria were cultured in 100 mL of LB medium (10 g/L tryptone, 5 g/L yeast extract, 5 g/L NaCl) with ampicillin (100 μg/mL) and chloramphenicol (30 μg/mL) overnight at 37 °C, 220 rpm. The culture was diluted to a total volume of 2.5 liters in LB medium (supplemented with ampicillin and chloramphenicol) to an optical density at A_{600}=0.1 and cultured for 2–3 hours. Upon reaching an optical density at A_{600}=0.5, gene expression was induced by addition of isopropyl-β-D-thiogalactopyranoside to the culture (final concentration 1 mM). The bacterial culture was further cultured for 4 hours at 30 °C, 140 rpm, and then pelleted by centrifugation (4000 g/4 °C/10 min). Bacterial pellets were resuspended in lysis buffer (50 mM Tris-HCl, pH 7.5; 0.15 M NaCl, 0.75% CHAPS). Cell suspensions were subsequently enriched with lysozyme (1 mg/mL), phenylmethylsulfonyl fluoride (1 mM), turbonuclease (1:1000), and $MgCl_2$ (1 mM), and then sonicated with an ultrasonic sonicator Sonoplus, probe VS 70T, for 15 cycles (10 s sonication, 50 s pause, 35W)

at 4 °C. Bacterial lysates were obtained by centrifugation for 30 minutes at 10,000 g/4 °C. His6-GST-tagged proteins were captured on a GSTrap glutathione agarose column (GE Healthcare), eluted with binding buffer (50 mM Tris-HCl, pH 7.5; 0.15 M NaCl) enriched with 20 mM glutathione, and subjected to TEV protease cleavage (1 mg of protease per 10 mg of purified protein) overnight at 4 °C. To remove His6-GST and His6-TEV protease, protein mixtures were applied to a HisTrap column (GE Healthcare). Fractions containing purified proteins were collected in a 96-well plate via a fractionator. After concentration, proteins were solubilized in final testing buffers (25 mM Tris-HCl pH 8.0, 300 mM NaCl and 1mM TCEP) using Zeba spin desalting columns that separate molecules with a molecular weight up to 10 kDa (Thermo Fisher Scientific). The purity of all isolated proteins was verified by SDS-PAGE electrophoresis and staining with Coomassie Brilliant Blue. The TEV protease was prepared in the laboratory following the method from lit.[19]

Preparation and purification of human galectin-3-CRD (*h*gal-3-CRD)

The DNA sequence of galectin 3 glycodomain (AA 113-250) was PCR amplified (oligonucleotides pET_G3D_F 5'-TTTAAGAAGGAGATATACATATGCCACTGATTGTGCCTTA-3' and pET_G3D_R 5'-GGTGCTCGAGTGCGGCCGCATCATATCATGGTATATGAAG -3') from plasmid LGALS3 (Origene; RC208785) and subcloned into NdeI and HindIII restricted vector pET-22b(+)using Gibson assembly. G3D was expressed in E. coli strain BL21 (DE3). The expression was induced in cells grown in LB media at 37 °C and 180 rpm to the growth density of approximately OD600 = 0.5 using 0.4 mM IPTG and further grown at 22 °C for 16 hours. Cell pellet from 1 liter of LB media (approximately 3 ml) was resuspended in 20 ml of Lysis buffer (0.1 M Na-phosphate buffer pH 7.4, 0.5 M NaCl, 5 mM β-mercaptoethanol, 5 mM MgCl2, 0.5 mg/ml lysozyme and 125 U Novagen® Benzonase) and sonicated for 2 minutes (MSE Soniprep 150; 75% power and amplitude 14 microns). After incubation on ice for 30 minutes, the cell lysate was spun for 30 minutes at 20 000 x g. The cleared lysate was run through chromatographic column containing apropriate amount of lactosyl-Sepharose (binding capacity approximately 10 mg/ml), prepared as described before.[20] The column was washed with 5 column volumes of Wash buffer (50 mM Na-phosphate buffer pH 7.4, 1 M NaCl and 5 mM β-mercaptoethanol) and galectin was eluted using appropriate amount of elution buffer (50 mM Na-phosphate buffer pH 7.4, 0.1 M NaCl, 5 mM β-mercaptoethanol and 0.1 M β-lactose). The galectin was further purified by gel filtration (column SuperdexTM 75 10/300 GL, GE Healthcare) using phosphate buffered saline (PBS) containing 5 mM β-mercaptoethanol as mobile phase. The eluted protein was concentrated (Amicon® Ultra – 15, Ultracel® - 10K; Merck Millipore), 10 x dialyzed 1:200 against PBS containing 5 mM β-mercaptoethanol in D-tubeTM Dialyzer Mega (MWCO 3.5 kDa; Merck Millipore) and further stored at 4 °C.

D. Constant current chronopotentiometric analysis

*H*gal-1 was diluted in 30 mM tris-HCl in the presence of 0.1 M NaCl (pH = 7.4). Ferrocene compounds **6**, **25**, and **36** were dissolved in dimethyl sulfoxide and then diluted in 30 mM tris-HCl in the presence of 0.1 M NaCl (pH = 7.4). The final concentrations were: 2 μM *h*Gal-1, 24 μM tris(2-carboxyethyl)phosphine (TECP), 40 μM N-acetyllactosamine or compound **6**, **25** or **36.** In the ice, *h*gal-1/full-length *h*gal-3 was incubated alone or with saccharide compound for 15 min.

Electrochemical measurements were performed using an Autolab analyzer (PGSTAT30, EcoChemie the Netherlands) connected with VA-Stand 663 (Metrohm Switzerland) with a three-electrode system. A hanging mercury drop electrode (HMDE with area 0.4 mm^2) as a working electrode, Ag|AgCl|3M KCl as a reference one, and Pt wire as an auxiliary electrode were used in a standard thermostatic cell at a controlled temperature of 15 ºC open to air if not stated otherwise. Data were collected using GPES version 4.9. Experiments were replicated at least 3 times for each measurement.

At an open circuit potential, the incubated samples were adsorbed onto the HMDE electrode surface from a 5 μL drop for an accumulation time, t_A, of 60 s. Then, the protein complex-modified HMDE electrode was transferred to a blank electrolyte containing 50 mM Na–phosphate buffer (pH = 7.4). For all measurements, parameters E_B -0.3 V against the Ag|AgCl|3M KCl for t_B of 5 s, accompanied by stirring of 1500 rpm, were used.

E. Determination of the affinity to galectins

Determination of fluorescence probe (S3) K_d to *h*gal-1 and *h*gal-3-CRD by direct fluorescence polarization titration

The fluorescence probe **S3** direct fluorescence polarization titration to *h*gal-1 and *h*gal-3-CRD has been done according to the prescribed procedures (Fig. S5 Tab. S4).[15] Briefly, *h*gal-1 was titrated (from 6 nM to 60000 nM) in presence of 100 nM probe **S3** in PBS supplemented with 0.01% Triton X-100 and *h*gal-3-CRD was titrated in the same buffer (from 0.3 nM to 3000 nM) in presence of 5 nM probe S7. K_d were calculated using One Site Total Binding's model GraphPad Prism software (version 10.0.2, GraphPad, USA).
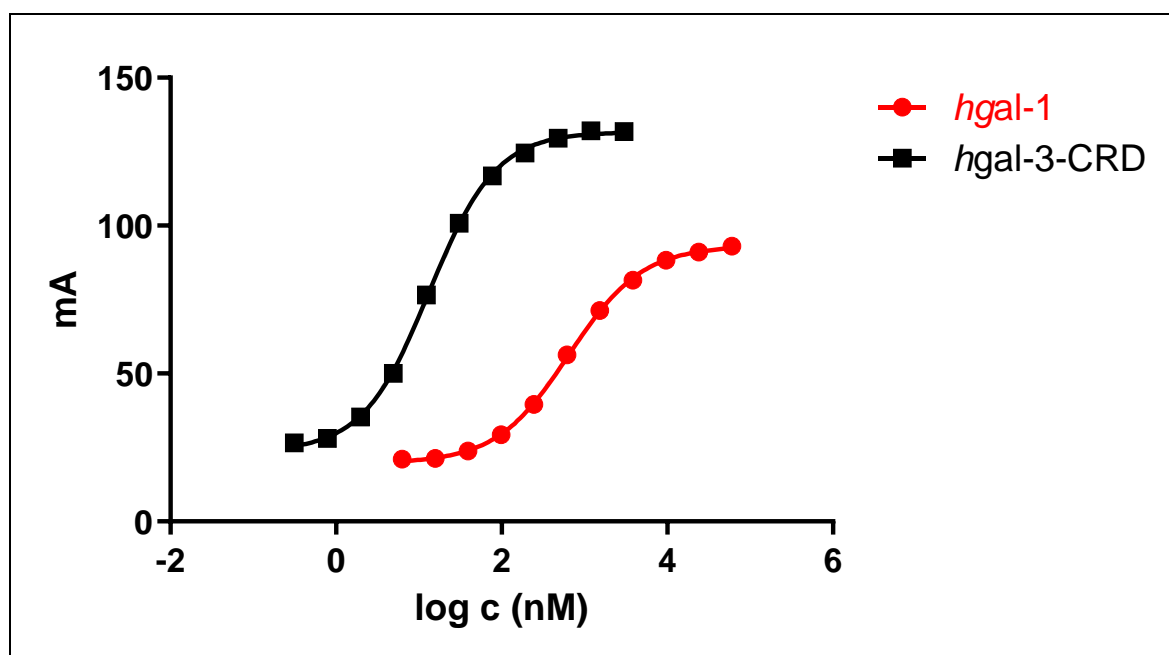
Figure S5. Direct fluorescence polarization titration curves of the fluorescence probe **S3** with *h*gal-1 and *h*gal-3-CRD.

Table S4: Calculated K_d (nM) of the fluorescence probe **S3** to *h*gal-1 and *h*gal-3-CRD.

	*h*gal-1	*h*gal-3-CRD
K_d (nM)	650.8	13.37

Competitive fluorescence polarization (FP)

FP experiments were performed analogically to the procedures reported in lit.[15,21] with Tecan Spark multiplate reader (Tecan, Switzerland) using excitation 485 ± 20 nm and emission 535 ± 20 nm in 384 well black polystyrene microplate (Corning 4514, USA) with the temperature set up to 25 °C.

Affinities to *h*gal-1 were determined in PBS buffer with 0.01% Triton X-100 using protein concentration 500 nM, fluorescence probe concentration 100 nM and at least eleven different concentrations (depending of the expected affinity) of the tested compound in triplicates. Affinities to *h*gal-3-CRD were determined in PBS buffer 0.01% Triton X-100 using protein concentration 50 nM, fluorescence probe concentration 5 nM and eleven different concentrations (depending of the expected affinity) of tested compound in triplicates. Compounds were pre-spotted into the 384 well plate using Echo 650 (Backmann Coulter, USA) liquid handler and 5 µl of galectin and probe mixture was added using Certus Flex (Fritz Gyger AG, Switzerland) liquid handler. Anisotropy was measured after 30–60 min incubation at 25 °C. Raw anisotropy data from the reader were plotted against concentration using GraphPad Prism software (version 10.0.2, GraphPad, USA) and nonlinear fitting "*[Inhibitor] vs. response -- Variable slope (four parameters)*" analysis was used to calculate the IC_{50} values (concentration, where half of the inhibition is achieved) for each titration. The IC_{50} values from each titration experiment were then used to calculate inhibition constant K_i using an online calculator (http://websites.umich.edu/~shaomengwanglab/software/calc_ki/index.html).[22] The titration curves are shown in the Figs. S6–S21. The triplicate measurements for each compound are shown in one graph using the error bars.
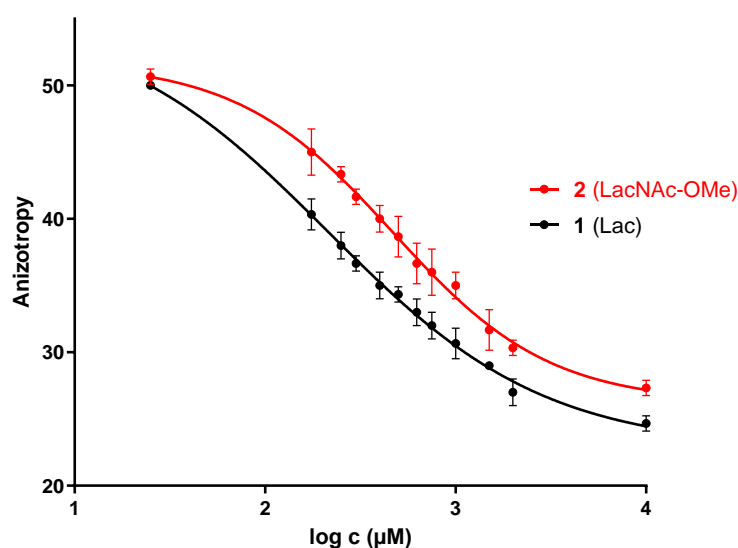
Figure S6. Fluorescence polarization titration curves of lactose (**1**) and methyl β-*N*-acetyllactosamine (**2**β-OMe) with human galectin-1.
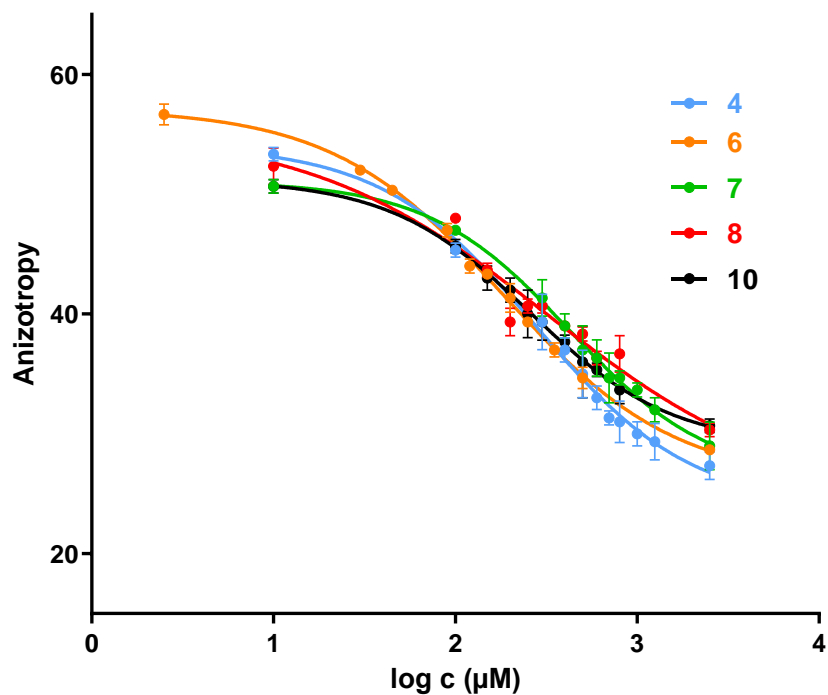
Figure S7. Fluorescence polarization titration curves of lactose-based inhibitors **4**, **6**, **7**, **8** and **10** with human galectin-1.
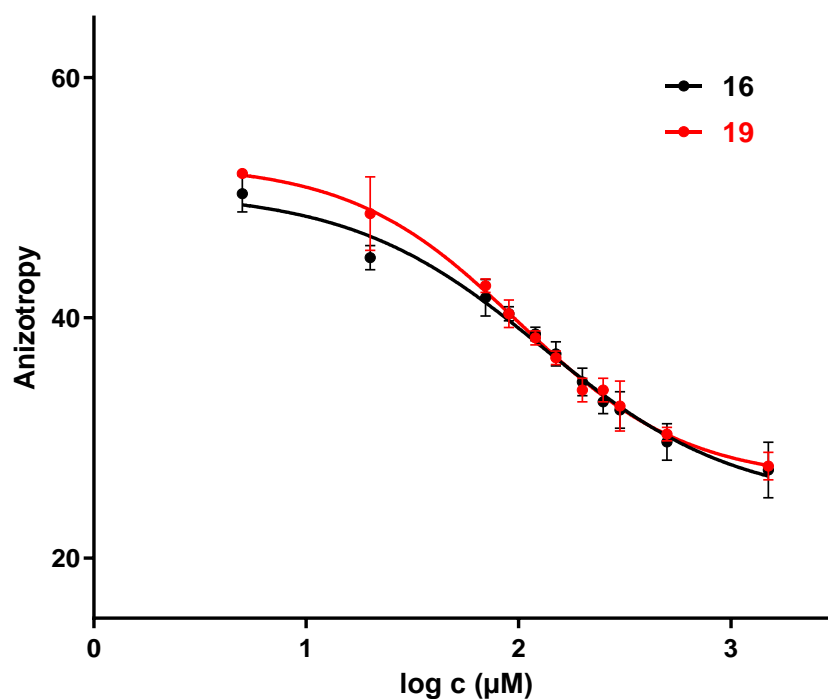
Figure S8. Fluorescence polarization titration curves of 1- and 2′-ferrocene modified *N*-acetyllactosamine inhibitors **16** and **19** with human galectin-1.
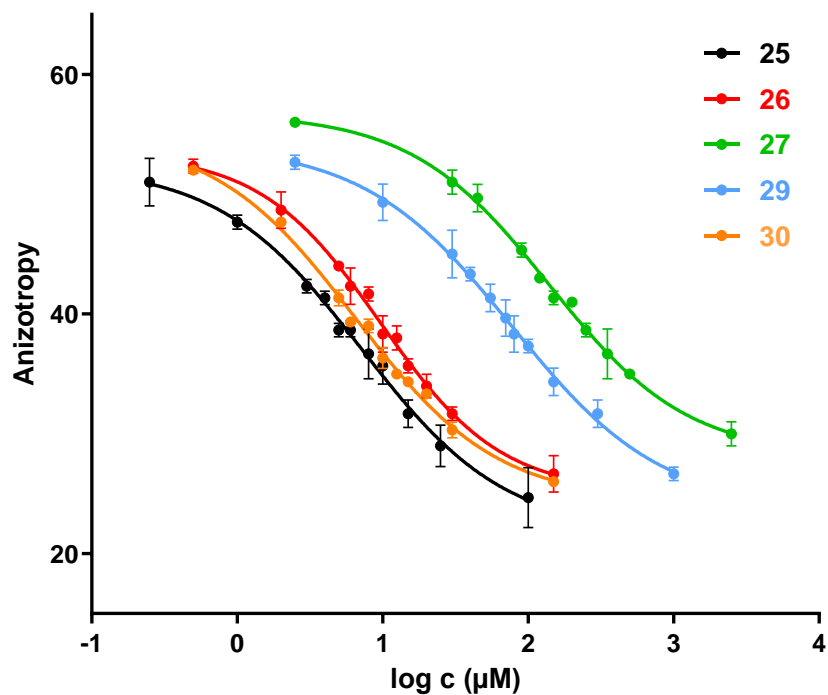
Figure S9. Fluorescence polarization titration curves of 3′- modified *N*-acetyllactosamine-based inhibitors **25–27**, **29** and **30** with human galectin-1.
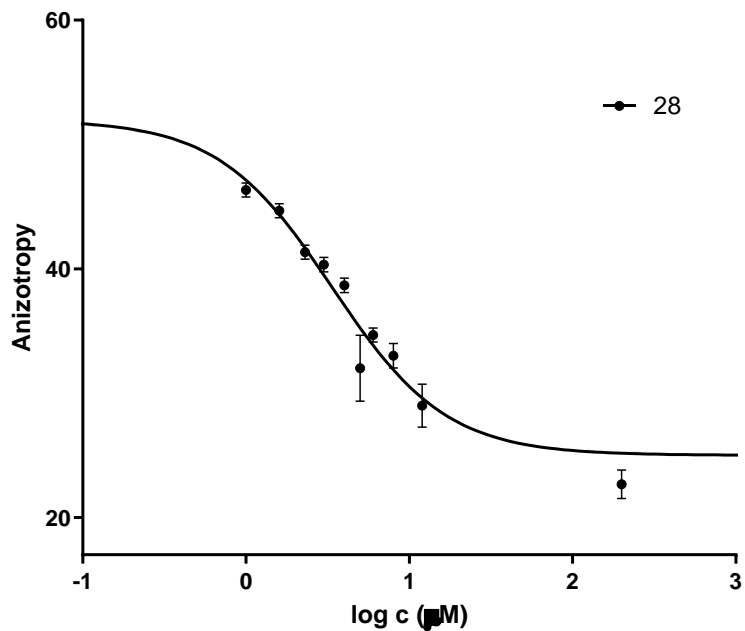
Figure S10. Fluorescence polarization titration curves of the inhibitor **28** with human galectin-1.
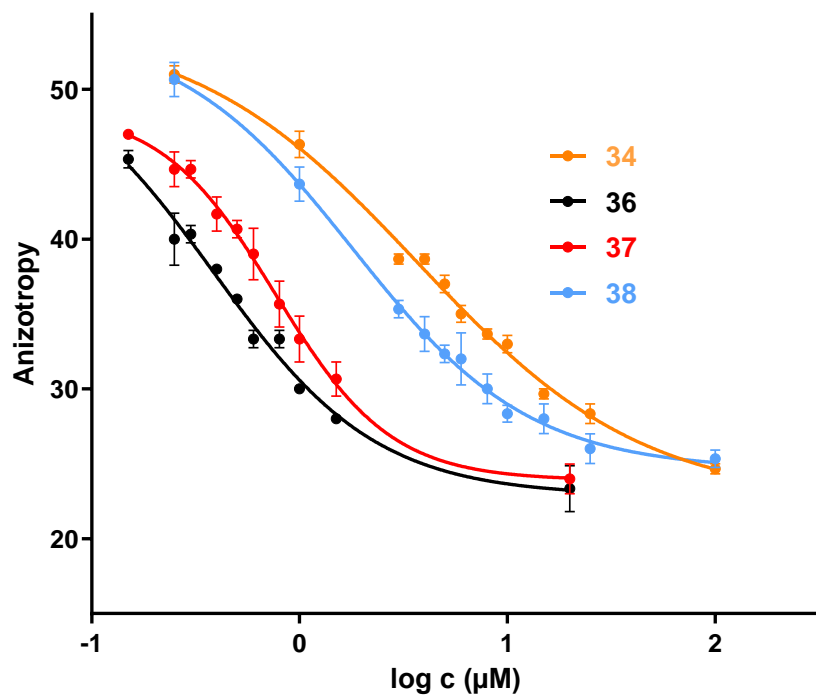
Figure S11. Fluorescence polarization titration curves of thiodigalactoside-based inhibitors **34**, **36–38** with human galectin-1.
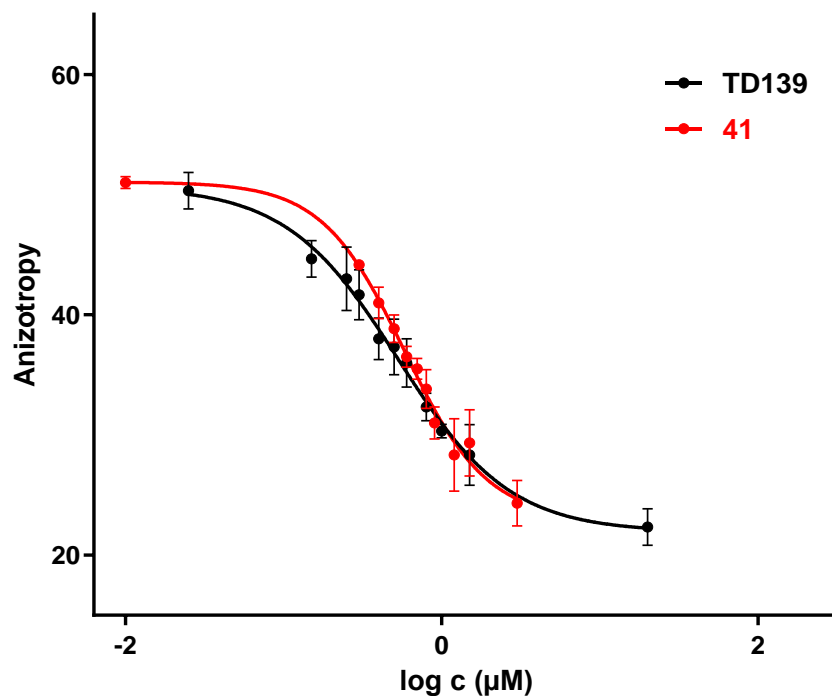
Figure S12. Fluorescence polarization titration curves of unsymmetrical thiodigalactoside-based inhibitors **41** and **TD139** with human galectin-1.
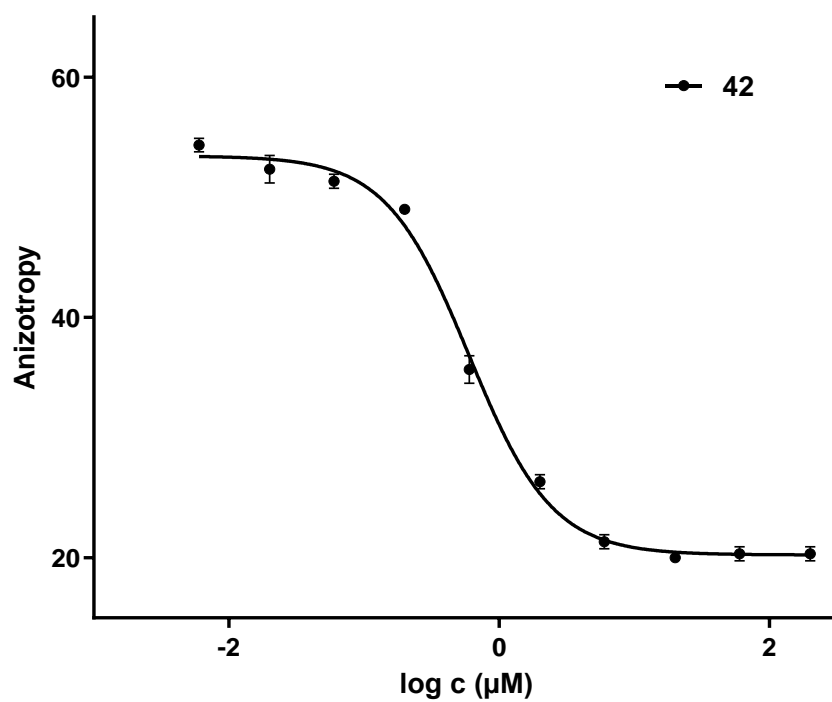
Figure S13. Fluorescence polarization titration curves of unsymmetrical thiodigalactoside-based inhibitor **42**.
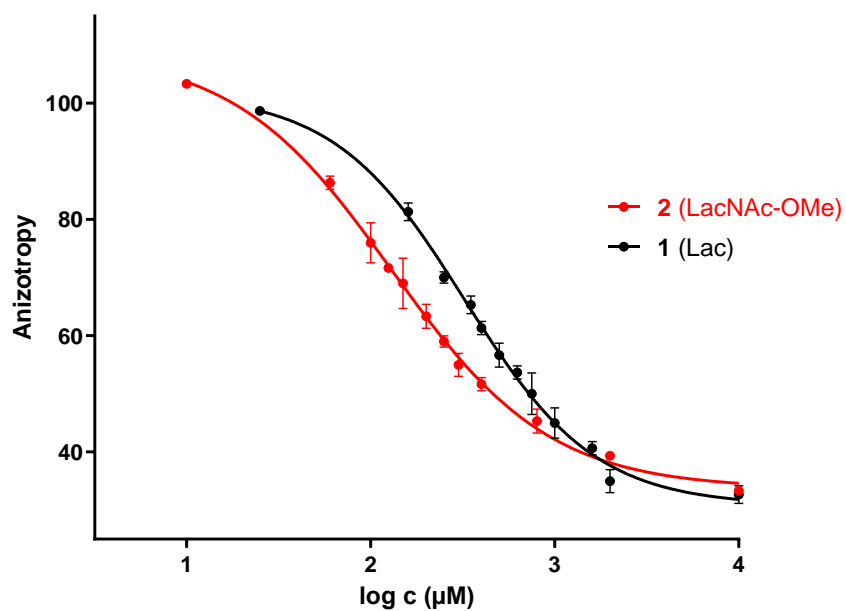
Figure S14. Fluorescence polarization titration curves of **1** and **2**β-OMe with human galectin-3-CRD.
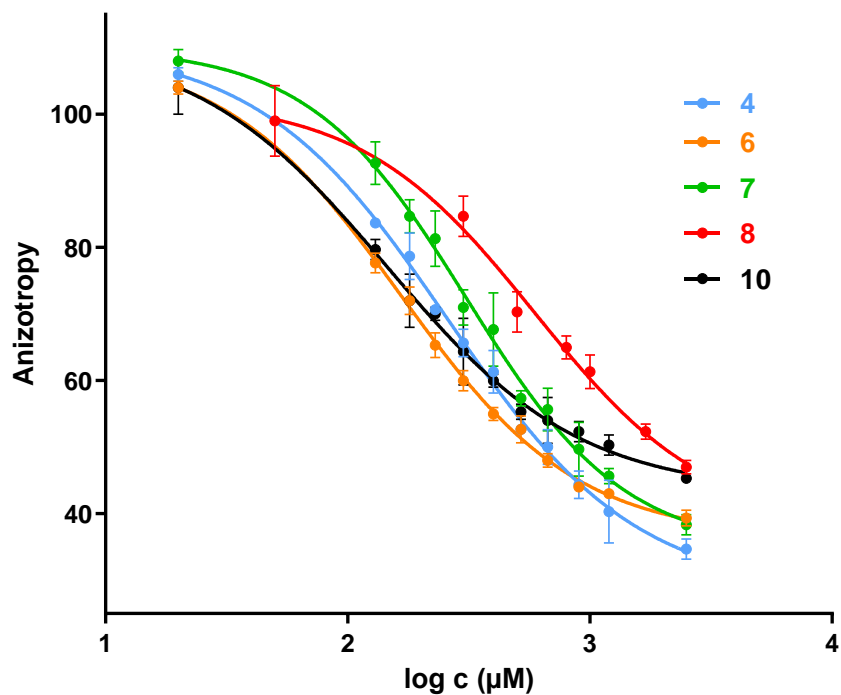
Figure S15. Fluorescence polarization titration curves of lactose-based inhibitors **4**, **6**, **7**, **8**, and **10** with human galectin-3-CRD.
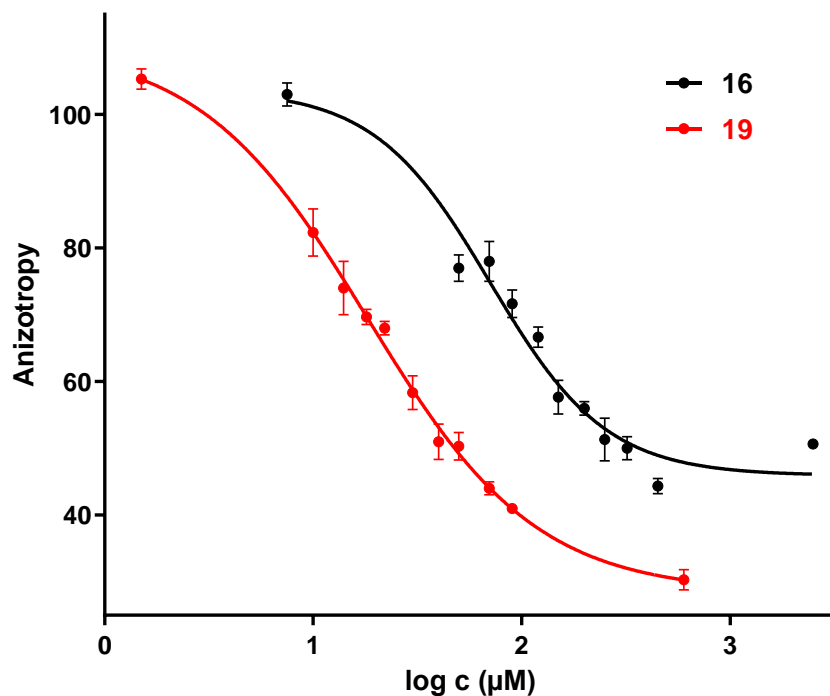
Figure S16. Fluorescence polarization titration curves of 1- and 2′-ferrocene modified *N*-acetyllactosamine inhibitors **16** and **19** with human galectin-3-CRD.
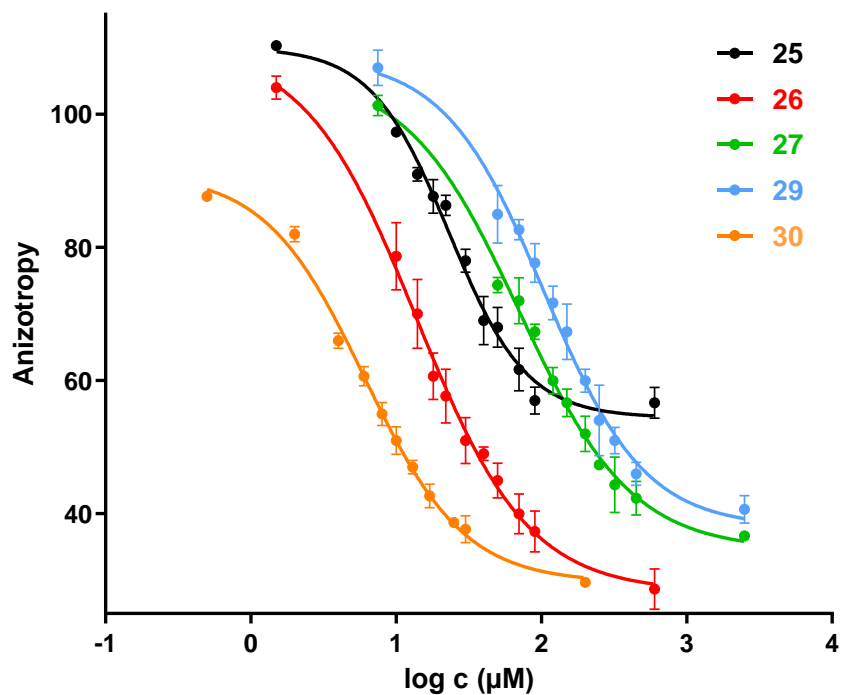
Figure S17. Fluorescence polarization titration curves of 3′- modified *N*-acetyllactosamine-based inhibitors **25–27**, **29**, and **30** with human galectin-3-CRD.
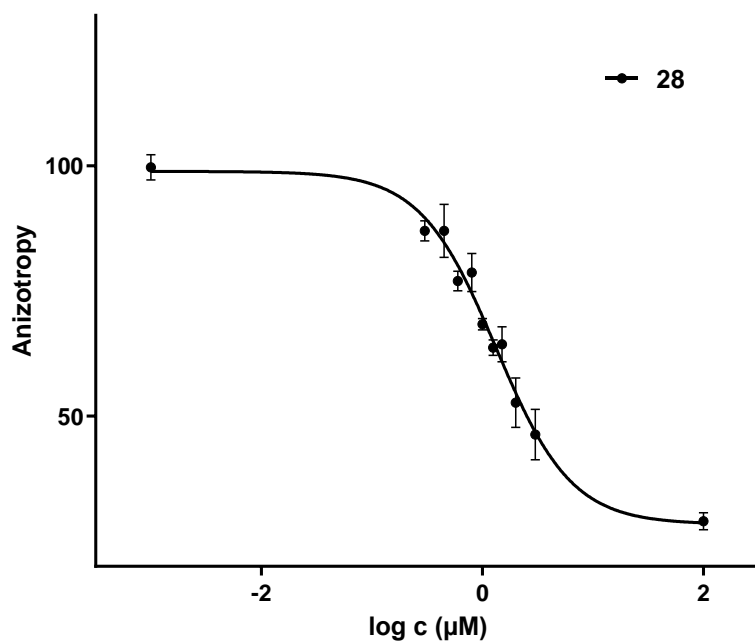
Figure S18. Fluorescence polarization titration curves of inhibitor **28** with human galectin-3-CRD.
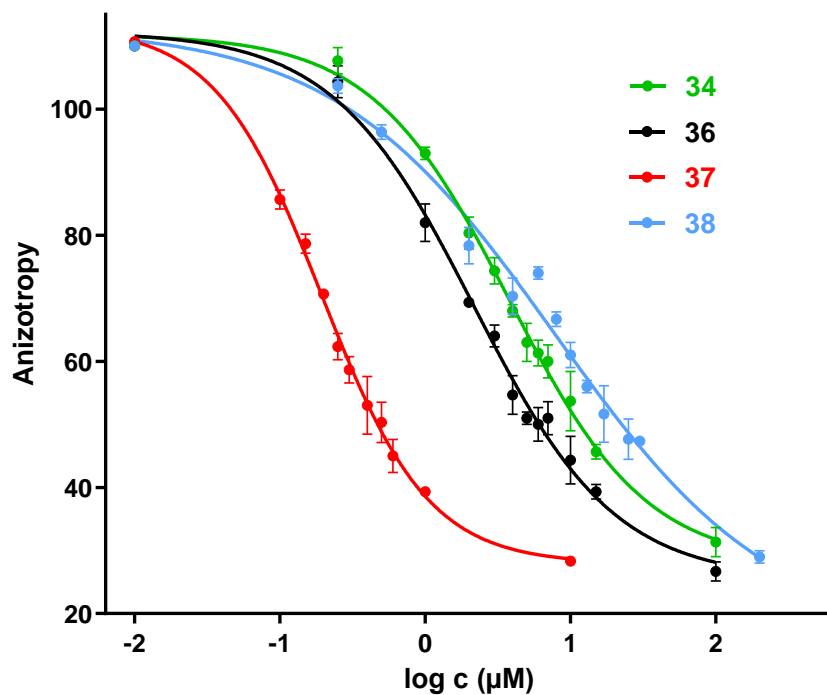
Figure S19. Fluorescence polarization titration curves of thiodigalactoside-based inhibitors **34**, **36–38** with human galectin-3-CRD.
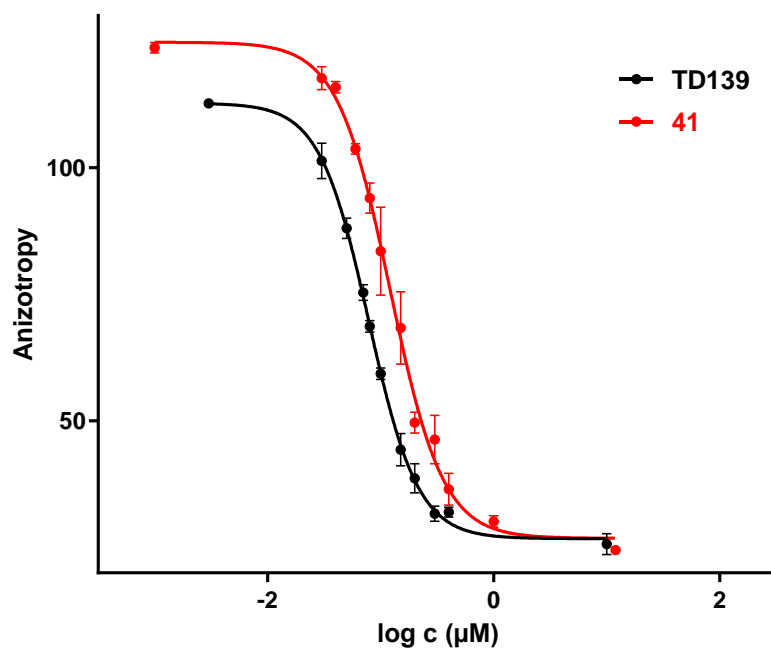
Figure S20. Fluorescence polarization titration curves of unsymmetrical thiodigalactoside-based inhibitors **41** and **TD139** with human galectin-3-CRD.
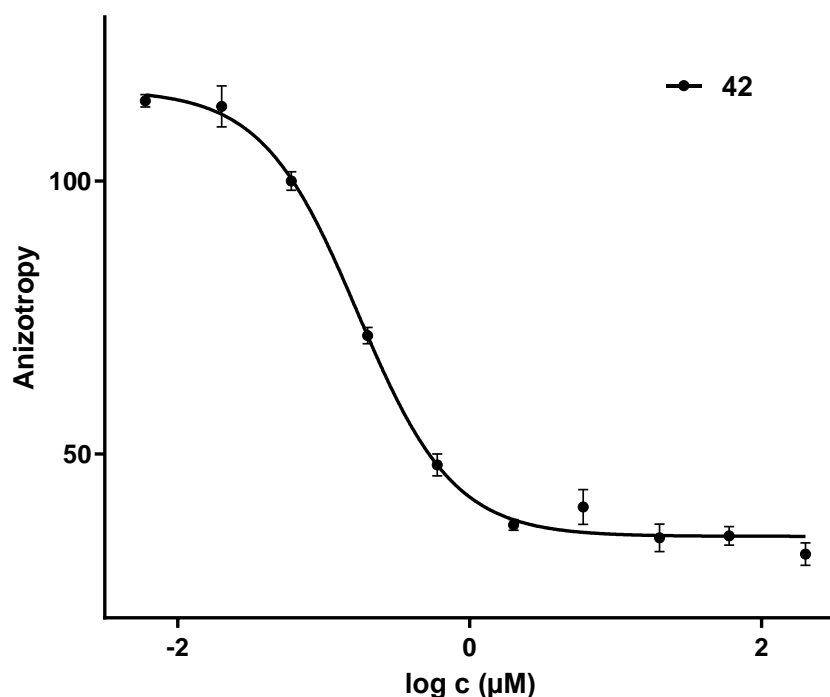
Figure S21. Fluorescence polarization titration curves of unsymmetrical thiodigalactoside-based inhibitor **42** with human galectin-3-CRD.

Intrinsic tryptophan fluorescence

The excitation of 9 μM Gal-1, resp. 3 μM Gal-3, in phosphate-buffered saline (PBS) (pH = 7.4) with 6 mM trehalose, was done at 285 nm, and emission spectra were recorded from 302 to 400 nm. All emission spectra were registered using an ISS PC1 photon counting spectrofluorometer (ISS, USA) in a quartz cuvette with a 1 cm path length and at a temperature of 25 °C. The excitation and emission slit widths were fixed at 4 nm each. Fluorescence intensity was normalized; the fluorescence intensity maximum of $h$gal-1/$h$gal-3 with saccharide compound, I_A, was subtracted from the fluorescence intensity maximum of free galectin titrated with an adequate amount of PBS, I_B. The obtained value was divided by the fluorescence intensity max of free $h$gal, i.e. $(I_B-I_A)/I_B$. The binding constant, K_D value, was calculated using the One Site -Specific Binding's model ($Y=B_{max}*X)/(K_D +X)$, where X is the ligand concentration, Y is the fluorescence intensity, B_{max} is the maximum specific binding and K_D is the equilibrium binding constant) in Origin Software.[23] The titration curves are shown in the Figs. S22–S55.
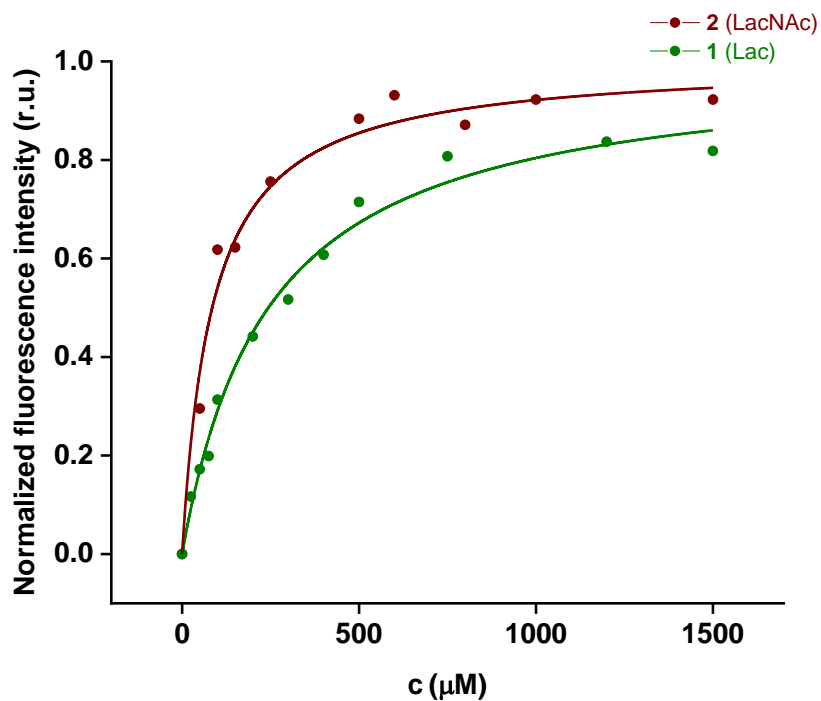
Figure S22. Normalized fluorescence intensity of *h*gal-1 with lactose (**1**) and *N*-acetyllactosamine (**2**).
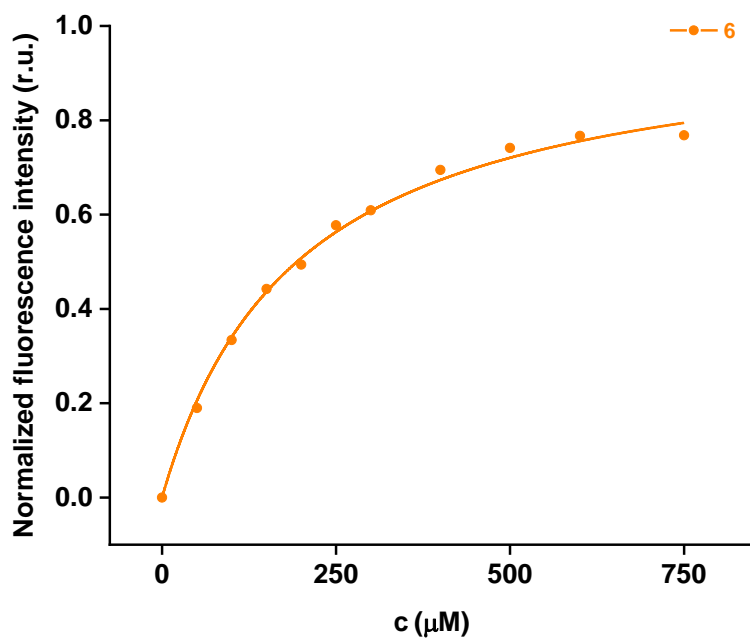
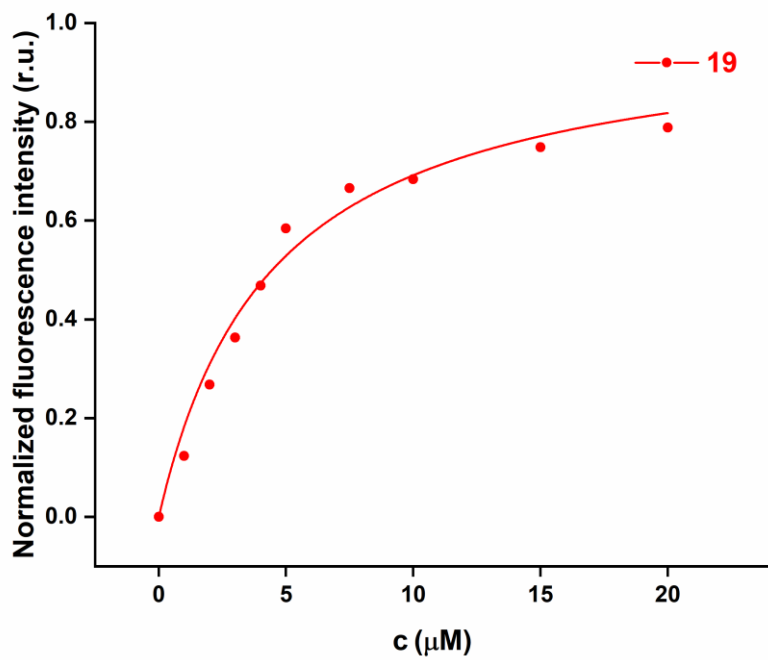**Figure S23**. Normalized fluorescence intensity of *h*gal-1 with **6.**
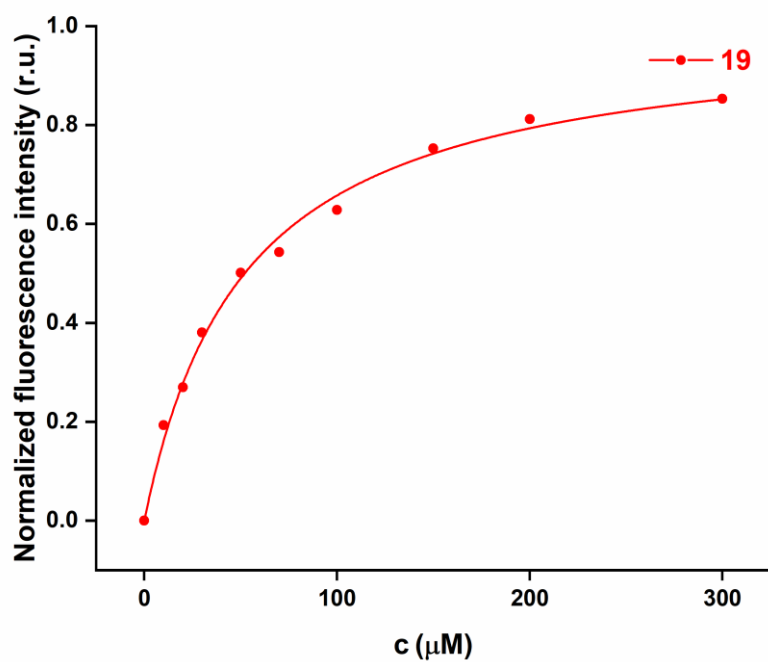
Figure S24. Normalized fluorescence intensity of *h*gal-1 with **19.**
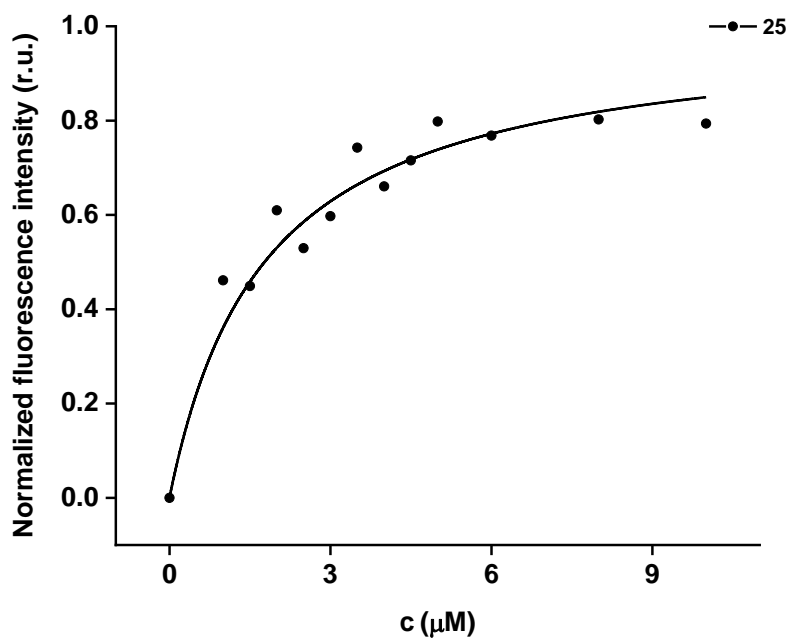
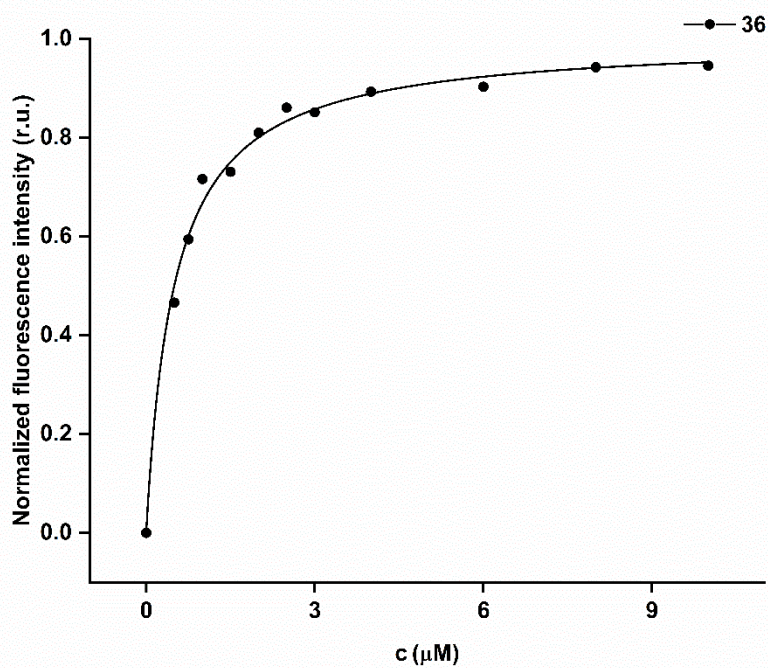**Figure S25**. Normalized fluorescence intensity of *h*gal-1with **25.**
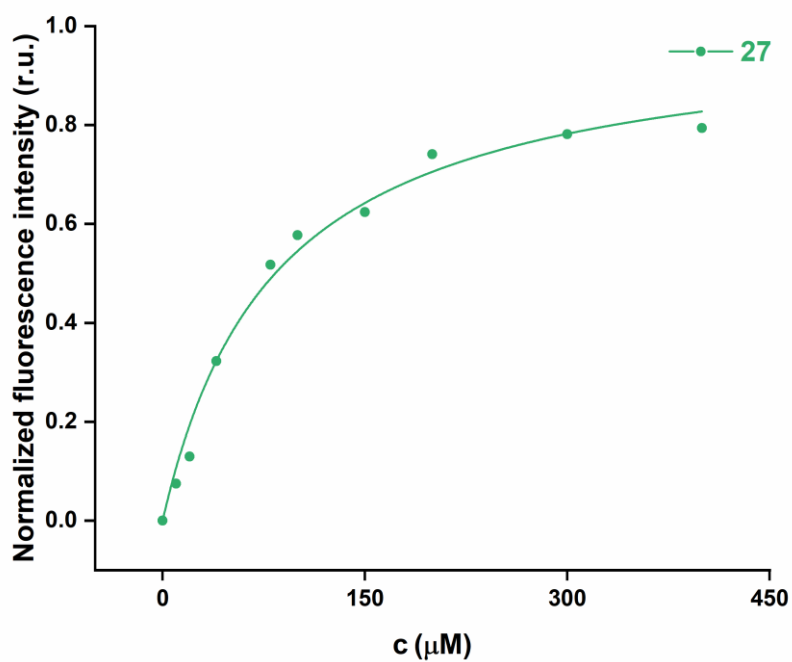
Figure S26. Normalized fluorescence intensity of *h*gal-1with **27.**
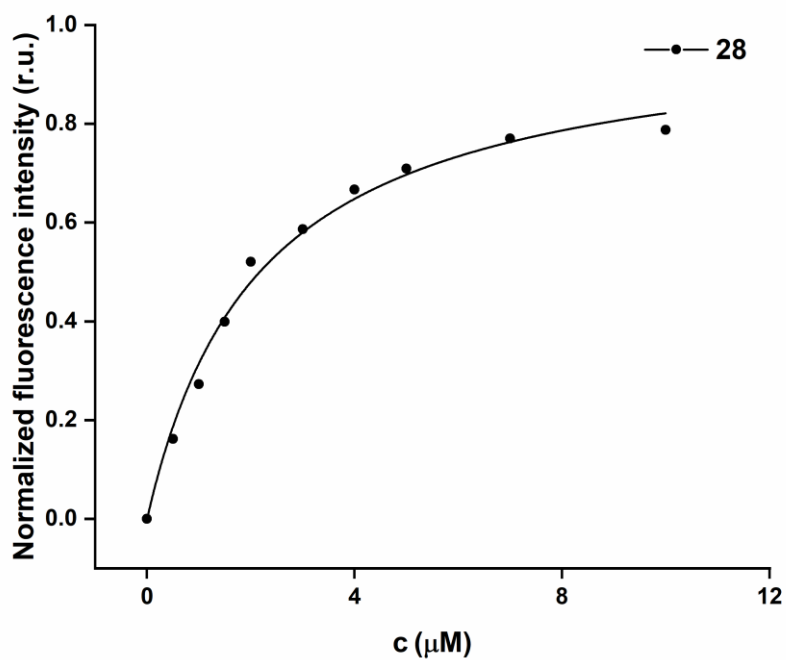
Figure S27. Normalized fluorescence intensity of *h*gal-1with **28.**
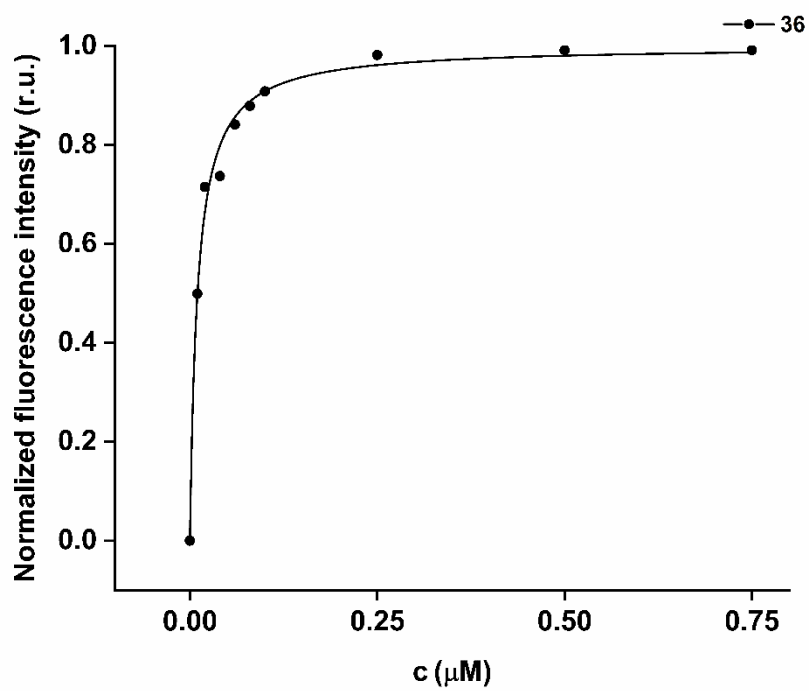
Figure S28. Normalized fluorescence intensity of *h*gal-1with **36.**
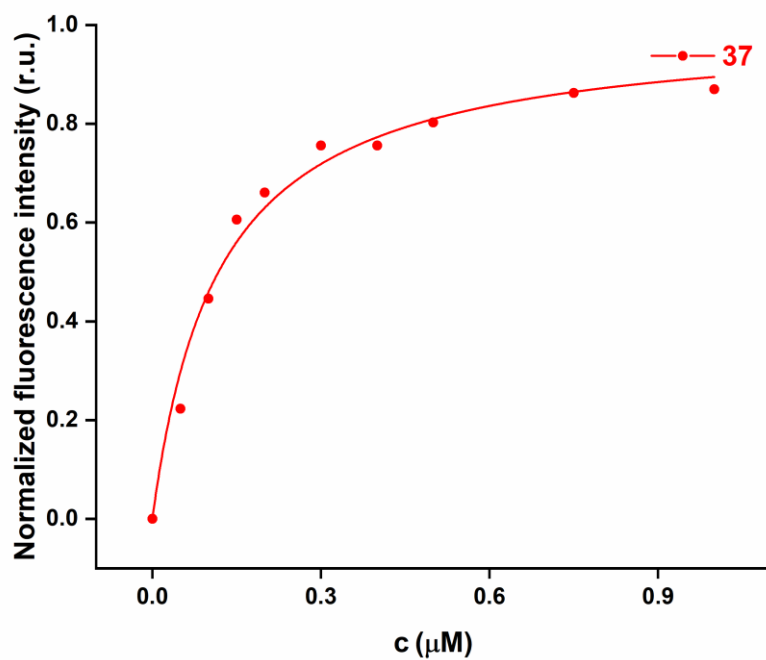
Figure S29. Normalized fluorescence intensity of *h*gal-1with **37.**
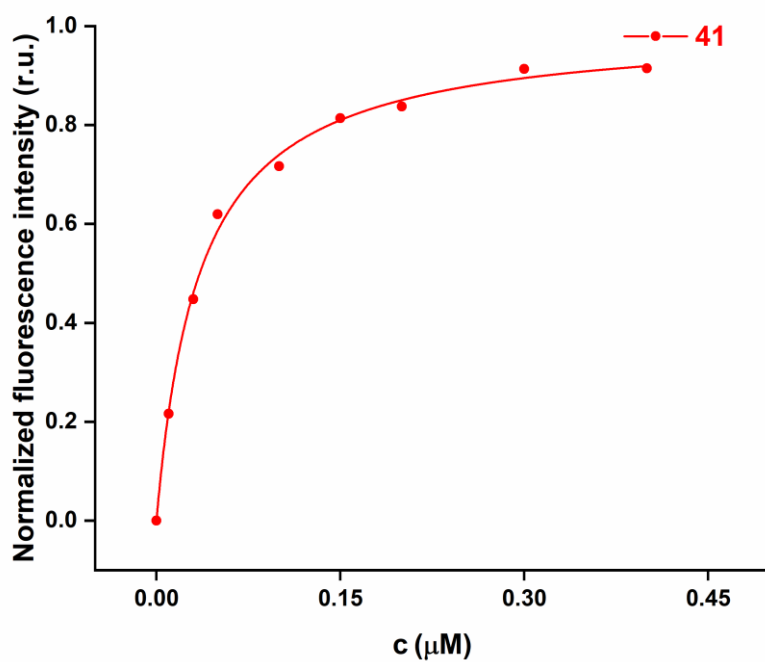
Figure S30. Normalized fluorescence intensity of *h*gal-1with **41.**
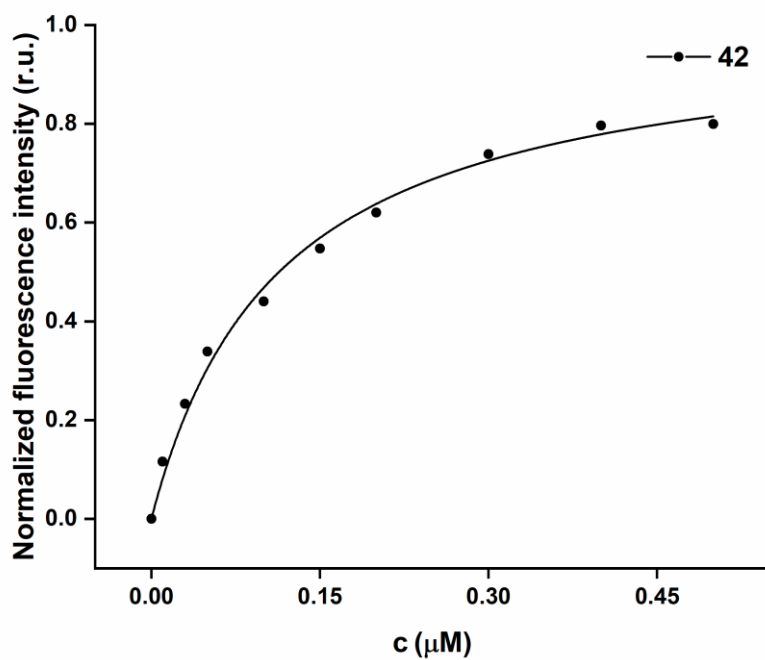
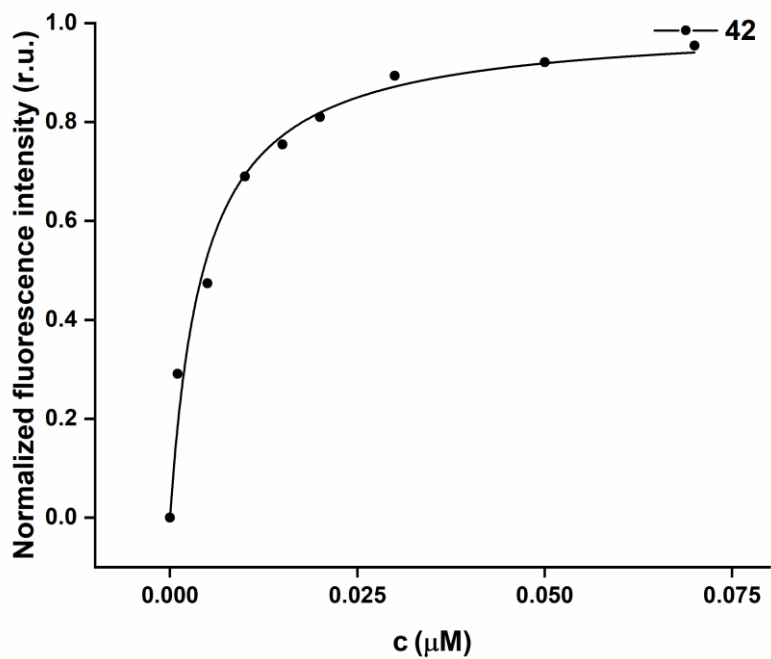**Figure S31**. Normalized fluorescence intensity of *h*gal-1with **42.**
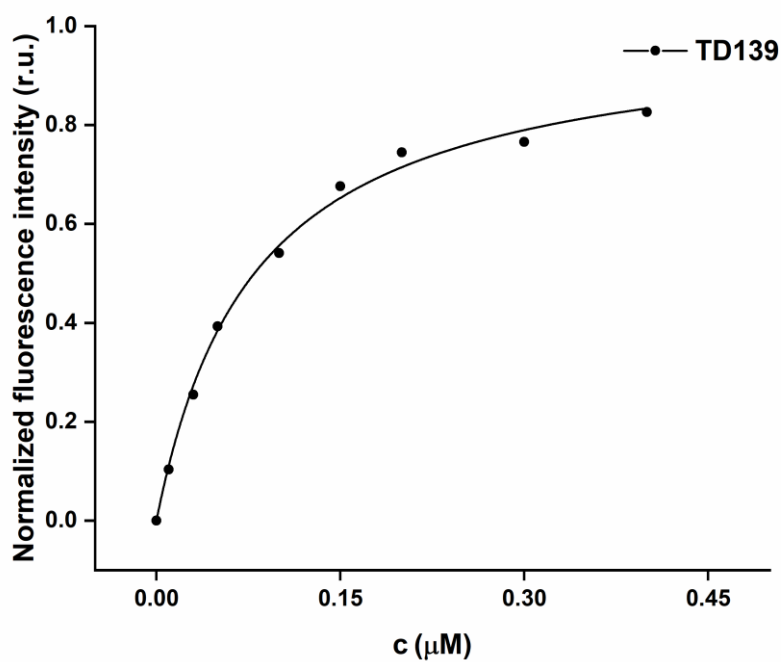
Figure S32. Normalized fluorescence intensity of *h*gal-1with **TD139.**
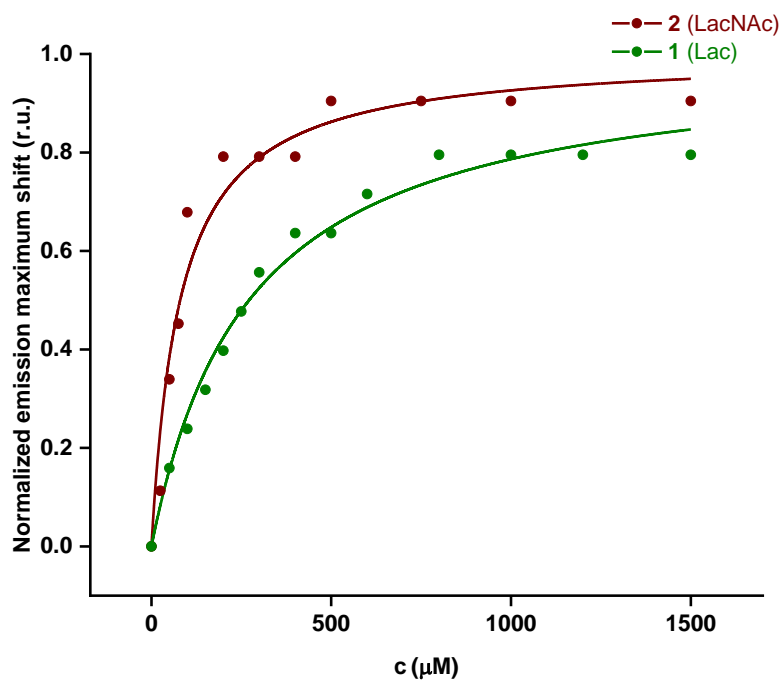
Figure S33. Normalized fluorescence intensity of full-length *h*gal-3 with lactose (**1**) and *N*-acetyllactosamine (**2**).
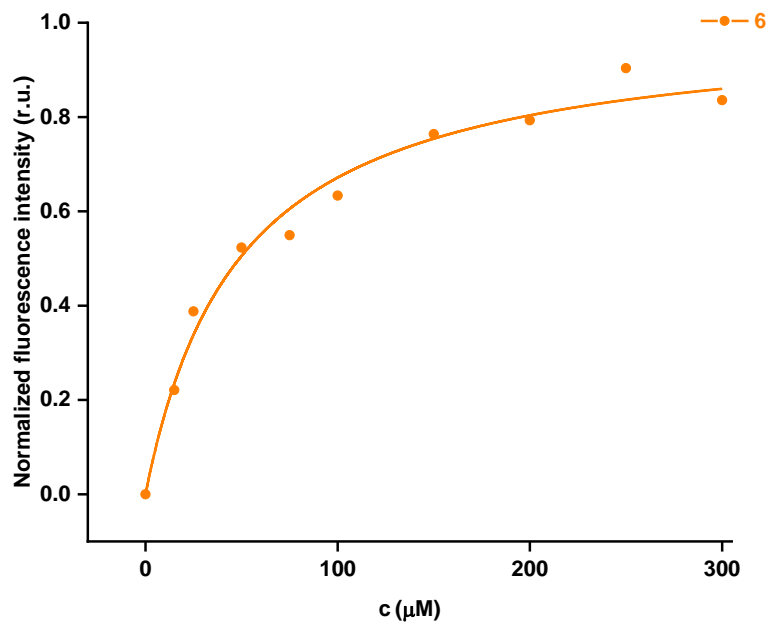
Figure S34. Normalized fluorescence intensity of full-length *h*gal-3with **6.**

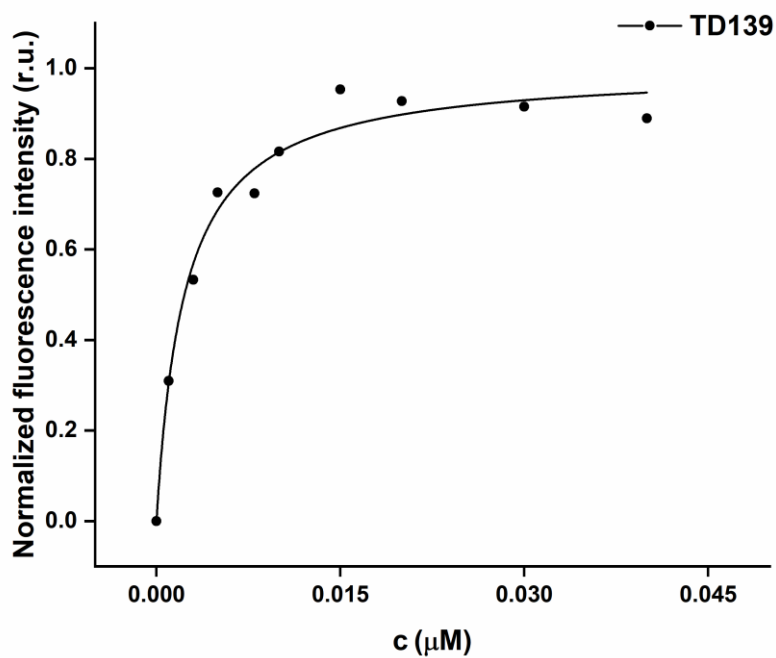**Figure S35**. Normalized fluorescence intensity of full-length *h*gal-3with **19.**
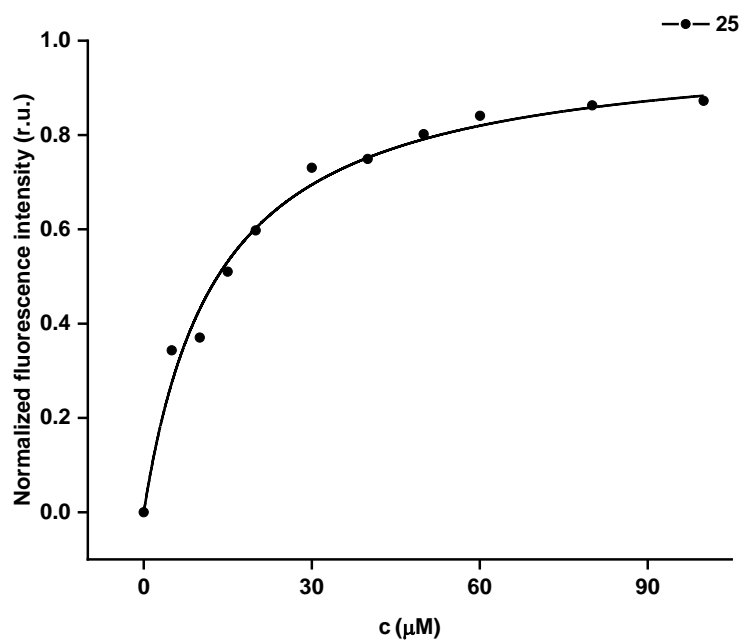
Figure S36. Normalized fluorescence intensity of full-length *h*gal-3with **25**.
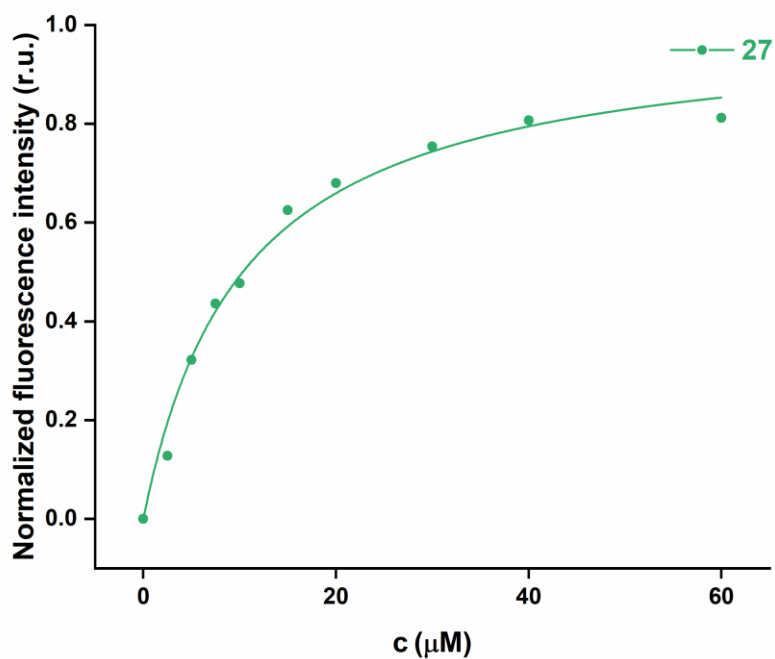
Figure S37. Normalized fluorescence intensity of full-length *h*gal-3with **27**.
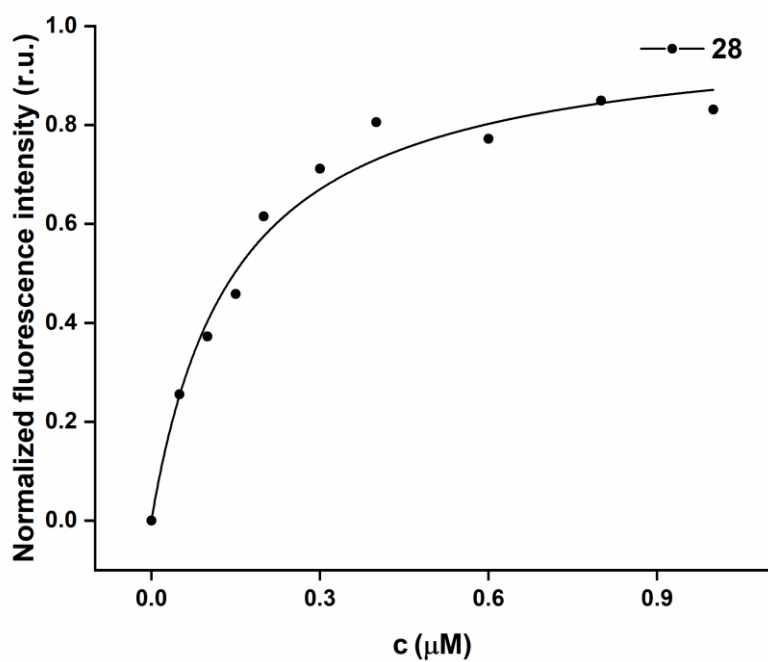
Figure S38. Normalized fluorescence intensity of full-length *h*gal-3with **28**.

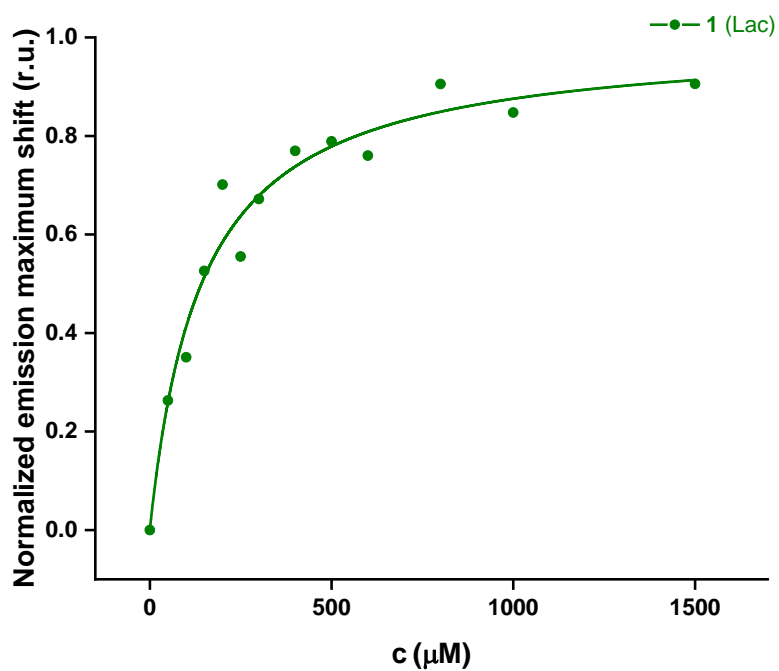**Figure S39**. Normalized fluorescence intensity of full-length *h*gal-3with **36**.
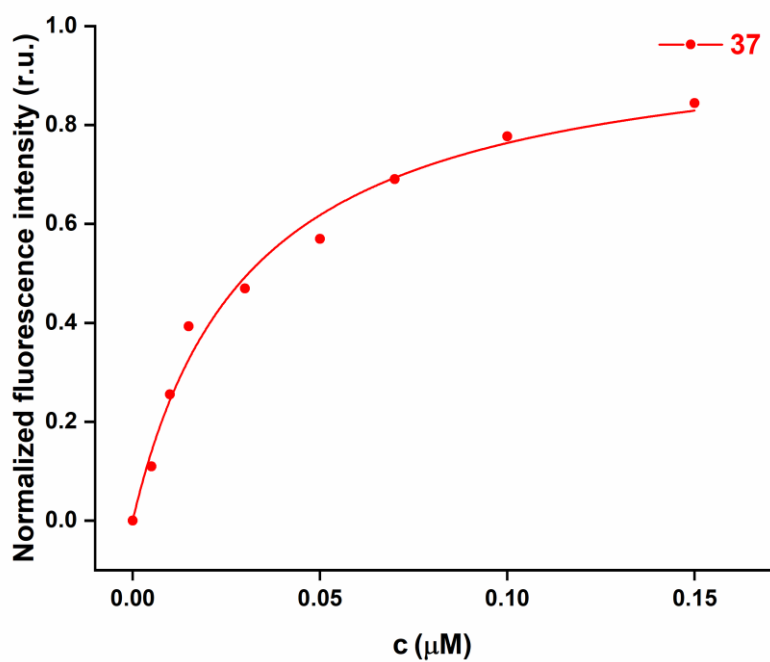
Figure S40. Normalized fluorescence intensity of full-length *h*gal-3with **37**.
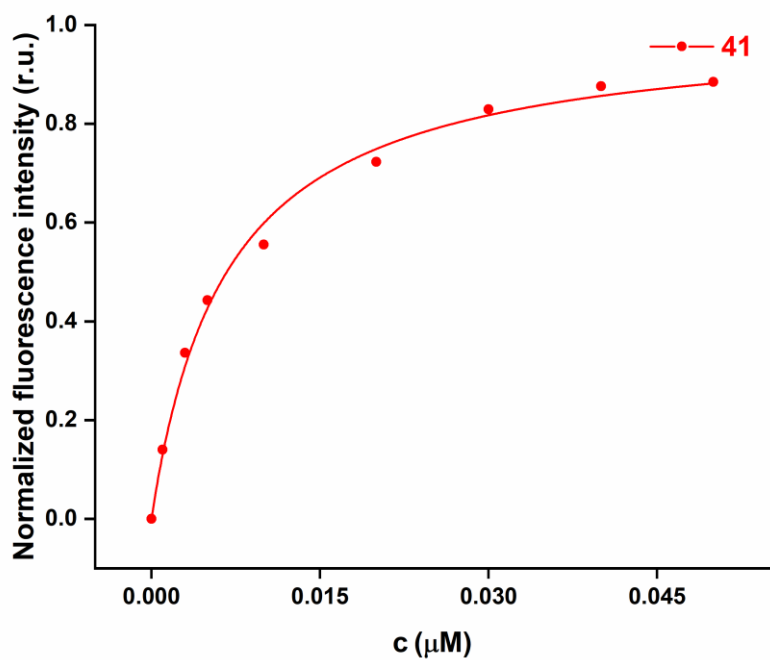
Figure S41. Normalized fluorescence intensity of full-length *h*gal-3with **41**.

Figure S42. Normalized fluorescence intensity of full-length *h*gal-3with **42**.

Figure S43. Normalized fluorescence intensity of full-length *h*gal-3with **TD139**.

Figure S44. Normalized fluorescence intensity of *h*gal-3-CRD with lactose (**1**).
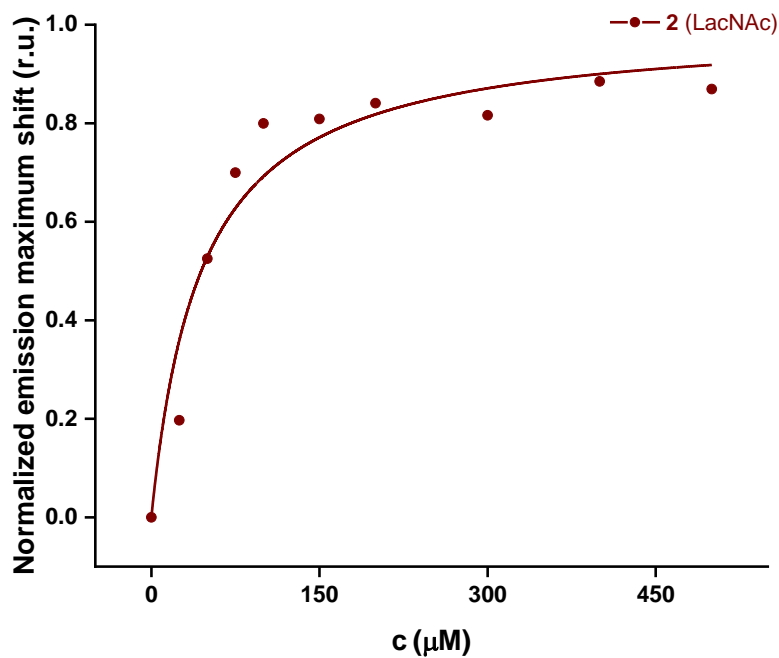
Figure S45. Normalized fluorescence intensity of *h*gal-3-CRD with N-acetyllactosamine (**2**).
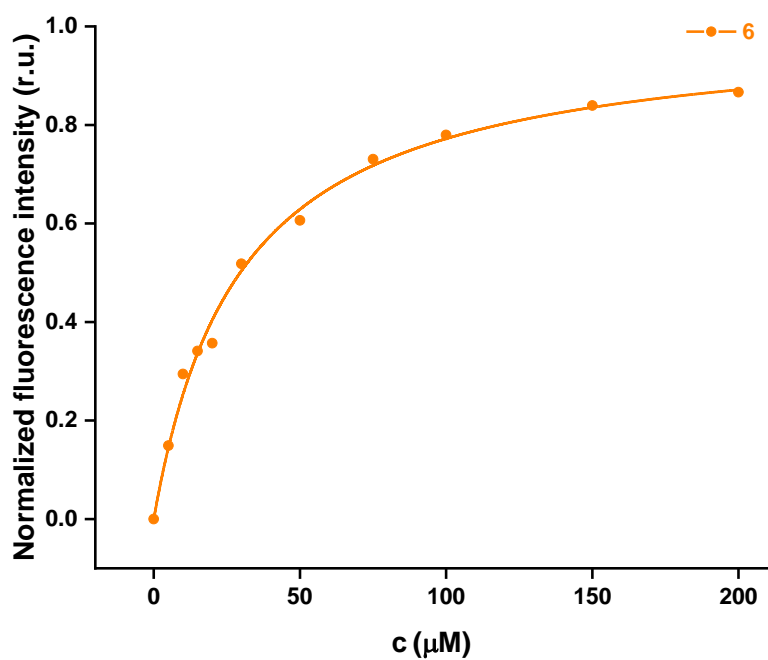
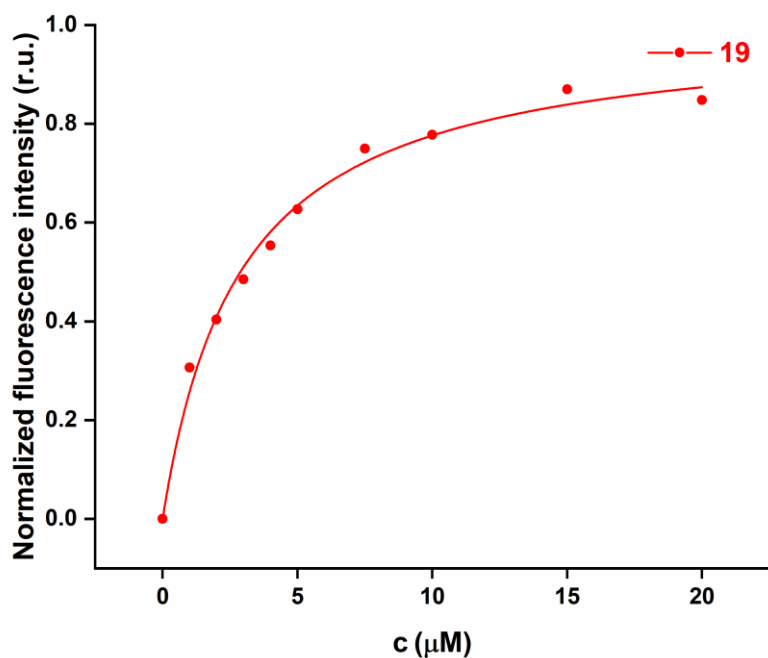**Figure S46**. Normalized fluorescence intensity of *h*gal-3-CRD with **6**.

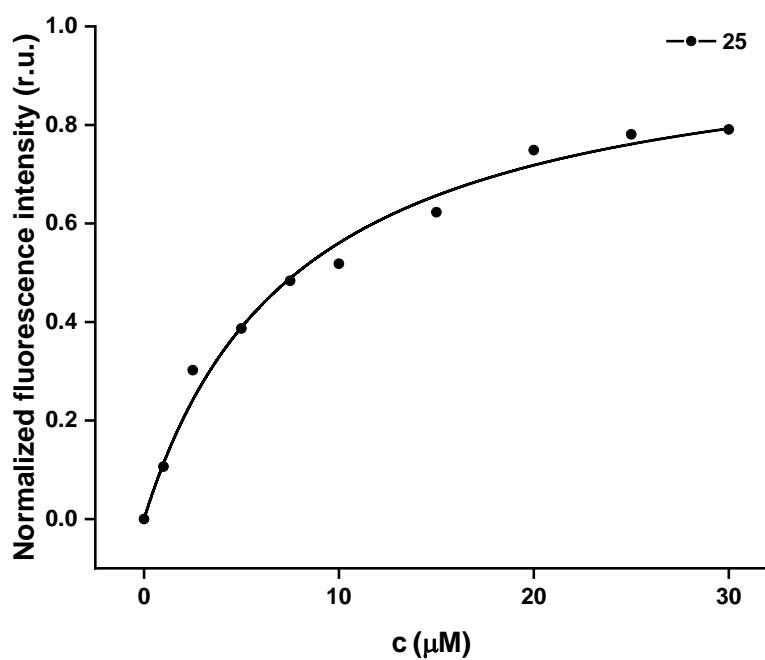**Figure S47**. Normalized fluorescence intensity of *h*gal-3-CRD with **19**.

Figure S48. Normalized fluorescence intensity of *h*gal-3-CRD with **25**.
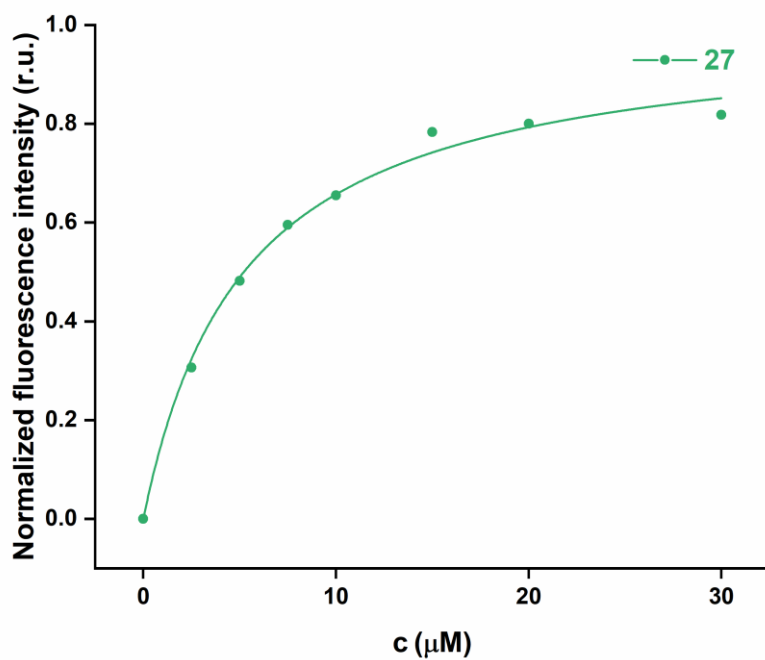

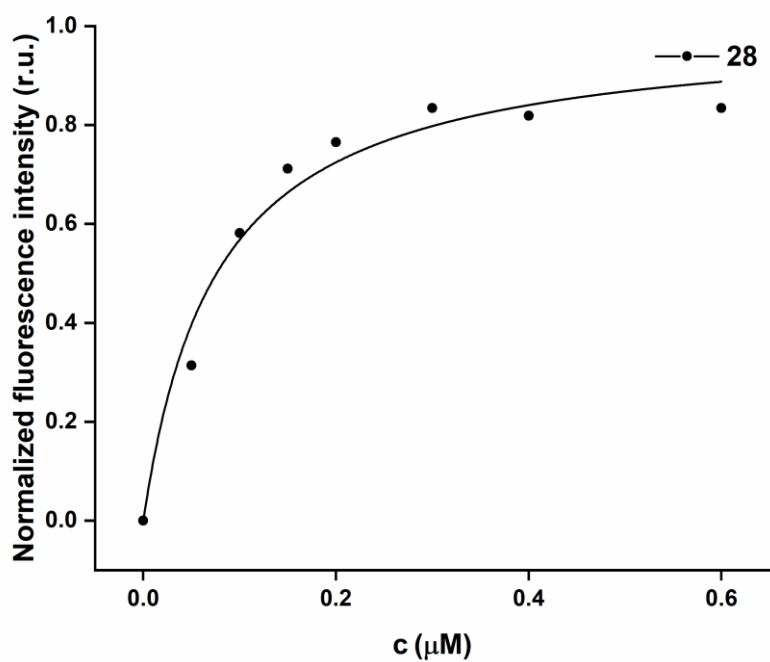**Figure S49**. Normalized fluorescence intensity of *h*gal-3-CRD with **27**.

Figure S50. Normalized fluorescence intensity of *h*gal-3-CRD with **28**.

Figure S51. Normalized fluorescence intensity of *h*gal-3-CRD with **36**.

Figure S52. Normalized fluorescence intensity of *h*gal-3-CRD with **37**.

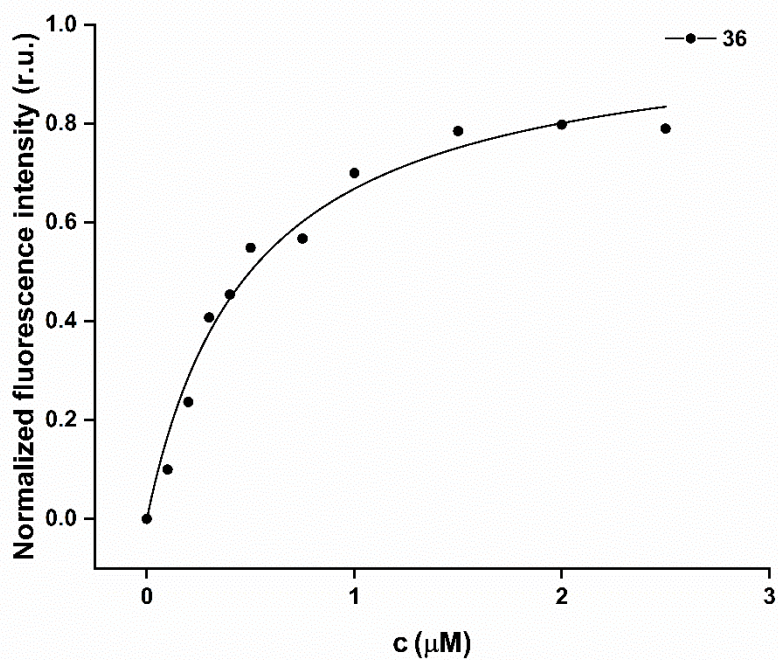**Figure S53**. Normalized fluorescence intensity of *h*gal-3-CRD with **41**.

Figure S54. Normalized fluorescence intensity of *h*gal-3-CRD with **42**.

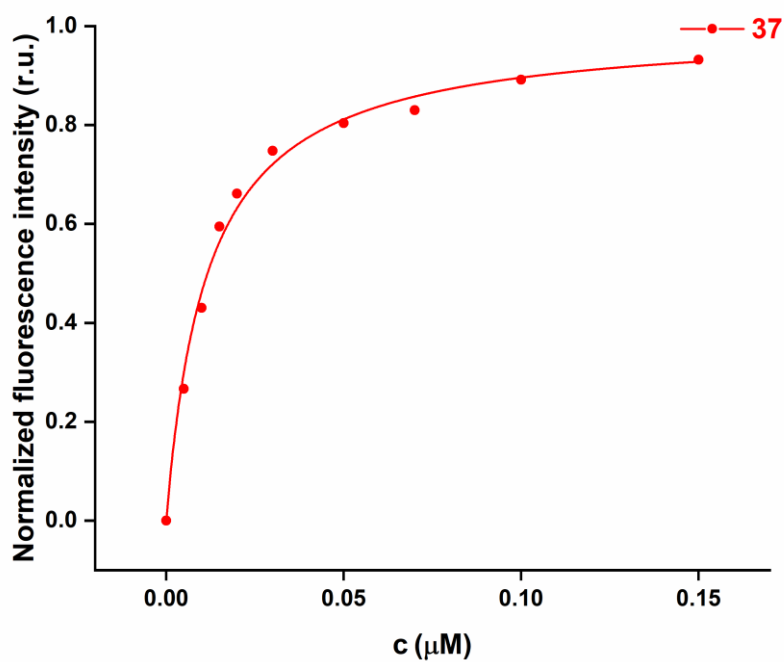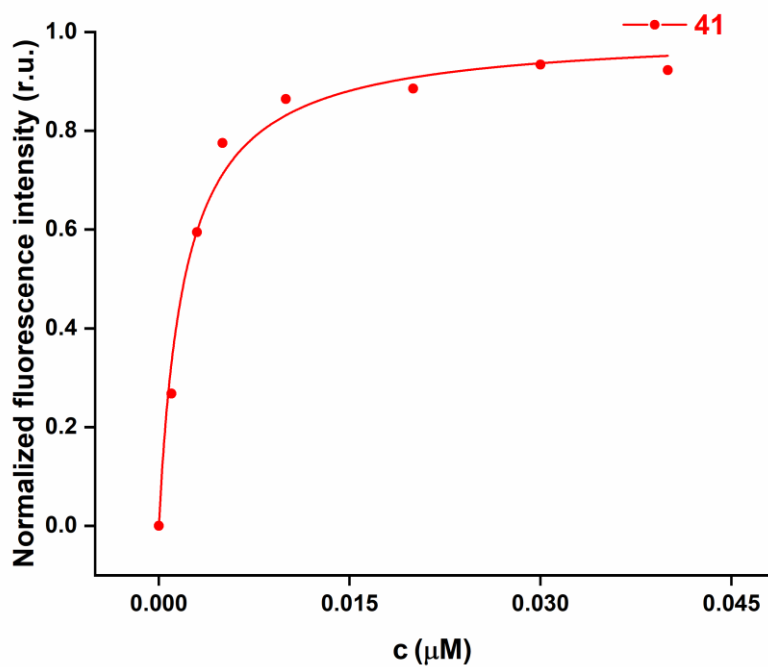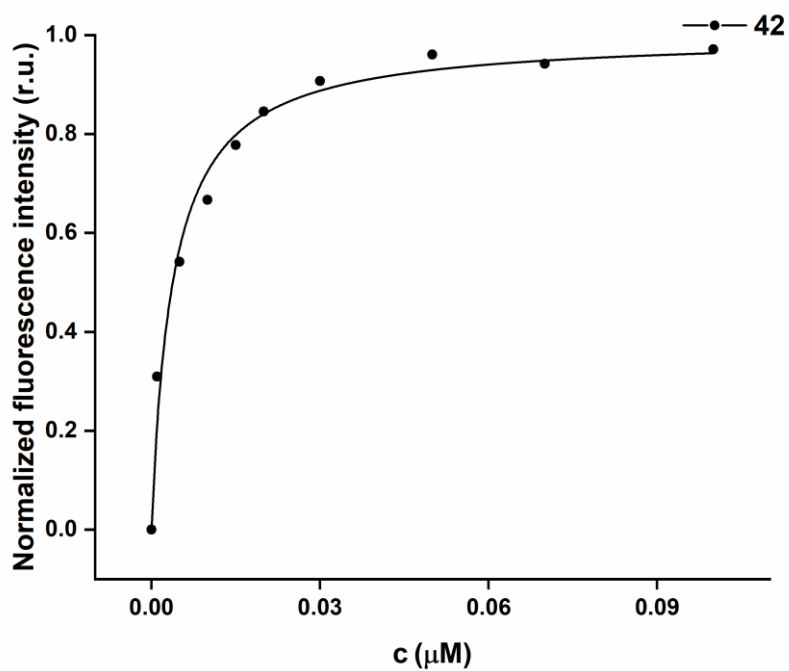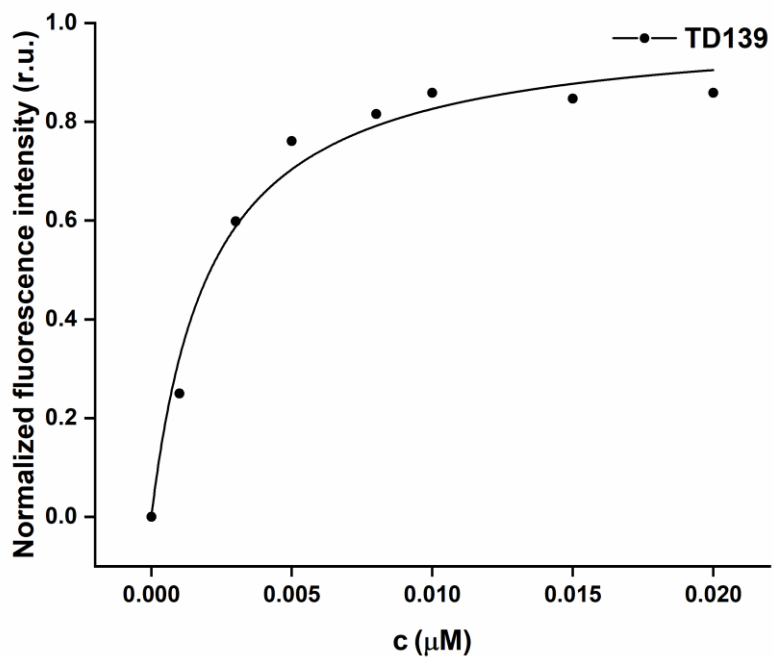**Figure S55**. Normalized fluorescence intensity of *h*gal-3-CRD with **TD139**.

S59

Isothermal titration calorimetry (ITC)

ITC experiments were performed analogically to the procedures reported in lit.[24] in dialysate buffer (25 mM Tris-HCl pH 8.0, 300 mM NaCl and 1mM TCEP). All samples were filtered with 0.22 μm cutoff filters (Millipore) and extensively degassed with stirring prior to use. ITC was performed using MICROCAL PEAQ-ITC (Malvern Instruments Ltd., United Kingdom) at 298 K. The tested compounds were dissolved in DMSO and diluted with prepared buffer to ligand concentration 200–500 μM. The stock protein solution was diluted with the prepared buffer to protein concentration 9–25 μM. The exact concentration used for each experiment is shown in tables S5–S28, heat changes and data fits are shown in Figs. S56–S77. The DMSO concentration in the inject tant and protein solution was matched to 1.5%. The titration experiment consisted of 19 injections of 2.0 μL ligand solution into cell with approx. 300 μL of protein solution. MICROCAL PEAQ-ITC Analysis Software (Malvern Instruments Ltd., United Kingdom) was used for the curve fitting of the experimental data as well as for calculation of the thermodynamic data. Measurement of all tested compounds was done in duplicates.

Table S5. Data for the isothermal titration calorimetry of **TD139** with $h$gal-1, 1st experiment.

c_{TD139} (μM)	c_{Gal-1} (μM)	K_d (μM)	ΔG (kcal/mol)	ΔH (kcal/mol)	$-T\Delta S$ (kcal/mol)	n
100	9	0.279	−8.9	−16.6	7.6	1.05

Figure S56. Raw heat and ΔH graphs of the isothermal titration calorimetry of **TD139** with $h$gal-1, 1st experiment.

Table S6. Data for the isothermal titration calorimetry of **TD139** with $h$gal-1, 2nd experiment.

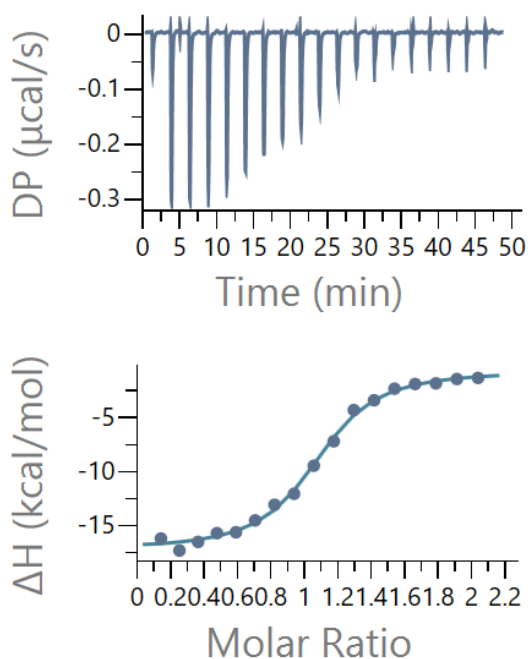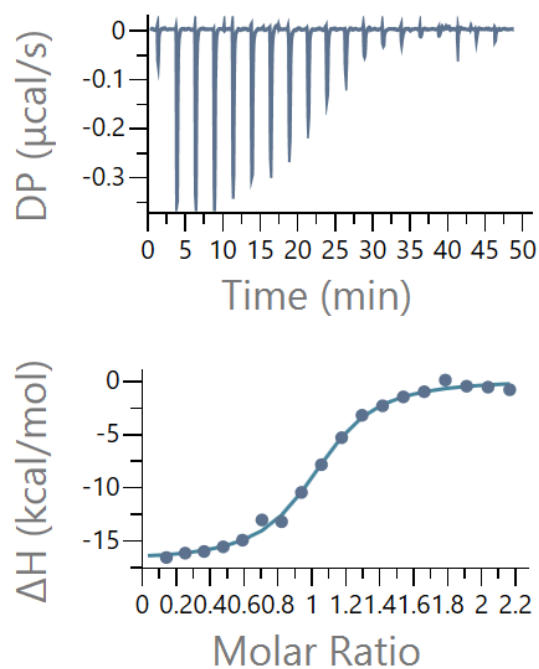| c_{TD139} (µM)	c_{Gal-1} (µM)	K_d (µM)	ΔG (kcal/mol)	ΔH (kcal/mol)	$-T\Delta S$ (kcal/mol)	n
100	9	0.278	−8.9	−17.1	8.2	1.00

Figure S57. Raw heat and ΔH graphs of the isothermal titration calorimetry of **TD139** with $h$gal-1, 2nd experiment.

Table S7. Data for the isothermal titration calorimetry of **25** with *h*gal-1, 1st experiment with n set to 1.00.

c_{25} (μM)	c_{Gal-1} (μM)	K_d (μM)	ΔG (kcal/mol)	ΔH (kcal/mol)	$-T\Delta S$ (kcal/mol)	n
300	25	10.5	−6.8	ND*	ND*	1.00

*ND = not determined.

Figure S58: Raw heat and ΔH graphs of the isothermal titration calorimetry of **25** with *h*gal-1, 1st experiment.

Table S8: Data for the isothermal titration calorimetry of **25** with *h*gal-1, 2nd experiment with n set to 1.00.

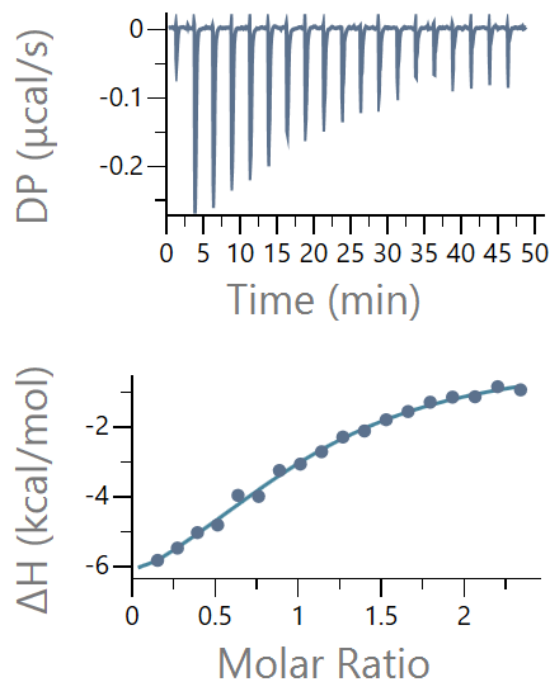| c_{25} (µM)	c_{Gal-1} (µM)	K_d (µM)	ΔG (kcal/mol)	ΔH (kcal/mol)	$-T\Delta S$ (kcal/mol)	n
300	25	13.3	−6.7	ND*	ND*	1.00

*ND = not determined.
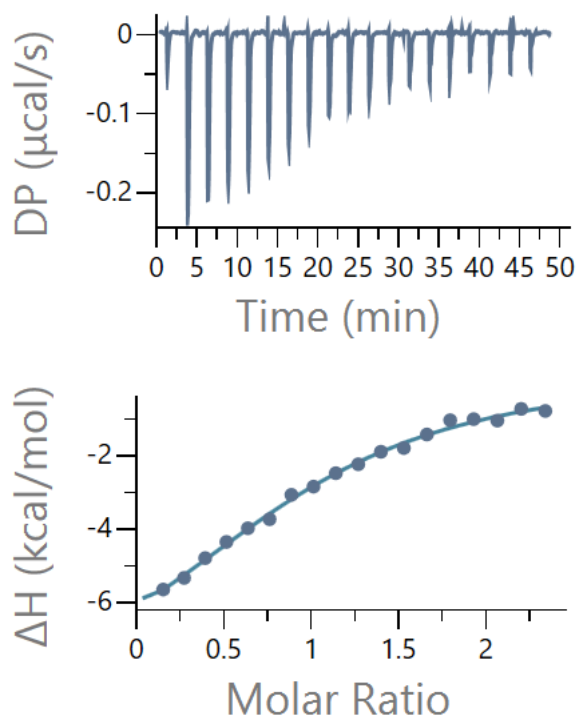
Figure S59. Raw heat and ΔH graphs of the isothermal titration calorimetry of **25** with *h*gal-1, 2nd experiment.

Table S9: Data for the isothermal titration calorimetry of **36** with *h*gal-1, 1st experiment.

c_{35} (µM)	c_{Gal-1} (µM)	K_d (µM)	ΔG (kcal/mol)	ΔH (kcal/mol)	$-T\Delta S$ (kcal/mol)	n
200	12	0.261	−9.0	−13.8	4.9	1.00

The raw heat and ΔH graphs of this titration are shown in the main text.

Table S10: Data for the isothermal titration calorimetry of **36** with *h*gal-1, 2ⁿᵈ experiment.

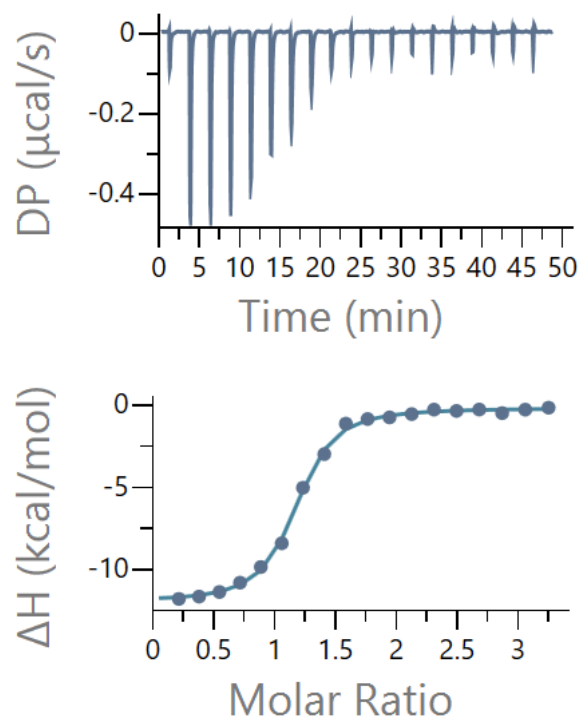| c_{35} (μM)	c_{Gal-1} (μM)	K_d (μM)	ΔG (kcal/mol)	ΔH (kcal/mol)	−TΔS (kcal/mol)	n
200	12	0.255	−9.0	−11.8	2.8	1.11

Figure S60. Raw heat and ΔH graphs of the isothermal titration calorimetry of **36** with *h*gal-1, 2ⁿᵈ experiment.

Table S11: Data for the isothermal titration calorimetry of **37** with *h*gal-1, 1st experiment.

c_{36} (μM)	$c_{\text{Gal-1}}$ (μM)	K_d (μM)	ΔG (kcal/mol)	ΔH (kcal/mol)	$-T\Delta S$ (kcal/mol)	n
200	15	0.292	−8.9	−9.2	0.3	1.03

Figure S61. Raw heat and ΔH graphs of the isothermal titration calorimetry of **37** with *h*gal-1, 1st experiment.

Table S12: Data for the isothermal titration calorimetry of **37** with *h*gal-1, 2nd experiment.

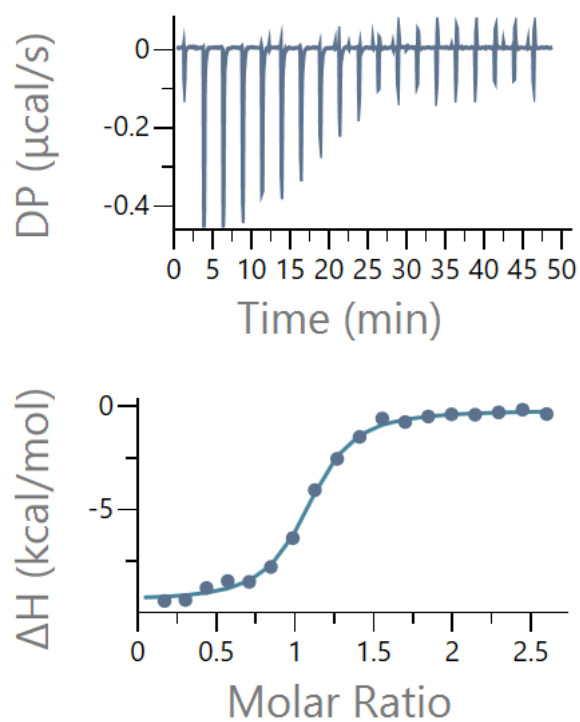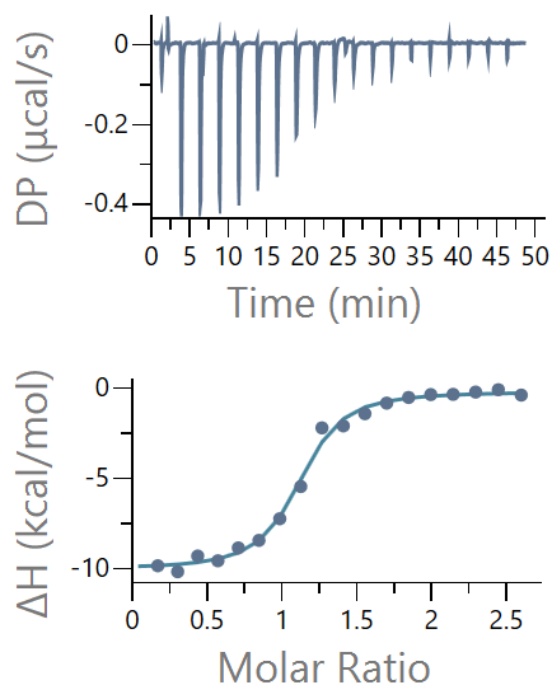| c_{36} (µM)	c_{Gal-1} (µM)	K_d (µM)	ΔG (kcal/mol)	ΔH (kcal/mol)	$-T\Delta S$ (kcal/mol)	n
200	15	0.284	−8.9	−9.9	0.9	1.06

Figure S62. Raw heat and ΔH graphs of the isothermal titration calorimetry of **37** with *h*gal-1, 2nd experiment.

Table S13: Data for the isothermal titration calorimetry of **41** with *h*gal-1, 1st experiment.

c_{41} (µM)	c_{Gal-1} (µM)	K_d (µM)	ΔG (kcal/mol)	ΔH (kcal/mol)	$-T\Delta S$ (kcal/mol)	n
200	11	0.326	−8.9	−10.2	1.3	1.03

Figure S63. Raw heat and ΔH graphs of the isothermal titration calorimetry of **41** with *h*gal-1, 1st experiment.

Table S14: Data for the isothermal titration calorimetry of **41** with *h*gal-1, 2nd experiment.

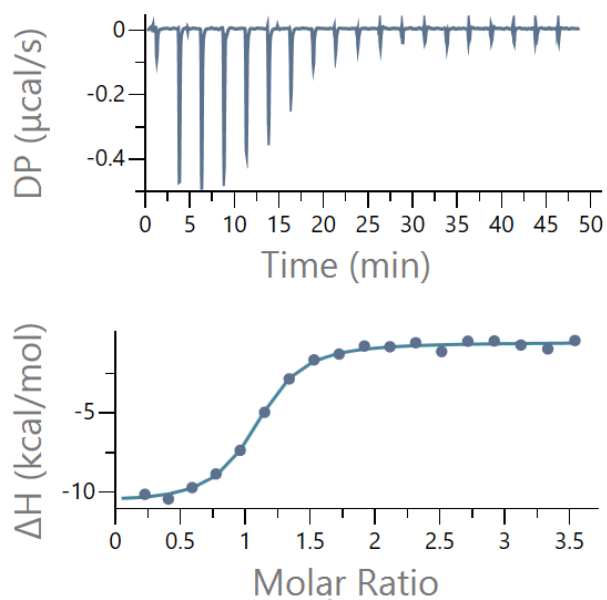| c_{41} (µM)	c_{Gal-1} (µM)	K_d (µM)	ΔG (kcal/mol)	ΔH (kcal/mol)	$-T\Delta S$ (kcal/mol)	n
200	15	0.353	−8.8	−10.1	1.3	1.03

Figure S64. Raw heat and ΔH graphs of the isothermal titration calorimetry of **41** with *h*gal-1, 2nd experiment.

Table S15: Data for the isothermal titration calorimetry of **42** with *h*gal-1, 1st experiment.

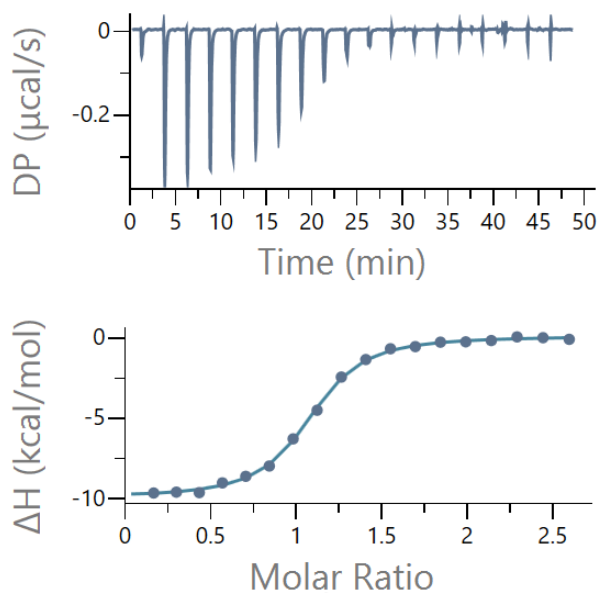| c_{42} (µM)	c_{Gal-1} (µM)	K_d (µM)	ΔG (kcal/mol)	ΔH (kcal/mol)	$-T\Delta S$ (kcal/mol)	n
200	17	0.388	−8.8	−9.4	0.6	1.02

Figure S65. Raw heat and ΔH graphs of the isothermal titration calorimetry of **42** with *h*gal-1, 1st experiment.

Table S16: Data for the isothermal titration calorimetry of **42** with *h*gal-1, 2nd experiment.

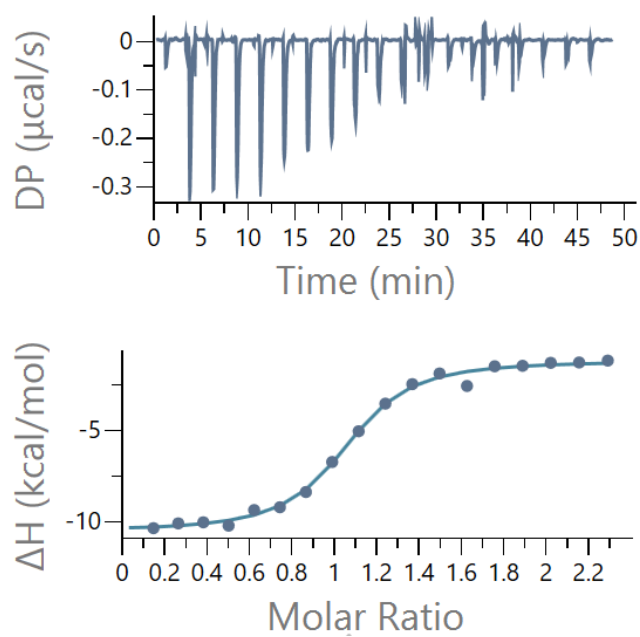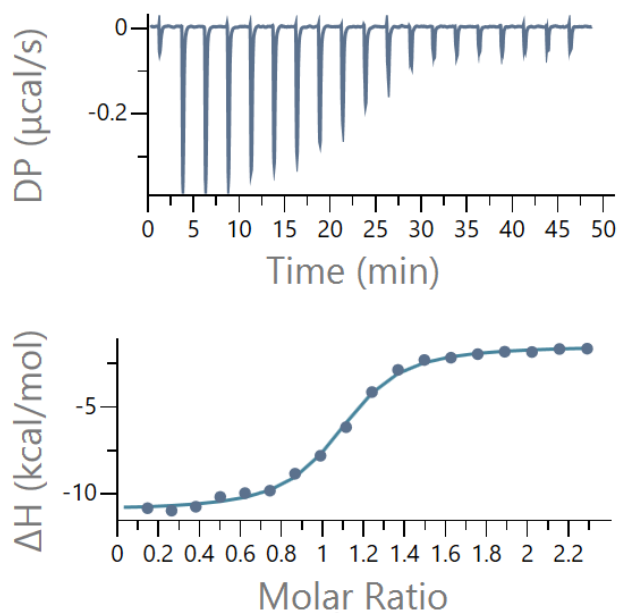| c_{42} (µM)	c_{Gal-1} (µM)	K_d (µM)	ΔG (kcal/mol)	ΔH (kcal/mol)	$-T\Delta S$ (kcal/mol)	n
200	17	0.344	−8.8	−9.5	0.6	1.05

Figure S66. Raw heat and ΔH graphs of the isothermal titration calorimetry of **42** with *h*gal-1, 2nd experiment.

Table S17: Data for the isothermal titration calorimetry of **TD139** with *h*gal-3-CRD, 1st experiment.

c_{TD139} (μM)	$c_{Gal-3-CRD}$ (μM)	K_d (μM)	ΔG (kcal/mol)	ΔH (kcal/mol)	$-T\Delta S$ (kcal/mol)	n
200	10	0.021	−10.5	−16.6	5.1	1.07

Figure S67. Raw heat and ΔH graphs of the isothermal titration calorimetry of **TD139** with *h*gal-3-CRD, 1st experiment.

Table S18: Data for the isothermal titration calorimetry of **TD139** with *h*gal-3-CRD, 2nd experiment.

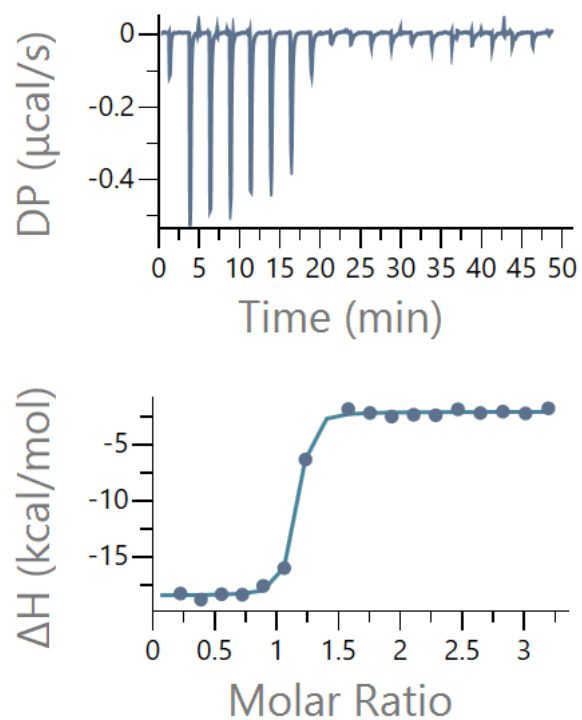| c_{TD139} (μM)	$c_{Gal\text{-}3\text{-}CRD}$ (μM)	K_d (μM)	ΔG (kcal/mol)	ΔH (kcal/mol)	$-T\Delta S$ (kcal/mol)	n
200	10	0.017	−10.6	−16.1	5.5	1.08

Figure S68. Raw heat and ΔH graphs of the isothermal titration calorimetry of **TD139** with *h*gal-3-CRD, 2nd experiment.

Table S19: Data for the isothermal titration calorimetry of **25** with *h*gal-3-CRD, 1st experiment with n set to 1.00.

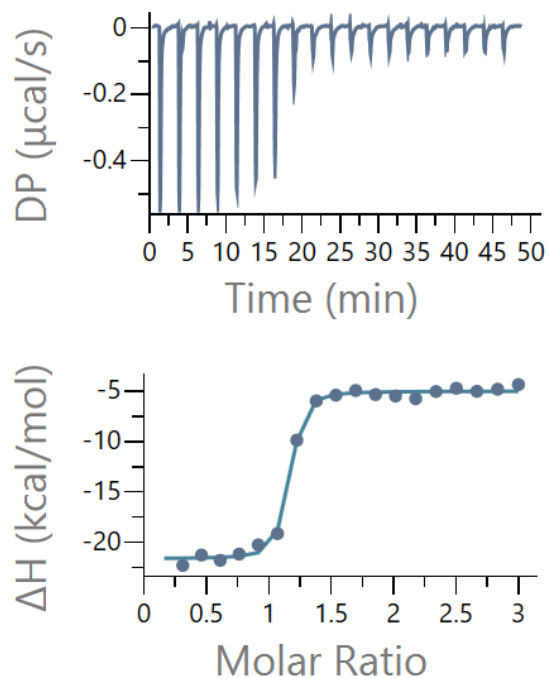| c_{25} (µM)	$c_{Gal-3-CRD}$ (µM)	K_d (µM)	ΔG (kcal/mol)	ΔH (kcal/mol)	$-T\Delta S$ (kcal/mol)	n
500	28	16.5	−5.7	ND*	ND*	1.00

*ND = not determined.

Figure S69. Raw heat and *ΔH* graphs of the isothermal titration calorimetry of **25** with *h*gal-3-CRD, 1st experiment.

Table S20: Data for the isothermal titration calorimetry of **25** with *h*gal-3-CRD, 2nd experiment with n set to 1.00.

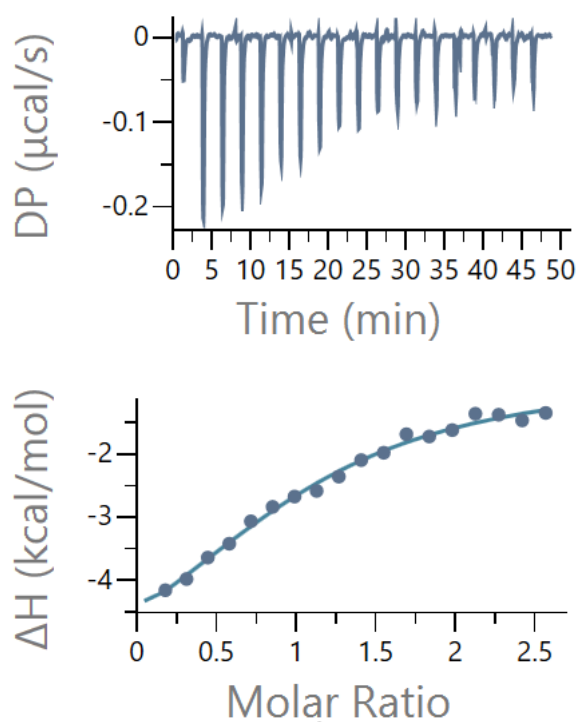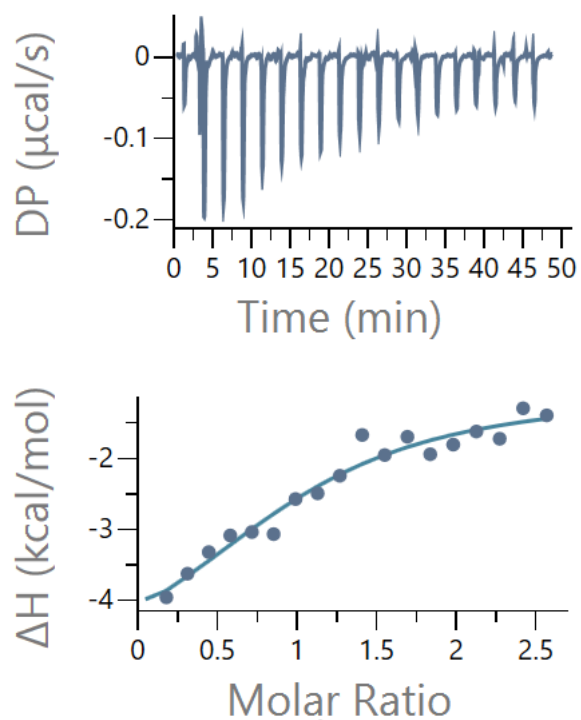| c_{25} (µM)	$c_{Gal-3-CRD}$ (µM)	K_d (µM)	ΔG (kcal/mol)	ΔH (kcal/mol)	$-T\Delta S$ (kcal/mol)	n
500	28	12.8	−6.7	ND*	ND*	1.00

*ND = not determined.

Figure S70. Raw heat and *ΔH* graphs of the isothermal titration calorimetry of **25** with *h*gal-3-CRD, 2nd experiment.

Table S21: Data for the isothermal titration calorimetry of **36** with $h$gal-3-CRD, 1st experiment.

c_{35} (µM)	$c_{Gal\text{-}3\text{-}CRD}$ (µM)	K_d (µM)	ΔG (kcal/mol)	ΔH (kcal/mol)	$-T\Delta S$ (kcal/mol)	n
200	11	0.894	−8.3	−12.8	4.5	1.09
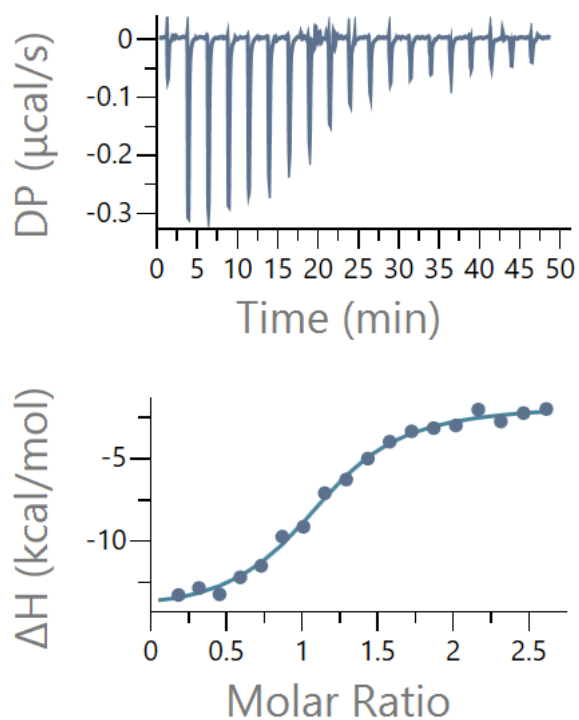
Figure S71. Raw heat and ΔH graphs of the isothermal titration calorimetry of **36** with $h$gal-3-CRD, 1st experiment.

Table S22: Data for the isothermal titration calorimetry of **36** with $h$gal-3-CRD, 2nd experiment.

c_{35} (µM)	$c_{Gal\text{-}3\text{-}CRD}$ (µM)	K_d (µM)	ΔG (kcal/mol)	ΔH (kcal/mol)	$-T\Delta S$ (kcal/mol)	n
200	11	0.951	−8.2	−12.5	−4.3	1.06

The raw heat and ΔH graphs of this titration are shown in the main text.

Table S23: Data for the isothermal titration calorimetry of **37** with *h*gal-3-CRD, 1ˢᵗ experiment.

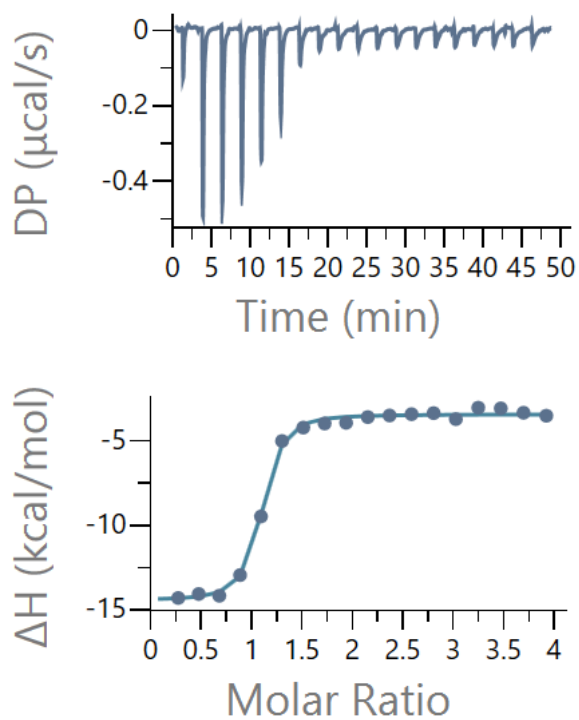| c_{36} (μM)	$c_{Gal-3-CRD}$ (μM)	K_d (μM)	ΔG (kcal/mol)	ΔH (kcal/mol)	−TΔS (kcal/mol)	n
300	11	0.092	−9.6	−11.4	1.8	1.05

Figure S72. Raw heat and ΔH graphs of the isothermal titration calorimetry of **37** with *h*gal-3-CRD, 1ˢᵗ experiment.

Table S24: Data for the isothermal titration calorimetry of **37** with $h$gal-3-CRD, 2nd experiment.

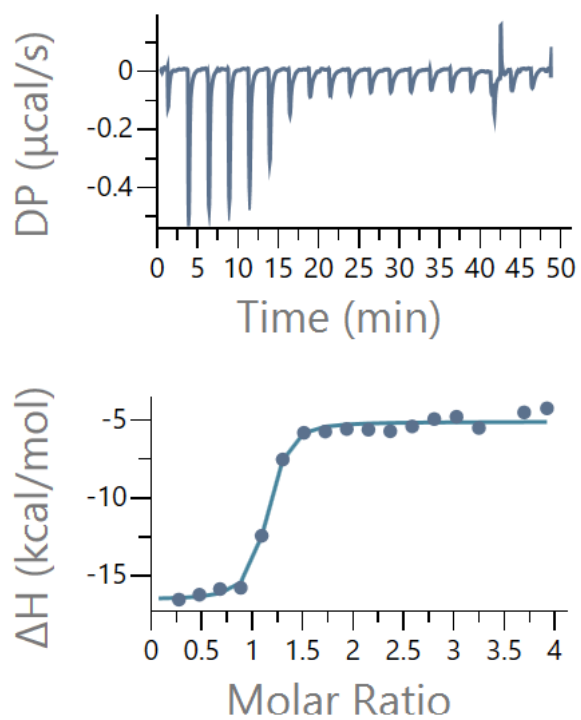| c_{36} (µM)	$c_{\text{Gal-3-CRD}}$ (µM)	K_d (µM)	ΔG (kcal/mol)	ΔH (kcal/mol)	$-T\Delta S$ (kcal/mol)	n
300	11	0.099	−9.5	−11.0	1.5	1.00

Figure S73. Raw heat and ΔH graphs of the isothermal titration calorimetry of **36** with $h$gal-3-CRD, 2nd experiment.

Table S25: Data for the isothermal titration calorimetry of **41** with *h*gal-3-CRD, 1nd experiment.

c_{41} (μM)	$c_{\text{Gal-3-CRD}}$ (μM)	K_d (μM)	ΔG (kcal/mol)	ΔH (kcal/mol)	$-T\Delta S$ (kcal/mol)	n
100	11	0.018	−10.6	−13.1	2.5	1.06

Figure S74. Raw heat and ΔH graphs of the isothermal titration calorimetry of **41** with *h*gal-3-CRD, 1nd experiment.

Table S26: Data for the isothermal titration calorimetry of **41** with *h*gal-3-CRD, 2nd experiment.

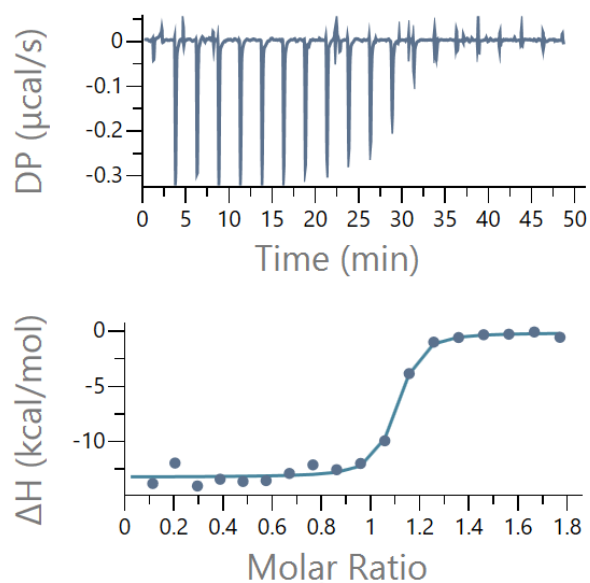| c_{41} (μM)	$c_{\text{Gal-3-CRD}}$ (μM)	K_d (μM)	ΔG (kcal/mol)	ΔH (kcal/mol)	$-T\Delta S$ (kcal/mol)	n
200	11	0.027	−10.3	−14.9	4.6	1.00

Figure S75. Raw heat and ΔH graphs of the isothermal titration calorimetry of **41** with *h*gal-3-CRD, 2nd experiment.

Table S27: Data for the isothermal titration calorimetry of **42** with *h*gal-3-CRD, 1ⁿᵈ experiment.

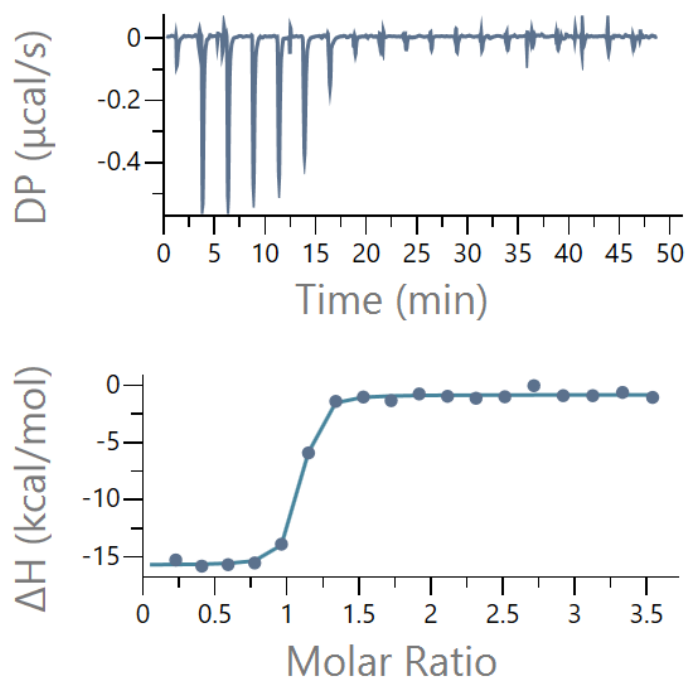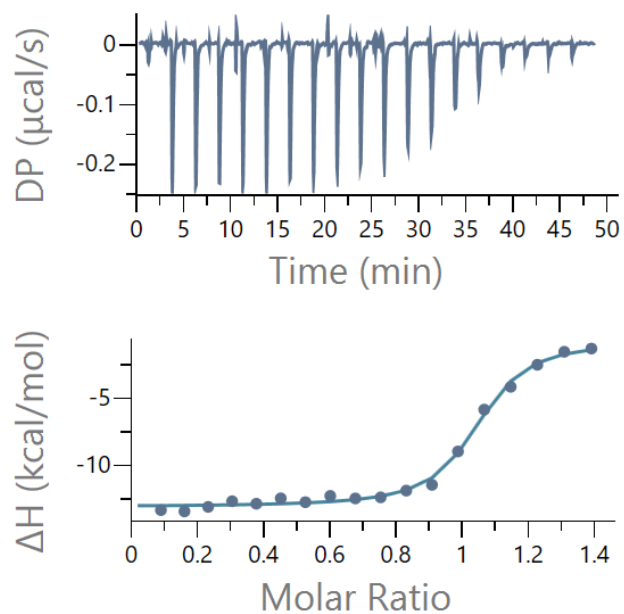| c_{42} (μM)	$c_{Gal-3-CRD}$ (μM)	K_d (μM)	ΔG (kcal/mol)	ΔH (kcal/mol)	$-T\Delta S$ (kcal/mol)	n
100	14	0.073	−9.7	−12.2	2.5	1.01

Figure S76. Raw heat and ΔH graphs of the isothermal titration calorimetry of **42** with *h*gal-3-CRD, 1ⁿᵈ experiment.

Table S28: Data for the isothermal titration calorimetry of **42** with *h*gal-3-CRD, 2nd experiment.

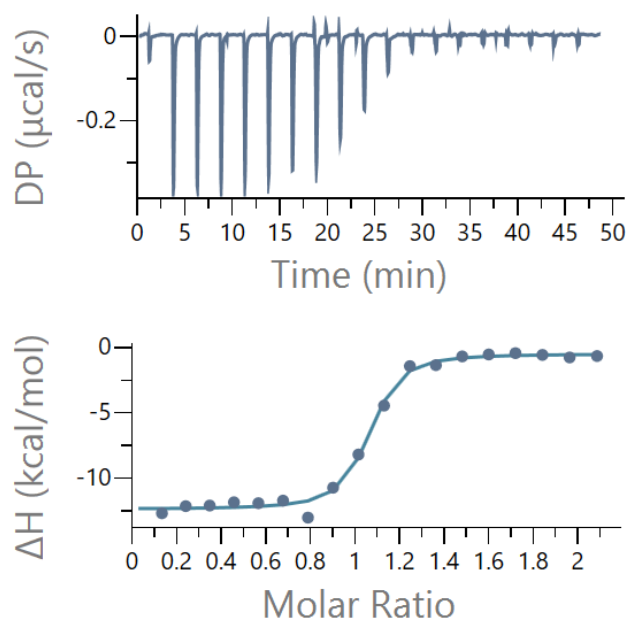| c_{42} (µM)	$c_{Gal-3-CRD}$ (µM)	K_d (µM)	ΔG (kcal/mol)	ΔH (kcal/mol)	$-T\Delta S$ (kcal/mol)	n
150	14	0.059	−9.9	−11.9	2.0	1.01

Figure S77. Raw heat and ΔH graphs of the isothermal titration calorimetry of **42** with *h*gal-3-CRD, 2nd experiment.

F. Modeling the affinity of the ligand to galectin

We proposed a simple computational procedure to estimate the differences in binding affinities of compounds **34**, **36** and **42** to *h*gal-1 and *h*gal-3-CRD. The approach was based on the combination of the molecular dynamics of the ligand-galectin complex followed by an estimate of the ligand binding enthalpy for a set of sampled MD geometries. MD simulation were performed in Desmond,[25,26] binding enthalpies were calculated at the semiempirical level in MOPAC.[27]

Initial structures of the galectin complex with compounds **34**, **36** and **42** were constructed using X-ray structures of TD139 with *h*gal-1 (PDB code 4Y24) or *h*gal-3-CRD (PDB code 5H9P) as templates. TD139 was then replaced with the optimized (PM6[28] level in MOPAC[27]) structure of the compounds studied (Figs. 6, S78–S83). The original 4Y24 complex of *h*gal-1 with TD139 is a dimer, but only the monomeric unit was considered in this work. The obtained initial structures of *h*gal-1 and *h*gal-3-CRD with compounds **34**, **36** or **42** were placed in a periodic orthorhombic array defined by a 10 Å buffer distance using the System Builder tool in Desmond.[25, 26] The box was then filled with water molecules.

One complex was thus surrounded by approximately 5000 water molecules. The protein and ligand were described using the OPLS4 force field[29] and the TIP4PEW model[30] was used to describe the water. The system was relaxed prior to MD simulations using the default relaxation protocol in Desmond,[25, 26] which includes simulated annealing and short constrained and unconstrained simulations under NVT and then NpT conditions. A production run of 100 ns was performed on a relaxed system (NpT ensemble at 300 K and 1 atm; Nosé-Hoover thermostat; Martyna-Tobias-Klein barostat with a coupling constant of 2.0 ps) using a time step of 1 fs. Geometries were sampled at 1 ns intervals, resulting in 100 geometries. Long-range electrostatic interactions were calculated using the particle mesh Ewald method. The cutoff radius of the Coulomb interactions was 9.0 Å. Non-bonding forces were calculated using the r-RESPA integrator.

The sampled geometries were then optimized in MOPAC[27] at the PM6-D3H4X level[31] using the MOZYME approximation[32] (utilizing the localized molecular orbital method developed for MOPAC) till the gradient norm was less than 10. The iron atoms in compounds **34**, **36** and **42** were described as fully ionic with a 2+ charge using the "METAL" keyword in MOPAC. The net charge of the $h$gal-1 complexes was −3, while the $h$gal-3-CRD complexes had a charge of +3. The solvent effect was approximated using the COSMO model[33] with a dielectric constant of 78.4 corresponding to water. Selected MD structures of the complexes were also separated into galectin and ligand, and these individual components were optimized separately under the same conditions as the complexes. The binding enthalpies were then calculated as: $\Delta H_{bind} = H_{complex} - (H_{galectin} + H_{ligand})$, where $H_{complex}$, $H_{galectin}$ and H_{ligand} are the final heats of formation of the optimized structures. The resulting binding enthalpies then represent the average of ΔH_{bind} obtained for all considered MD geometries. The quality of the resulting enthalpies obtained at the PM6-D3H4X level also depends on the quality of the optimized structure. More stringent criteria may also bring some improvement in the calculated values. It is obvious from the comparison of the calculated ΔH_{bind} (Table 5, entry 3) and experimentally determined ΔH for diferrocene **36** (Table 4, entries 4 and 8) that the calculation overestimates the values of the binding enthalpies. This may be due to several reasons. First, we consider 100 MD geometries of a ligand-galectin complex, for which we determine the ΔH_{bind} values, and the resulting value is their average. However, the standard deviation of the individual values from the mean is relatively high (up to 20 kcal/mol), which is probably due to the large fluctuation of the energy in relation to changes in the geometries considered. The reduction of galectin flexibility by certain constraints in the MD or in the subsequent optimization, as well as more stringent optimisation criteria, could potentially improve the quantitative agreement with the experiment. For the purposes of the paper, however, the qualitative nature of the predictions seems sufficient.[34] Other sources of inaccuracy may be an incomplete description of iron atoms by semiempirical methods,[28] overestimation of charge-charge interactions in MD[35] (which is reflected in the resulting geometries) or imperfection of the solvation model describing the solvent effect.[36]
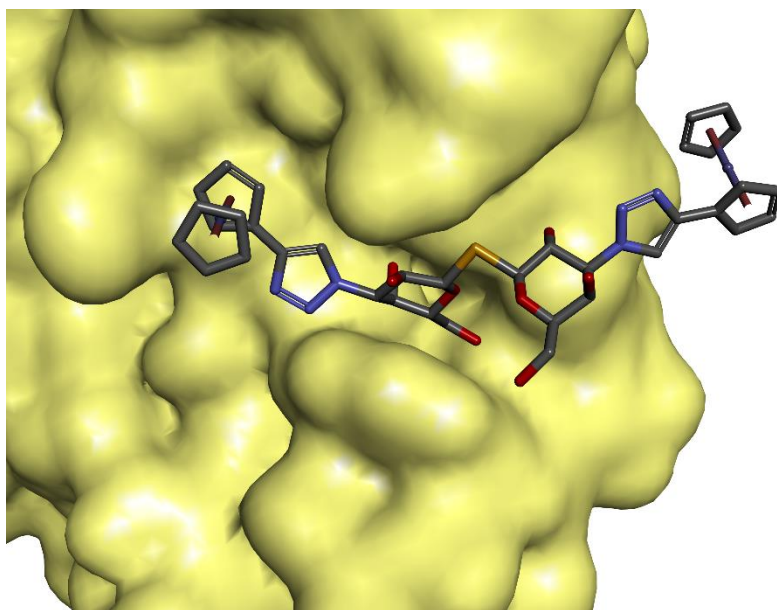
Figure S78. Starting geometry of complex of compound **36** with *h*gal-1 in molecular dynamics calculations.
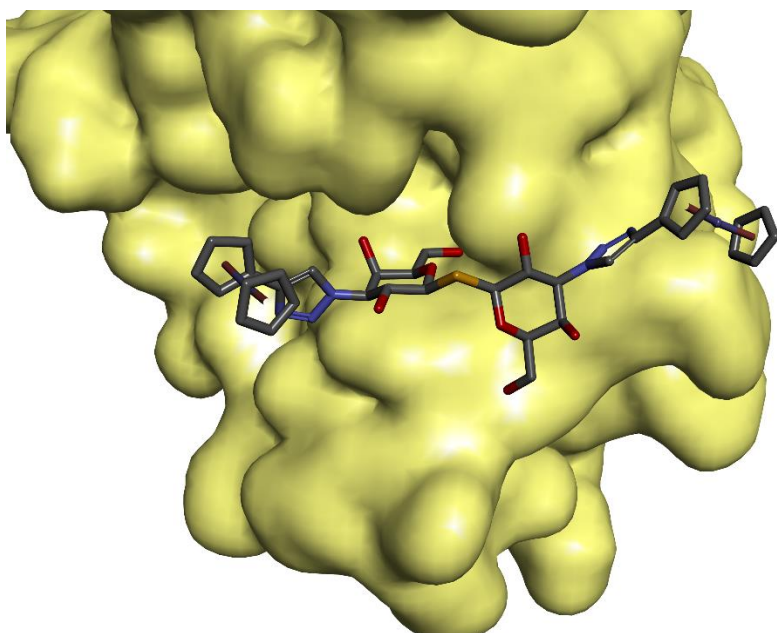

Figure S79. Starting geometry of complex of compound **36** with *h*gal-3 in molecular dynamics calculations.
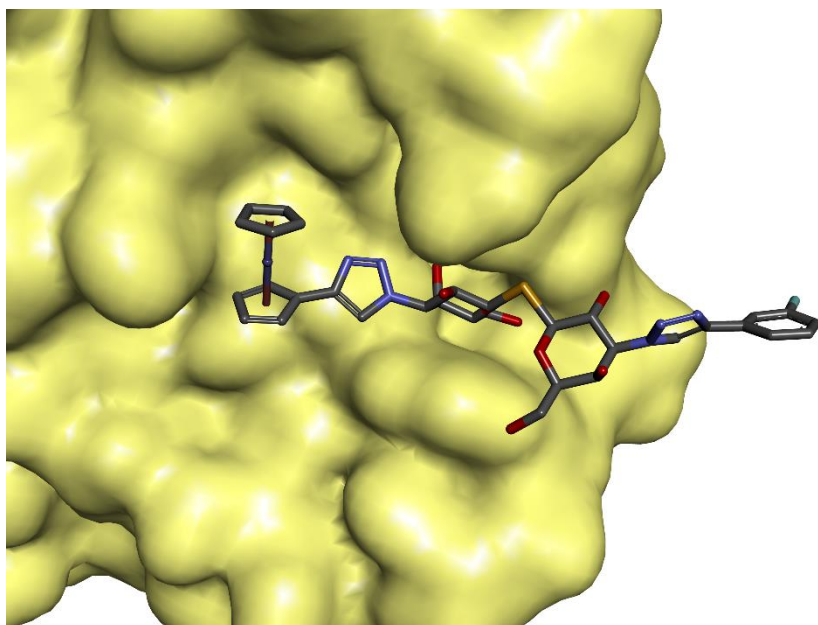
Figure S80. Starting geometry of complex of compound **42** with *h*gal-1 in molecular dynamics calculations. The ferrocene moiety is in subsites A and B.

Figure S81. Starting geometry of complex of compound **42** with *h*gal-1 in molecular dynamics calculations. The ferrocene moiety is in subsite E.

Figure S82. Starting geometry of complex of compound **42** with *h*gal-3-CRD in molecular dynamics calculations. The ferrocene moiety is in subsites A and B.
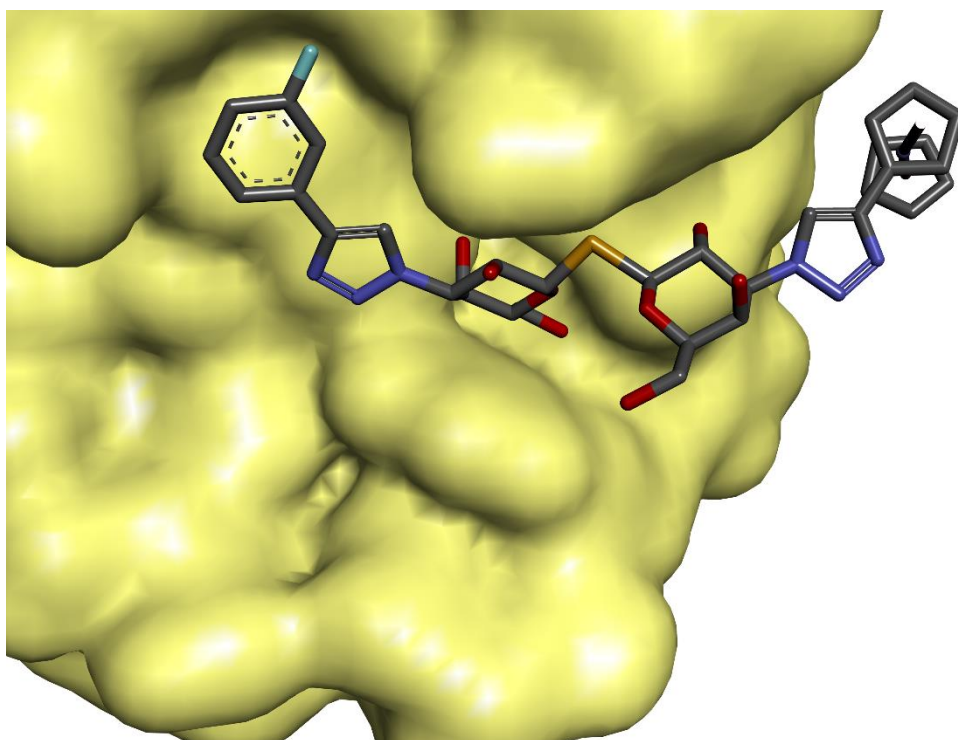
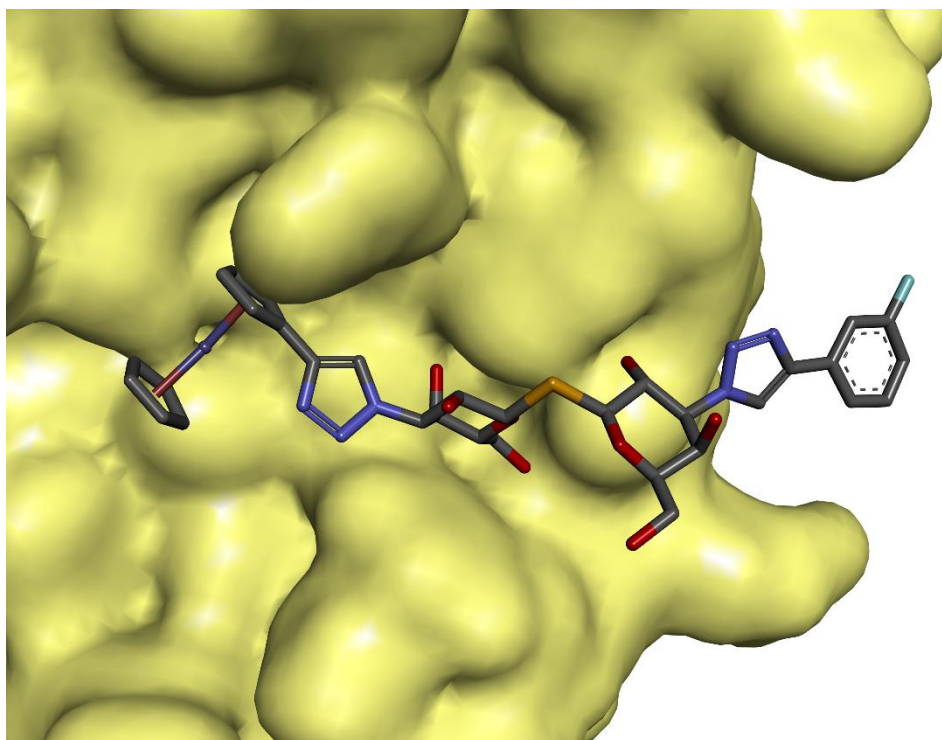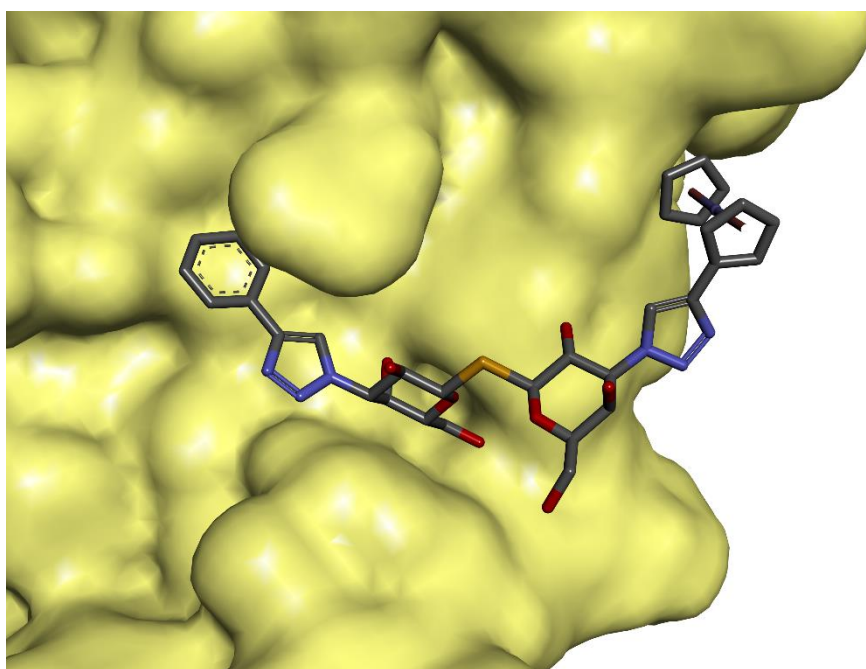

Figure S83. Starting geometry of complex of compound **42** with *h*gal-3-CRD in molecular dynamics calculations. The ferrocene moiety is in subsite E.

G. $^{19}F\{^1H\}$ NMR Experiments with Human Galectins

$^{19}F\{^1H\}$NMR spectra of compounds **28**, **42**, and **TD139** with *h*gal-1 and -3-CRD were recorded at 5 °C, using Bruker Avance 400 (^1H at 400.1 MHz, ^{19}F at 376.4 MHz) equipped with BBO probe optimized for X-nuclei detection. The experiments were performed using the 5 s relaxation delay, 3 s of acquisition time, 16 dummy scans and typically more than 6000 scans. The ^{19}F resonances were referenced to the line of an external standard hexafluorobenzene in $CHCl_3$ (δ/ppm; −163.00). The spectra were processed in MestreNova software (version 12.0.3) by 512 K zero-filling, 20 Hz exponential apodization, and multipoint baseline correction using cubic spine interpolation algorithm with the default setting of RMS calculation span (300 points). All samples were measured in PBS buffered aqueous solution (50 mM phosphate, 150 mM NaCl, 1 mM TCEP, pH = 7.4) with a content of 10% D_2O. We used Norell$^©$ Standard Series^{TM} 5 mm NMR tubes for all experiments. We have performed two NMR experiments for each combination of ligand (**28**, **42**, or **TD139**) and protein (*h*gal-1 and -3), therefore 12 experiments in total. Firstly, a sub-stoichiometric quantity of the ligand was added to a solution of the protein, allowing the observation of ^{19}F resonances, which correspond only to the bound states. Subsequently, the concentration of the ligand was increased above that of the protein, allowing the observation of ^{19}F resonance corresponding to the unbound state of the ligand (**28**, **42**, or **TD139**). In addition to the signals of unbound and protein-bound ligands, we also observed a signal close to −120.3 ppm (Figs. S85–S90) and in some cases also a signal close to −81.3 ppm (Figs. S88, and S90). These signals were identified as fluorine-containing impurities in μM concentrations leaking from glass NMR tubes. The impurity with the chemical shift near −120.3 ppm was assigned as fluoride in accordance with previous report.[53] The second ^{19}F signal close to −81.3 ppm was not assigned to a specific compound, but a blank experiment confirmed its origin from the NMR tube. Heating the NMR tube containing **TD139** and *h*gal-1 to 90 °C overnight the protein to precipitate in the form of white precipitate. The filtrate after filtration did not contain the bound state signals, however, the impurity signals persisted (S91), confirming that these signals do not belong to the galectin.
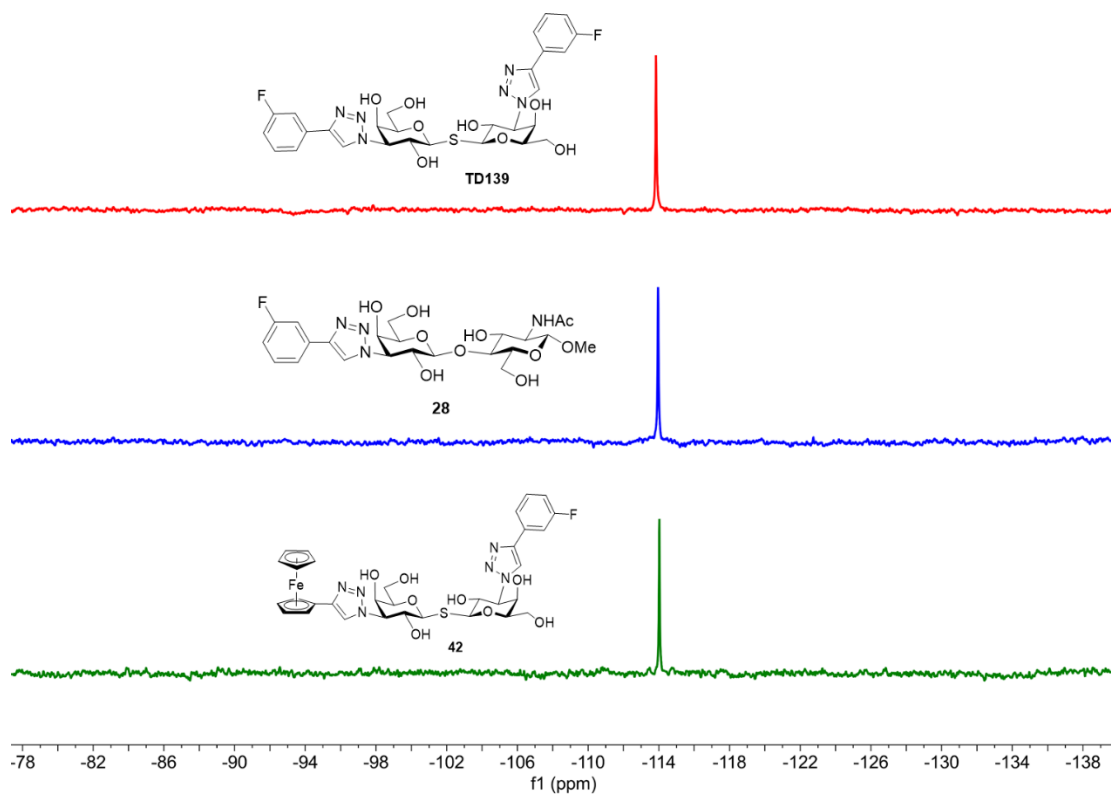
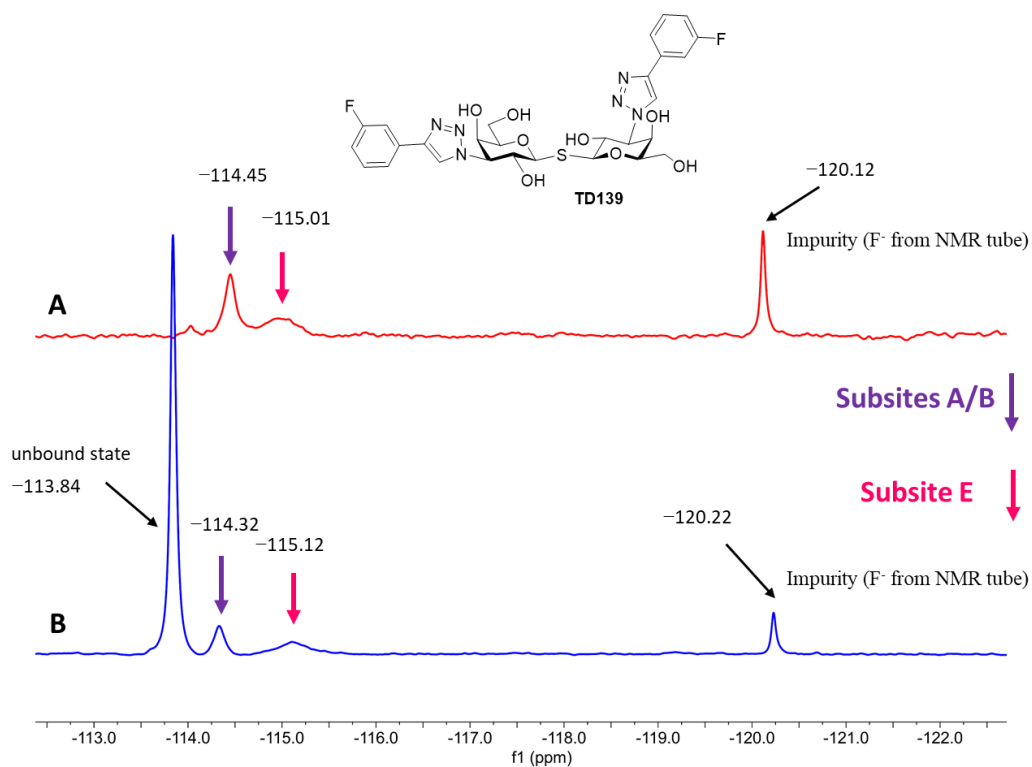**Figure S84.** $^{19}F\{^{1}H\}$ NMR spectra of compounds **TD139**, **28** and **42** in H_2O/D_2O 90:10 mixture.

Figure S85. $^{19}F\{^{1}H\}$ NMR spectrum of compound **TD139** in the presence of $h$gal-1. A) $c(\textbf{TD139}) = 100\ \mu M$, $c(h\text{gal-1}) = 150\ \mu M$. B) $c(\textbf{TD139}) = 500\ \mu M$, c($h$gal-1) $= 150\ \mu M$.
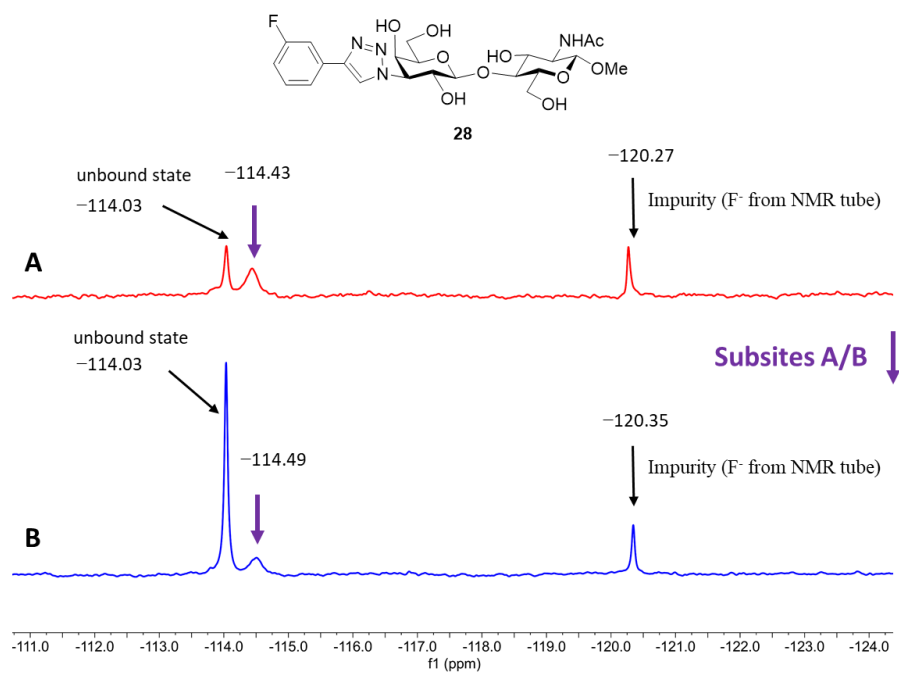
Figure S86. ^{19}F{^{1}H} NMR spectrum of compound **28** in the presence of $h$gal-1. A) $c(\mathbf{28}) = 100$ µM, $c(h\text{gal-1}) = 80$ µM. B) $c(\mathbf{28}) = 300$ µM, $c(h\text{gal-1}) = 80$ µM.
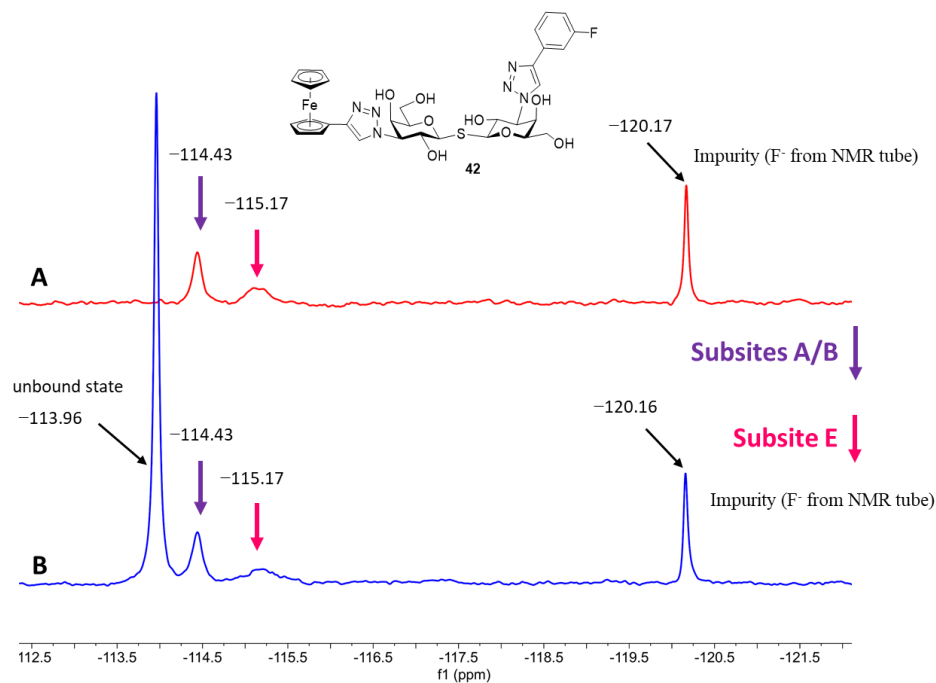
Figure S87. ^{19}F{^{1}H} NMR spectrum of compound **42** in the presence of $h$gal-1. A) $c(\mathbf{42}) = 100$ µM, $c(h\text{gal-1}) = 135$ µM. B) $c(\mathbf{42}) = 300$ µM, $c(h\text{gal-1}) = 135$ µM.
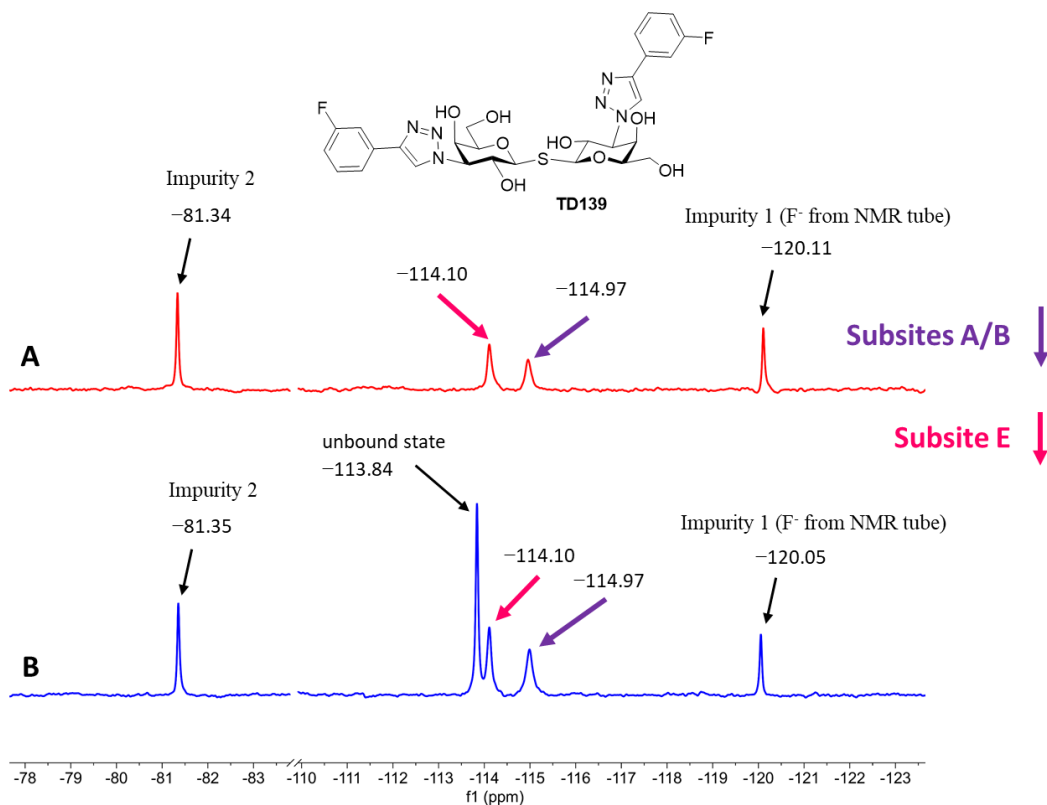
Figure S88. $^{19}F\{^1H\}$ NMR spectrum of compound **TD139** in the presence of $h$gal-3-CRD. A) $c(\mathbf{TD139})$ = 100 μM, $c(h$gal-3-CRD$)$ = 135 μM. B) $c(\mathbf{TD139})$ = 300 μM, $c(h$gal-3-CRD$)$ = 135 μM.
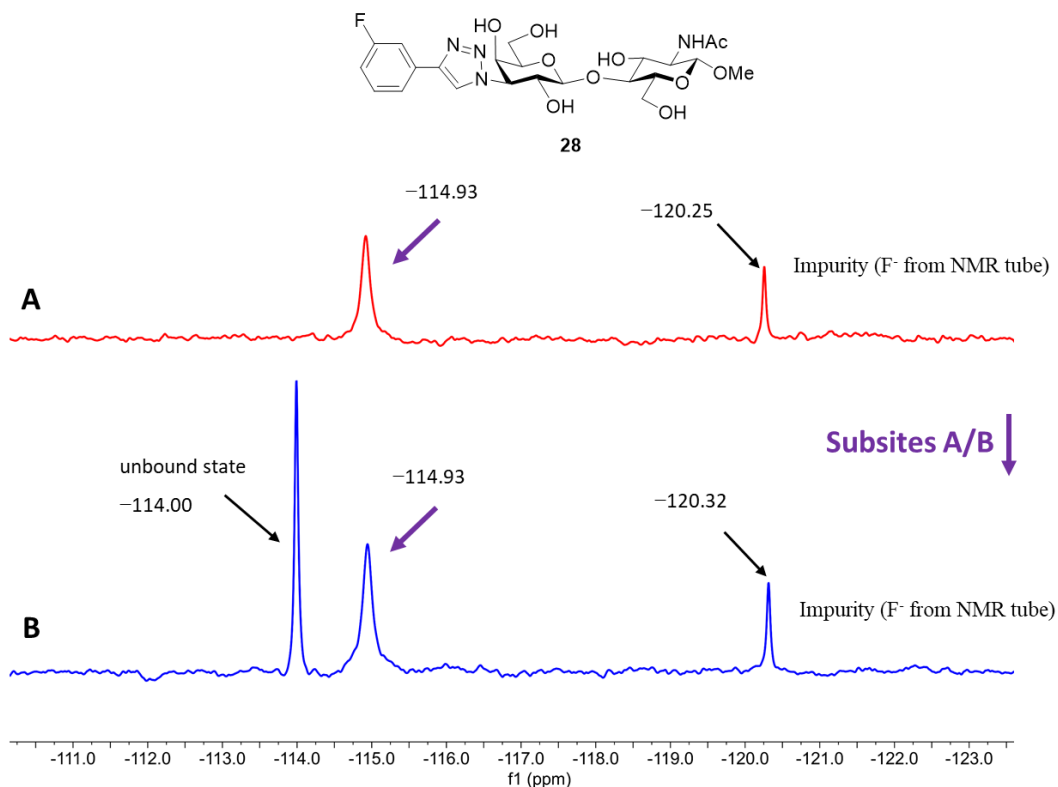
Figure S89. $^{19}F\{^1H\}$ NMR spectrum of compound **28** in the presence of $h$gal-3-CRD. A) $c(\mathbf{28})$ = 150 μM, $c(h$gal-3-CRD$)$ = 200 μM. B) $c(\mathbf{28})$ = 400 μM, $c(h$gal-3-CRD$)$ = 200 μM.
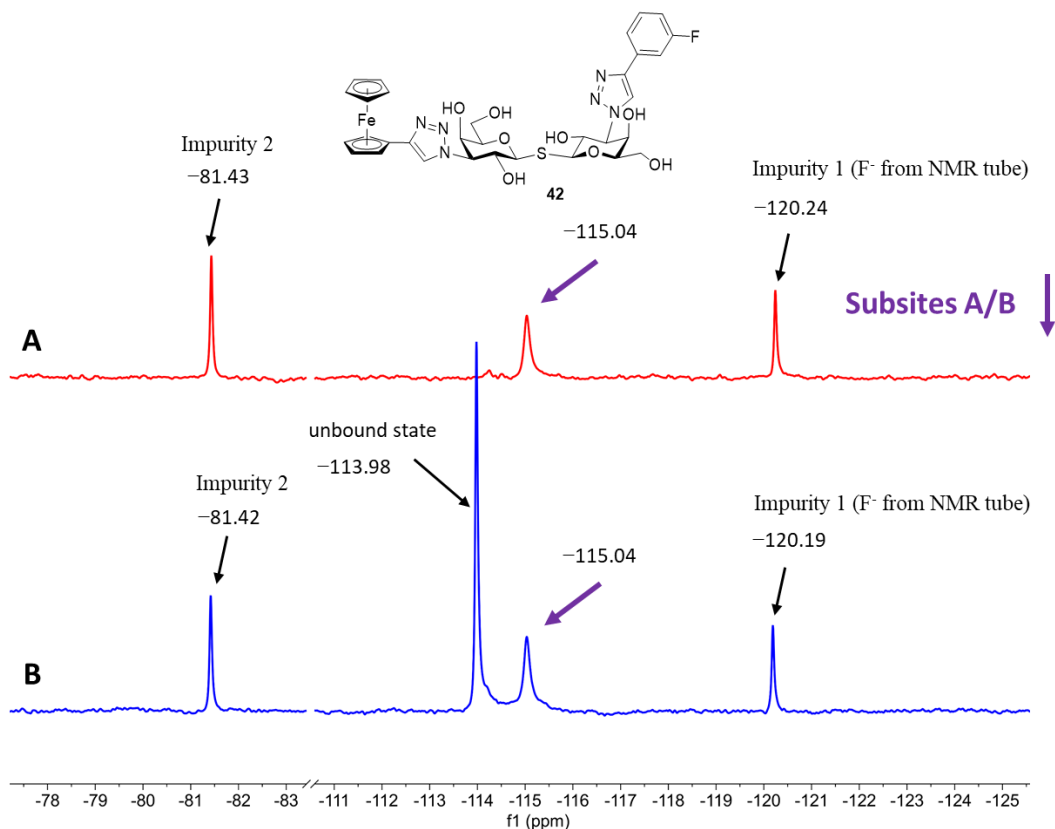
Figure S90. $^{19}F\{^{1}H\}$ NMR spectrum of compound **42** in the presence of $h$gal-3-CRD. A) $c(\mathbf{42}) = 100$ µM, $c(h$gal-3-CRD$) = 135$ µM. B) $c(\mathbf{42}) = 300$ µM, $c(h$gal-3-CRD$) = 135$ µM.
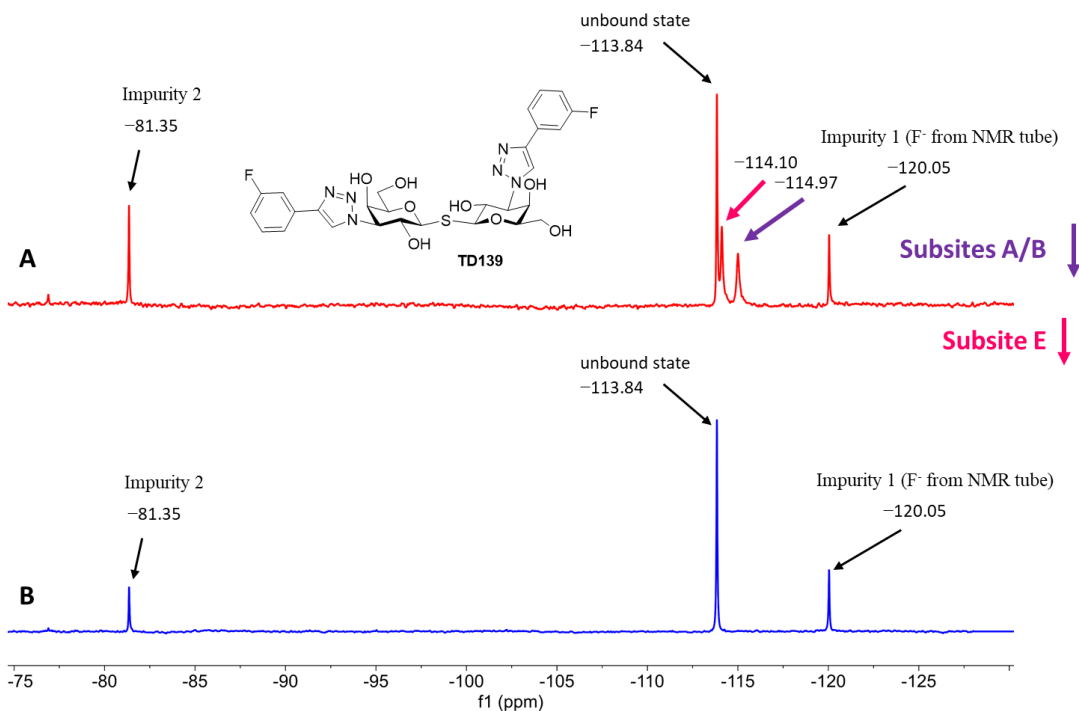
Figure S91. $^{19}F\{^{1}H\}$ NMR spektrum of **TD139** in the presence of $h$gal-3-CRD A) c(**TD139**) = 300 µM, c($h$gal-3-CRD) = 135 µM. B) Spectrum aquired after heating of the sample at 90 °C overnight and subsequent filtration of formed precipitate.

G. Cytotoxicity testing

The cells were maintained at 37 °C in humidified atmosphere with 5% CO_2. MDA-MB-231 and HEK-293 cells were cultured in high glucose Dulbecco's modified Eagle's medium, A2780 cells were cultured in RPMI-1640 medium and SK-OV-3 cells in McCoy's 5A Medium (all media were from Sigma-Aldrich (St. Louis, MO, USA)). Each media was supplemented with 10% fetal bovine serum (Gibco, ThermoFisher Scientific, Waltham, MA, USA), 300 μg/ml of L-glutamine (Sigma-Aldrich), and 100 μg/ml of HyClone Penicillin– Streptomycin 100X solution (BioSera, Nuaille, France). The culture medium was changed during each cell passage every 2–3 days. Cells were mycoplasma free throughout the experiments. Cells were grown to 60–80% confluence prior to seeding in a 96-well plate at a density of 5000 cells/well for cytotoxicity testing. The next day, these cells were exposed to selected compounds at concentrations from 0.15 to 300 μM for 72 h. The cell viability was measured using colorimetric MTT assay as described previously.[54] Data from MTT assay were analyzed in GraphPad Prism software and expressed as IC_{50} values (compound concentrations that produce 50% of cell metabolic inhibition). Errors were calculated as standard deviations (SD). All experiments were performed independently at least three times.

H. References:

(1) Rauthu, S. R.; Shiao, T. C.; Andre, S.; Miller, M. C.; Madej, É.; Mayo, K. H.; Gabius, H. J.; Roy, R. Defining the Potential of Aglycone Modifications for Affinity/Selectivity Enhancement against Medically Relevant Lectins: Synthesis, Activity Screening, and HSQC-Based NMR Analysis. *ChemBioChem* **2015**, *16* (1), 126–139.

(2) Machida, T.; Lang, K.; Xue, L.; Chin, J. W.; Winssinger, N. Site-specific glycoconjugation of protein via bioorthogonal tetrazine cycloaddition with a genetically encoded trans-cyclooctene or bicyclononyne. *Bioconjug. chem.* **2015**, *26* (5), 802–806.

(3) Šardzík, R.; Noble, G. T.; Weissenborn, M. J.; Martin, A.; Webb, S. J.; Flitsch, S. L. Preparation of aminoethyl glycosides for glycoconjugation. *Beilstein J. Org. Chem.* **2010**, *6*, 699–703.

(4) Jacobson, J. M.; Kitov, P. I.; Bundle, D. R. The synthesis of a multivalent heterobifunctional ligand for specific interaction with Shiga toxin 2 produced by E. coli O157: H7. *Carbohydr. Res.* **2013**, *378*, 4–14.

(5) Bröder, W.; Kunz, H. A new method of anomeric protection and activation based on the conversion of glycosyl azides into glycosyl fluorides. *Carbohydr. Res.* **1993**, *249* (1), 221–241.

(6) Helland, A.-C.; Hindsgaul, O.; Palcic, M. M.; Stults, C. L.; Macher, B. A. Methyl 3-amino-3-deoxy-β-D-galactopyranosyl-(1→ 4)-2-acetamido-2-deoxy-β-D-glucopyranoside: an inhibitor of UDP-D-galactose: β-D-galactopyranosyl-(1→ 4)-2-acetamido-2-deoxy-D-glucose (1→ 3)-α-D-galactopyranosyltransferase. *Carbohydr. Res.* **1995**, *276* (1), 91–98.

(7) Kurfiřt, M.; Dračínský, M.; Červenková Šťastná, L.; Cuřínová, P.; Hamala, V.; Hovorková, M.; Bojarová, P.; Karban, J. Selectively Deoxyfluorinated N-Acetyllactosamine Analogues as 19F NMR Probes to Study Carbohydrate-Galectin Interactions. *Chem. – Eur. J.* **2021**, *27* (51), 13040–13051.

(8) Xia, C.; Zhang, W.; Zhang, Y.; Chen, W.; Nadas, J.; Severin, R.; Woodward, R.; Wang, B.; Wang, X.; Kronenberg, M.; et al. The Roles of 3′ and 4′ Hydroxy Groups in α-Galactosylceramide Stimulation of Invariant Natural Killer T Cells. *ChemMedChem* **2009**, *4* (11), 1810–1815.

(9) Kovalová, A.; Prouza, V.; Zavřel, M.; Hájek, M.; Dzijak, R.; Magdolenová, A.; Pohl, R.; Voburka, Z.; Parkan, K.; Vrabel, M. Selection of Galectin-Binding Ligands from Synthetic Glycopeptide Libraries. *ChemPlusChem* **2023**, e202300567.

(10) Zhang, H.; Laaf, D.; Elling, L.; Pieters, R. J. Thiodigalactoside–bovine serum albumin conjugates as high-potency inhibitors of galectin-3: an outstanding example of multivalent presentation of small molecule inhibitors. *Bioconjug. Chem.* **2018**, *29* (4), 1266–1275.

(11) St-Gelais, J.; Leclerc, C.; Giguère, D. Synthesis of fluorinated thiodigalactoside analogues. *Carbohydr. Res.* **2022**, *511*, 108481.

(12) Cumpstey, I.; Salomonsson, E.; Sundin, A.; Leffler, H.; Nilsson, U. J. Double affinity amplification of galectin–ligand interactions through arginine–arene interactions: synthetic, thermodynamic, and computational studies with aromatic diamido thiodigalactosides. *Chem. – Eur. J.* **2008**, *14* (14), 4233–4245.

(13) St-Gelais, J.; Denavit, V.; Giguère, D. Efficient synthesis of a galectin inhibitor clinical candidate (TD139) using a Payne rearrangement/azidation reaction cascade. *Org. Biomol. Chem.* **2020**, *18* (20), 3903-3907.

(14) van Hattum, H.; Branderhorst, H. M.; Moret, E. E.; Nilsson, U. J.; Leffler, H.; Pieters, R. J. Tuning the preference of thiodigalactoside-and lactosamine-based ligands to galectin-3 over galectin-1. *J. Med. Chem.* **2013**, *56* (3), 1350–1354.

(15) Peterson, K.; Kumar, R.; Stenström, O.; Verma, P.; Verma, P. R.; Håkansson, M.; Kahl-Knutsson, B.; Zetterberg, F.; Leffler, H.; Akke, M. Systematic tuning of fluoro-galectin-3 interactions provides thiodigalactoside derivatives with single-digit nM affinity and high selectivity. *J. Med. Chem.* **2018**, *61* (3), 1164–1175.

(16) Špaček, J.; Daňhel, A.; Hasoň, S.; Fojta, M. Label-free detection of canonical DNA bases, uracil and 5-methylcytosine in DNA oligonucleotides using linear sweep voltammetry at a pyrolytic graphite electrode. *Electrochem. Commun.* **2017**, *82*, 34–38.

(17) Hasoň, S., Ostatná, V., Fojt, L., Fojta, M. Arrangements of DNA purine bases on pyrolytic graphite electrode surface. Electrochemical characterization and atomic force microscopy imaging. *Electrochim. Acta* **2023**, 441, 141772.

(18) Alba, A. F.; Totoricaguena-Gorriño, J.; Campos-Arias, L.; Peřinka, N.; Ruiz-Rubio, L.; Vilas-Vilela, J. L.; Lanceros-Méndez, S.; del Campo, F. J. Laser-induced highly oriented pyrolytic graphite for high-performance screen-printed electrodes. *Mater. Adv.* **2021**, *2* (18), 5912–5921.

(19) Tropea, J. E.; Cherry, S.; Waugh, D. S. Expression and purification of soluble His 6-tagged TEV protease. *High throughput protein expression and purification: methods and protocols* **2009**, 297-307.

(20) Pace, K. E.; Hahn, H. P.; Baum, L. G. Preparation of recombinant human galectin-1 and use in T-cell death assays. In *Methods in enzymology* **2003**, *363*, 499–518.

(21) Sörme, P.; Kahl-Knutsson, B.; Huflejt, M.; Nilsson, U. J.; Leffler, H. Fluorescence polarization as an analytical tool to evaluate galectin–ligand interactions. *Anal. Biochem.* **2004**, *334* (1), 36–47.

(22) Nikolovska-Coleska, Z.; Wang, R.; Fang, X.; Pan, H.; Tomita, Y.; Li, P.; Roller, P. P.; Krajewski, K.; Saito, N. G.; Stuckey, J. A. Development and optimization of a binding assay for the XIAP BIR3 domain using fluorescence polarization. *Anal. Biochem.* **2004**, *332* (2), 261–273.

(23) Sindrewicz, P.; Li, X.; Yates, E. A.; Turnbull, J. E.; Lian, L.-Y.; Yu, L.-G. Intrinsic tryptophan fluorescence spectroscopy reliably determines galectin-ligand interactions. *Sci. Rep.* **2019**, *9* (1), 11851.

(24) Hsieh, T.-J.; Lin, H.-Y.; Tu, Z.; Lin, T.-C.; Wu, S.-C.; Tseng, Y.-Y.; Liu, F.-T.; Hsu, S.-T. D.; Lin, C.-H. Dual thio-digalactoside-binding modes of human galectins as the structural basis for the design of potent and selective inhibitors. *Sci. Rep.* **2016**, *6* (1), 29457.

(25) Bowers, K. J.; Chow, E.; Xu, H.; Dror, R. O.; Eastwood, M. P.; Gregersen, B. A.; Klepeis, J. L.; Kolossvary, I.; Moraes, M. A.; Sacerdoti, F. D.; Salmon, J. K.; Shan, Y.; Shaw, D. E. Scalable algorithms for molecular dynamics simulations on commodity clusters. *Proceedings of the ACM/IEEE Conference on Supercomputing (SC06)* **2006**, Tampa, Florida, USA, page 43.

(26) *Schrödinger Release 2024-1: Desmond Molecular Dynamics System*; Schrödinger: New York, NY, **2024**.

(27) *MOPAC2016*; Stewart Computational Chemistry: Colorado Springs, CO, USA, **2016**.

(28) Stewart, J. J. P. Optimization of Parameters for Semiempirical Methods V: Modification of NDDO Approximations and Application to 70 Elements. *J. Mol. Modeling* **2007**, *13*, 1173–1213.

(29) Lu, C.; Wu, C.; Ghoreishi, D.; Chen, W.; Wang, L.; Damm, W.; Ross, G. A.; Dahlgren, M. K.; Russell, E.; Von Bargen, C. D.; et al. OPLS4: Improving Force Field Accuracy on Challenging Regimes of Chemical Space. *J. Chem. Theory Comput.* **2021**, *17*, 4291–4300.

(30) Horn, H. W.; Swope, W. C.; Pitera, J. W.; Madura, J. D.; Dick, T. J.; Hura, G. L.; Teresa Head-Gordon, T. Development of an improved four-site water model for biomolecular simulations: TIP4P-Ew. *J. Chem. Phys.* **2004**, *120*, 9665–9678.

(31) Brahmkshatriya, P. S.; Dobeš, P.; Fanfrlik, J.; Řezáč, J.; Paruch, K.; Bronowska, A.; Lepšík, M.; Hobza, P. Quantum Mechanical Scoring: Structural and Energetic Insights into Cyclin-Dependent Kinase 2 Inhibition by Pyrazolo[1,5-a]pyrimidines. *Curr. Comput.-Aid. Drug.* **2013**, *9*, 118–129.

(32) Stewart, J. J. P. Optimization of parameters for semiempirical methods VI: more modifications to the NDDO approximations and re-optimization of parameters. *J. Mol. Model.* **2013**, *19*, 1–32.

(33) Klamt, A.; Schüümann, G. COSMO: A New Approach to Dielectric Screening in Solvents with Explicit Expressions for the Screening Energy and its Gradient. *J. Chem. Soc. Perkin Trans.* **1993**, *2*, 799–805.

(34) Pecina, A.; Fanfrlík, J.; Lepšík, M.; Řezáč, J. SQM2.20: Semiempirical quantum-mechanical scoring function yields DFT-quality protein–ligand binding affinity predictions in minutes. *Nat. Commun.* **2024**, *15*, 1127.

(35) Kirby, B. J.; Jungwirth, P. Charge Scaling Manifesto: A Way of Reconciling the Inherently Macroscopic and Microscopic Natures of Molecular Simulations. *J. Phys. Chem. Lett.* **2019**, *10*, 7531−7536.

(36) Kříž, K.; Řezáč, J. Reparametrization of the COSMO Solvent Model for Semiempirical Methods PM6 and PM7. *J. Chem. Inf. Model.* **2019**, *59*, 229–235.

(37) Lee, C.; Yang, W.; Parr, R. G. Development of the Colle-Salvetti correlation-energy formula into a functional of the electron density. *Phys. Rev. B* **1988**, *37* (2), 785–790.

(38) Becke, A. D. Density-functional thermochemistry. II. The effect of the Perdew–Wang generalized-gradient correlation correction. *The Journal of chemical physics* **1992**, *97* (12), 9173–9177.

(39) Stephens, P. J.; Devlin, F. J.; Chabalowski, C. F.; Frisch, M. J. Ab initio calculation of vibrational absorption and circular dichroism spectra using density functional force fields. *J. Phys. Chem.* **1994**, *98* (45), 11623–11627.

(40) Vosko, S. H.; Wilk, L.; Nusair, M. Accurate spin-dependent electron liquid correlation energies for local spin density calculations: a critical analysis. *Can. J. Phys.* **1980**, *58* (8), 1200–1211.

(41) Grimme, S.; Antony, J.; Ehrlich, S.; Krieg, H. A consistent and accurate ab initio parametrization of density functional dispersion correction (DFT-D) for the 94 elements H-Pu. *J. Chem. Phys.* **2010**, *132* (15).

(42) Grimme, S.; Hansen, A.; Brandenburg, J. G.; Bannwarth, C. Dispersion-corrected mean-field electronic structure methods. *Chem. Rev,* **2016**, *116* (9), 5105–5154.

(43) Barone, V.; Cossi, M. Quantum Calculation of Molecular Energies and Energy Gradients in Solution by a Conductor Solvent Model. *J. Phys. Chem. A* **1998**, *102* (11), 1995–2001.

(44) Cossi, M.; Rega, N.; Scalmani, G.; Barone, V. Energies, structures, and electronic properties of molecules in solution with the C-PCM solvation model. *J. Comput. Chem.* **2003**, *24* (6), 669–681.

(45) London, F. Théorie quantique des courants interatomiques dans les combinaisons aromatiques. *J. Phys. Radium* **1937**, *8* (10), 397–409.

(46) McWeeny, R. Perturbation theory for the Fock-Dirac density matrix. *Phys.l Rev.* **1962**, *126* (3), 1028.

(47) Ditchfield, R. Self-consistent perturbation theory of diamagnetism: I. A gauge-invariant LCAO method for NMR chemical shifts. *Mol. Phys.* **1974**, *27* (4), 789–807.

(48) Wolinski, K.; Hinton, J. F.; Pulay, P. Efficient implementation of the gauge-independent atomic orbital method for NMR chemical shift calculations. *J. Am. Chem. Soc.* **1990**, *112* (23), 8251–8260.

(49) Cheeseman, J. R.; Trucks, G. W.; Keith, T. A.; Frisch, M. J. A comparison of models for calculating nuclear magnetic resonance shielding tensors. *J. Chem. Phys.* **1996**, *104* (14), 5497–5509.

(50) Sternberg, U.; Klipfel, M.; Grage, S. L.; Witter, R.; Ulrich, A. S. Calculation of fluorine chemical shift tensors for the interpretation of oriented 19F-NMR spectra of gramicidin A in membranes. *Phys. Chem. Chem. Phys.* **2009**, *11* (32), 7048–7060.

(51) Weigend, F.; Ahlrichs, R. Balanced basis sets of split valence, triple zeta valence and quadruple zeta valence quality for H to Rn: Design and assessment of accuracy. *Phys. Chem. Chem. Phys.* **2005**, *7* (18), 3297-3305.

(52) Weigend, F. Accurate Coulomb-fitting basis sets for H to Rn. *Phys. Chem. Chem. Phys.* **2006**, *8* (9), 1057–1065.

(53) Matwani, K.; Cornish, J.; DeBenedictis, E. A.; Heller, G. T. Micromolar fluoride contamination arising from glass NMR tubes and a simple solution for biomolecular applications. *bioRxiv* **2024**, 579991.

(54) Hodik T., Lamac M., Červenková Šťastná L., Karban J., Koubkova L., Hrstka R., Cisarova I. and Pinkas J., *Organometallics*, **2014**, *33*, 2059–2070.